FLEXURAL STRENGTHENING OF REINFORCED

CONCRETE BEAMS WITH EXTERNALLY

SIDE-BONDED CFRP LAMINATES

by

Ahmad S. D. Salama

A Thesis Presented to the Faculty of the
American University of Sharjah
College of Engineering
in Partial Fulfillment
of the Requirements
for the Degree of

Master of Science in
Civil Engineering

Sharjah, United Arab Emirates

April 2016

Approval Signatures

We, the undersigned, approve the Master's Thesis of Ahmad S. D. Salama

Thesis Title: Flexural Strengthening of Reinforced Concrete Beams with Externally Side-Bonded CFRP Laminates

Signature	**Date of Signature** *(dd/mm/yyyy)*

_____   _____
Dr. Rami Hawileh
Associate Professor, Department of Civil Engineering
Thesis Advisor

_____   _____
Dr. Jamal A. Abdalla
Professor, Department of Civil Engineering
Thesis Co-Advisor

_____   _____
Dr. Sherif Abdelaziz Yehia Mohamed Ahmed
Professor, Department of Civil Engineering
Thesis Committee Member

_____   _____
Dr. Bassam Abdel Jaber Abu-Nabah
Assistant Professor, Department of Mechanical
Thesis Committee Member

_____   _____
Dr. Osman Akan
Head, Department of Civil Engineering

_____   _____
Dr. Mohamed El-Tarhuni
Associate Dean, College of Engineering

_____   _____
Dr. Leland Blank
Dean, College of Engineering

_____   _____
Dr. Khaled Assaleh
Interim Vice Provost for Research and Graduate Studies

Acknowledgments

Dedication

For my family, my friends and my company; the supreme foundation of support and encouragement.

Abstract

Carbon fiber reinforcement polymer (CFRP) composite sheets and plates are widely used nowadays in civil engineering applications to externally strengthen structural concrete elements against deficiencies in flexure and shear. These deficiencies could be due to an increase in loading, earthquake damage, or even design and/or construction defects. The current state of the art technique used in flexural strengthening of reinforced concrete (RC) beams is the externally bonding of CFRP sheets or plates to the beam's tensile bottom surface (soffit). However, the beam's soffit may be obstructed and not always readily accessible for strengthening. Only the beam's sides that may be exposed become the only accessible area for strengthening using side-bonded CFRP sheets or plates. As a result, this study aims to evaluate the performance of RC beams externally strengthened in flexure with side-bonded CFRP composite sheets. Accordingly, a total of 25 beams has been cast and strengthened in flexure with different configurations of side-bonded CFRP sheets. The strengthening scheme, amount of steel and CFRP reinforcement were varied to examine their effect on the flexural strength and ductility of RC beams. The flexural strength and load-deflection response curves of the tested specimens were also predicted using the ACI 440.2R-08 design guidelines. The predicted results were in good agreement with the experimental results. It was concluded that the side-bonded strengthening scheme is less efficient than that of the conventional soffit-bonded one; however, it is a viable solution when the beam's soffit is not accessible for strengthening. The debonding mechanism of the side-bonded specimens justifies the efficiency reduction in this technique, since the stress distribution is not uniform along the CFRP sheets as in the soffit-bonded ones. However, as the reinforcement ratio increases, the performance of both strengthening schemes exhibit similar performance.

Search Terms: flexural strengthening, reinforced concrete; beams, FRP sheets, CFRP, external reinforcement.

Table of Contents

List of Figures

11

12

13

List of Tables

Chapter 1: Introduction

1.1. Background

Structures have greatly evolved over the course of history. Human shelters were first constructed using meager materials such as tree branches and twigs for shelter purposes against predators and climate. As the human population started to increase and civilizations were established, structures greatly grew in complexity and durability to meet their increased demands such as food storage structures or places to house their ceremonies. The evolution of building construction is marked by several advancements. One of the major advancements was in construction materials. Building materials gradually evolved from perishable to durable structures that have lasted for thousands of years. Nowadays, materials are synthesized solely for the purpose of restoration. Structure restoration, repair and strengthening have become an integral part of today's construction industry, whether it is for restoring historical structures, repairing damages caused by fires, fixing construction or design errors, strengthening structures due to changes in building usages or exposure to severe environmental conditions that cause deterioration.

Many techniques were developed to strengthen an existing structure or even to repair it. Some of these methods were section enlargements, external post-tensioning, bonding steel plates to concrete structures, steel jacketing and the use of fiber reinforced polymers (FRP). The use of Fiber-Reinforced Polymer (FRP) was first utilized in the aerospace and naval applications, which dates back to the early 1940s. The use of FRP in civil engineering applications for strengthening of existing structures was first developed in Japan during the early 1980s as an alternative to the use of steel plates due to the many added advantages, such as: larger contact area, lack of corrosion, flexibility in construction, and design and greater ease of installation [1, 2]. FRP was originally utilized to strengthen structural elements in order to improve shear capacity and ductility within the member [2]. As FRP started to gain popularity, researchers have conducted many studies over the course of the past two decades, which addressed the use of externally bonded fiber reinforced polymer (FRP) composites to reinforce concrete (RC) elements in the form of plates, sheets and near-surface-mounted (NSM) bars to improve their flexural and shear capacity [3].

Glass (GFRP), aramid (AFRP), and carbon fibers (CFRP) are common reinforcements used with FRP systems, which give the FRP system its strength and stiffness. Each type of fiber has its own physical and mechanical properties [4]. The tensile strength and stiffness of an FRP material are dependent on several factors, such as: type of fiber, orientation of fibers, quantity of fibers, and method and conditions in which the composite is produced. Choosing an appropriate type of FRP system depends on environmental, loading and durability considerations [4]. Under different harsh environmental conditions such as alkalinity, salt water, chemicals, ultraviolet light, high temperatures, high humidity and freezing-and-thawing cycles, the mechanical properties, like the tensile strength, ultimate tensile strain, and elastic modulus, of FRP systems change and the FRP system's durability is greatly affected. For example, areas with high alkalinity and high humidity favor the selection of carbon-fiber systems over glass-fiber systems. Moreover, in areas where the weather can be extremely hot or cold, carbon fibers have a coefficient of thermal expansion that is nearly zero whereas the glass fibers have a coefficient of thermal expansion similar to that of concrete. The ACI 440.2R-08 presents Table 1 in order to accommodate these environmental factors:

Table 1: Environmental Reduction Factors [5]

Exposure Condition	Fiber Type	Environmental Reduction Factor C_E
Interior Exposure	Carbon	0.95
	Glass	0.75
	Aramid	0.85
Exterior Exposure (bridges, piers, and unenclosed parking garages)	Carbon	0.85
	Glass	0.65
	Aramid	0.75
Aggressive environment (chemical plants and wastewater treatment plants)	Carbon	0.85
	Glass	0.50
	Aramid	0.70

As for the loading considerations, impact tolerance, creep-rupture and fatigue are important factors to consider in the design process. It is shown that designing for high impact tolerance, AFRP and GFRP systems exhibit better tolerance to impact than CFRP systems. As for the creep-rupture and fatigue conditions, CFRP systems

are highly resistant to creep-rupture under sustained loading and fatigue failure under cyclic loading, whereas GFRP systems do not exhibit such tolerance [4].

The common method of flexural strengthening of RC beams is made by externally bonding FRP plates or sheets to the bottom tensile surface (soffit) of the beams. This research will address the beam flexural benefits of using side-bonded CFRP sheets as opposed to the soffit-bonded CFRP sheets on RC beams. The beams used in the study are classified into three different groups in order to assess how different reinforcement ratios affect the side bonded and soffit bonded beams, which will allow for direct comparison in performance between the side bonded and soffit bonded beams. This research is solely aimed to target restrictions faced in the practical field. Many times engineers are faced with constrictions that will deem the beams' soffits inaccessible. This is when understanding the behavior of CFRP side bonded sheets becomes vital.

1.2. Research Significance

Aging infrastructures are growing in number around the world. A persistent question for these aging owners and governments is always posed, "Do we need to reconstruct or repair aging infrastructures?" To answer this question, one needs to consider the benefits of having a proactive approach when faced with issues in their structures. Being proactive, the life cycle costs of a structure can be greatly optimized; hence time and money will be saved and better exploited elsewhere.

CFRP laminates are being increasingly utilized within the construction industry. It has a very high tolerance to creep and fatigue conditions and is considered to be highly resistant under sustained and cyclic loading. Moreover, CFRP can aid in accounting for loading increases, seismic strengthening, accounting for the damage to structural parts, accounting for changes in the structural system and accounting for design or construction defects. This will be further elaborated in the Literature Review section of this research.

This study's aim is focused on using side-bonded CFRP laminates to enhance the flexural capacity of reinforced concrete beams as opposed to the commonly used soffit-bonding method. The behavior, benefits and the percentage of strength gain of using side-bonded are scarcely researched and still remain a vague concept to most practicing Engineers. Using side-bonded CFRP on RC beams can help solve many

problems faced on the field, such as strengthening Double-T beams, where the soffit of the RC beams is not accessible.

1.3. Research Objectives

This study aims to understand the behavior of bonding CFRP laminates to the side of the reinforced concrete beams in order to enhance the beam's flexural capacity. A total of 25 beams will be cast and tested in four-point bending. The specimen will be strengthened with side bonded CFRP laminates. The results will be compared with other beam specimens strengthened with the common method of soffit bonding.

The main objectives of this study are as follows:

1. Investigate the performance of RC beams externally strengthened in flexure with side-bonded CFRP composite sheets.
2. Compare the load-deflection response, strength and ductility of the specimens strengthened with side-bonded CFRP to that with regular soffit-bonded beams.
3. Investigate the effect of the amount of side-bonded reinforcement on the strength and ductility of the strengthened specimens.
4. Evaluate the effect of the amount of flexural reinforcement on the performance of the strengthened specimens.
5. Predict the flexural capacity of the tested specimens using the ACI 440.2R-08 design guidelines.
6. Develop analytical load-deflection curves using ACI 440.2R-08 flexibility model to validate the experimental results.

1.4. Thesis Organization

Chapter 1 gives an introduction to the thesis topic in general, and explains the significance of the research idea and methodology. Furthermore, the detailed objectives of the study are discussed. Chapter 2 presents the literature review; several papers have been summarized in relation to FRP composites and FRP flexural strengthening. Chapter 3 explains the experimental program developed in the study. Testing matrix, section details, testing setup, tested materials properties have been discussed in this chapter. The results of the experimental program are presented in Chapter 4. The results chapter discusses the load-deflection and strains curves, along with all the experimental observations and data. Moreover, chapter 5 has detailed

technical discussions for the results with different comparisons for each group of specimens. Chapter 6 is the last technical part of the thesis that validates the experimental results; this chapter has utilized ACI440-08.2R code to develop analytical load-deflection curves comparing them to the actual data. In addition, ultimate flexural loads for the specimens were calculated and compared to the data found in the testing program. Finally, chapter 7 concludes the overall topic, the results and the technical outcomes.

Chapter 2: Literature Review

2.1   General Overview

Repairing and retrofitting infrastructure have become a vital activity for governments and private property owners that are continuously seeking more economical solutions to maintain their infrastructure or even change its use all together. The age of demolition has long passed, and most governments are now greatly investing in research which aims to find more apt solutions to repair existing structures while maintaining their operation during their repair. Many repair systems have emerged, such as external post-tensioning and steel plates, which date back to the late 60's, have been used extensively ever since [6]. Even though these methods have their advantages, their outweighing disadvantages, such as transportation, corrosion and constructability, pushed researchers to find alternative solutions such as FRP [6]. Despite the high cost of the FRP material, there are many added benefits such as [4], [6]:

- High stiffness
- High tensile strength
- Low Weight
- High chemical resistance
- High temperature tolerance
- Low thermal expansion
- Constructability
- Lower manpower required for assembly
- Lower maintenance costs

This makes FRP a popular choice amongst practitioners nowadays when seeking a strengthening solution [5, 7]. FRP is mainly used to [8]:

- Account for loading increases in:
    - Live loads capacities of floor systems.
    - Live load capacities of parking garages.
    - Shear and flexural strengths of reinforced and prestressed beams.
    - Axial capacity of columns.
    - Live load capacities of parking garages.

- Seismic strengthening:
    - Column confinement for ductility improvement.
    - Concrete shear walls strengthening.
- Account for the damage to structural parts:
    - Strength deficiency due to deterioration and corrosion.
    - Restore strength of structural elements damaged by fire.
- Account for changes in structural systems:
    - Load redistribution due to removal of some structural elements.
    - New openings in slabs.
- Account for design or construction defects:
    - Deficient amount of shear or flexural reinforcement.
    - Deficient size and/or layout of reinforcement.
    - Low compressive strength of the used concrete.

The three most commonly used fibers are glass, aramid and carbon. Figure 1 depicts the stress-strain diagrams of the different FRP types versus that of steel [4]:
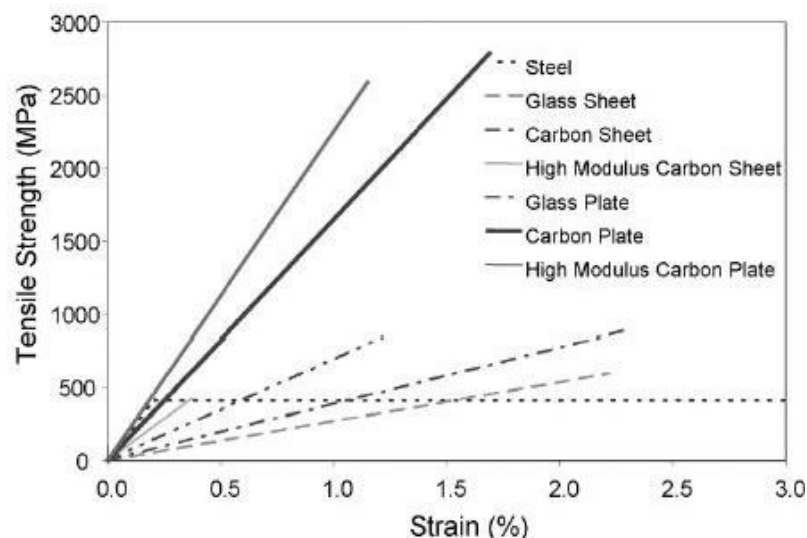
Figure 1: Stress-strain curves for different types of FRP [4]

Currently, codes and standards for designing, detailing and placing of externally bonded FRP systems are being developed in Europe, Japan, Canada and the U.S. Over the past 20 years, Japan has greatly contributed in the publication of several documents related to the use of FRP materials in concrete structures. Canadians too, have published a code named ISIS Manual number 3 that discusses Fiber Reinforced

Structures [9]. The U.S currently uses the ACI 440.2R-08 which is completely dedicated to the design and construction of FRP strengthened systems [5].

2.2   Glass Fiber Reinforced Polymer (GFRP) for Flexure Strengthening

GFRP, simply put, is long continuous interwoven fibers of glass. There are many types of glass that may be used to reinforce the FRP depending on the specific usage requirement. GFRP sheets typically tend to have a tensile strength of 2300 MPa, tensile elastic modulus of 76,000 MPa and an elongation of 2.8% [10]. Compared to CFRP, GFRP has a lower elastic modulus and tensile strength than the CFRP. However, many practitioners opt for GFRP due to its deforming ability, its high impact and break resistance, and lower cost compared to CFRP [11]. The graph in Figure 2 compares the stress-strain diagrams of GFRP with CFRP and steel [11]:
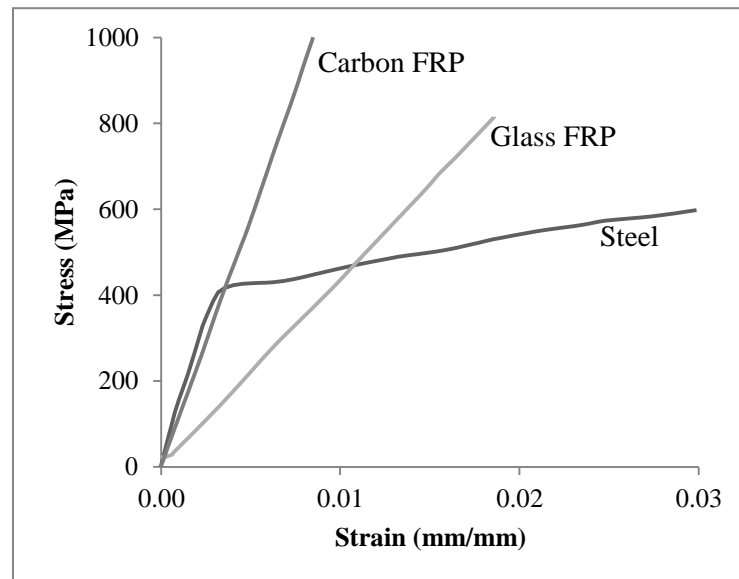
Figure 2: Stress-strain curves for GFRP, CFRP and steel [11]

Onal [12] has studied the behavior of 6 GFRP reinforced beams. He found that the GFRP beams had almost 1.45 times increase in flexural strength compared to the 3 control beams and 53.6% reduction in displacement. Moreover, Onal stated that there was 87.5% reduction in cracks in the GFRP reinforced beams compared to that found in the control beams.

Chiew [13] subjected 10 GFRP strengthened RC beams (with varied GFRP laminate thickness) and 2 control beams to monotonic 4 point loading. It was noted that the flexural strength and stiffness of the GFRP strengthened beams increased by almost 18-46% and 24 % respectively compared to the control beams. However, the

strengthened beam's ductility was decreased. Debonding of the external GFRP laminates (in a brittle manner) was the main mode of failure amongst the strengthened beams.

Mohite [14] studied a total of 4 GFRP strengthened beams 2 control beams. Contrary to the common practice of placing the FRP laminates on the tension side of the beam, Mohite was trying to analyze the flexural strength and deflection of the side bonded GFRP RC beams and to compare his findings to the control and GFRP tension side bonded beams. He found that the flexural strength of the side bonded and tension bonded increased by almost 10% compared to the control beam. Moreover, he observed that the tension sided beams' deflection increased by 75% and the side bonded beams' deflection increased by 152% when compared to the control beams.

2.3 Aramid Fiber Reinforced Polymer (AFRP) Laminates for Flexure Strengthening

Another fiber component that is used quite often is the Aramid to produce the Aramid Fiber Reinforced Polymers. Aramid itself is a strong synthetic fiber that maintains its high strengths at elevated temperatures. It is used most often in aerospace and military applications, in civil engineering applications. It is even used to synthesize heat resistant armors, gears and bicycle tires [15].

AFRP sheets typically tend to have a tensile strength of 3200-3600 MPa, tensile elastic modulus of 124,000-130,000 MPa and an elongation of 2.5-2.8% [14]. The below graph in Figure 3 compares the stress strain diagrams of steel and FRP materials [16]:
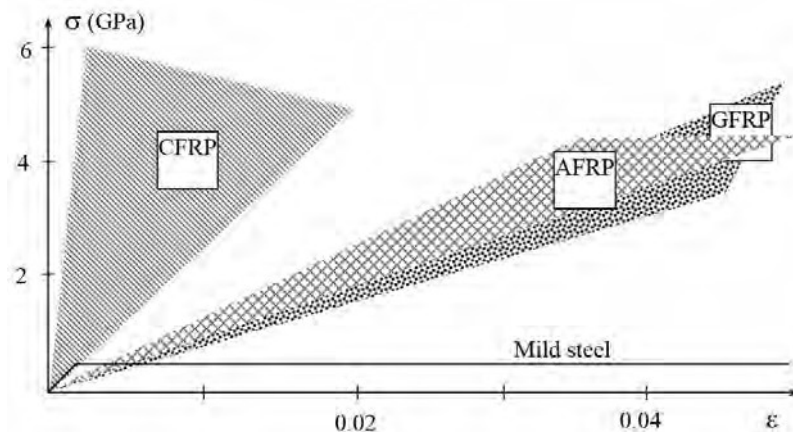
Figure 3: Stress-strain graph for different FRP composites [16]

Rashid et al. [17] tested 11 RC beams strengthened with AFRP and a control specimen. He found that the AFRP strengthened beams had a 52% increase in their moment capacity compared to the control. Rashid also observed that before the cracking, the AFRP beams had a comparable stiffness to the control beams, however, after initial cracking the AFRP beams witnessed drastic reduction in stiffness. Moreover, after the cracking commenced, the AFRP strengthened beams had higher deflections and larger crack widths than the controls.

Murali et al. [15] compiled 12 previous research papers that tested CFRP and AFRP strengthened beams and compared their findings to control beams. A total of 83 beams, with varying thicknesses of FRP laminates, were analyzed by Murali and it was found that the AFRP ultimate moments were almost 10% lower than that of CFRP. Both CFRP and AFRP beams predominant mode of failure was debonding. Also, Murali mentioned that the first cracking moment and deflections for the AFRP beams were lower than that of CFRP. Moreover, both AFRP and CFRP strengthened beams ultimate moment capacities were not extremely affected when exposed to wet/dry cycles using salt water.

More et al. [18] tested a total of 21 RC beams strengthened with AFRP to study the flexural capacities and effect of damage. Moreover, More was interested to study the effect of increasing the number of layers of AFRP laminates on the RC beams. He observed that all the strengthened beams exhibited limited deformation and cracking before the steel yielding. Moreover, the ultimate moment capacity of the strengthened beams seemed to increase as the number of layers increased, where the ultimate capacity of the beams strengthened with a single layer of GFRP increased by 27.59% and 48.27% for 2 layers.

2.4   Carbon Fiber Reinforced Polymer (CFRP) Laminates for Flexure Strengthening

Carbon fibers are simply fibers that are 5-10 μm in diameter made up of carbon atoms, which is what allows the fibers to have a high strength to weight ratio. CFRP sheets typically tend to have a tensile strength of 4830 MPa tensile elastic modulus of 227,500 MPa and an elongation of 2.1% [19].

CFRP had proven from past extensive research to provide increase in the flexural strength of the RC beams. Bonacci and Maalej [8] collected data from 23

different case studies, amounting to 127 beams, which studied the performance of RC beams strengthened in flexure with externally bonded FRP reinforcement. It was concluded that FRP debonding failure was prevalent among most test specimens. It was observed that almost a third of the specimens with externally bonded FRP showed strength increases of 50% or more in combination with considerable deflection capacity.

Hutchinson and Rahimi [20] tested the structural behavior of 2.3-m concrete beams with bonded external CFRP plates. It was observed that the externally bonded reinforced beams witnessed a 230% increase in their load-carrying capacity. However, it was concluded that the magnitude of performance was dependent on the flexural and shear steel reinforcement in the beams, and on the type and amount of externally bonded CFRP reinforcement. It was also observed that debonding limited the amount of gain in flexural capacity of the beams.

Lu and Ayoub [21] studied a large number of beam specimens in order to specifically focus on the causes of debonding failure of RC beams strengthened with FRP laminates. It was concluded that the reduction in tensile strength was due to several factors: (1) bond strength between FRP and concrete interface; (2) concrete strength; (3) thickness of FRP; (4) elastic modulus of FRP; (5) width of FRP laminate; and (6) development length of the FRP sheets.

Kotynia et al. [22] conducted a nonlinear numerical analysis using a displacement controlled 3D finite-element model in order to investigate the flexural and debonding behavior of the strengthened RC beams. In addition, a total of 10, 4.2 m long, RC beams that were strengthened in flexure using different CFRP arrangements were tested. It was observed that all the tested specimens failed by developing an intermediate crack, which eventually caused debonding of the bottom CFRP reinforcement. It was also concluded that the width of the flexural CFRP laminates greatly affected the debonding mechanism. In the case of the narrow laminates, the debonding occurred within the concrete cover, as opposed to the wide laminates, where the debonding observed along the steel reinforcement. Moreover the finite element analysis was able to accurately predict the mode of failure of all the tested specimens.

Ashour et al. [23] tested 16 CFRP strengthened RC beams and studied the effect of the amount of steel reinforcement and the arrangement of the CFRP sheets on the beam's performance. Three failure modes of beams with external CFRP laminates were observed: (1) laminate rupture; (2) laminate separation; and (3) peeling failure of the concrete cover attached to the laminate (dominant failure mode). It was also noticed that the ductility of all strengthened beams was reduced compared with that of the unstrengthened control beam. It was also observed that the externally bonded simply supported beams achieved greater performance than the continuous beams.

Most published papers discussed soffit externally bonded CFRP beams. In the practical world, installing CFRP on the soffit of the RC beams is not always possible. To overcome this obstacle, RC beams could be strengthened with side-bonded CFRP laminates, which is the subject of this research. Li [24] investigated the flexural performance of 8 RC cantilever beams strengthened by side-bonded CFRP sheet and a control beam. He reported that side-bonded CFRP laminates can affect crack width and crack pattern of the strengthened beams. Side-bonding the CFRP sheets extended the pre-crack stage of the RC beam immensely. This means that the first crack loads of CFRP side bonded RC beams are much higher than that of soffit bonded RC beams. However, Li stated that the yield and ultimate loads of the CFRP side bonded RC beams are generally the same as that of the CFRP soffit-bonded RC beams.

Hosen [25] analyzed the flexural behavior of 6 RC beams strengthened with different ratios of Side Near Surface Mounted (SNSM) reinforcement (3 steel and 3 CFRP) and a control beam tested under four-point loading until failure. He found that the yield and ultimate load carrying capacities of the beams strengthened by the CFRP SNSM increased by 2 and 2.38 times than that of the control beam and by 1.3 times than those beams strengthened with the steel SNSM. The cracking loads for the SNSM strengthened beams increased by 3.17 times and the crack width decreased compared to the control beam. Moreover, the CFRP SNSM beams had less crack widths than the steel SNSM beams. As for the deflection, the beams strengthened by the CFRP SNSM yielded the least deflection under loading. In addition, the experimental results were accurately predicted by analytical models.

This study focuses on testing the flexural capacity of RC simply-supported beams using externally side-bonded CFRP sheets. This topic was specifically chosen to further understand the increase in the flexural capacity of RC beams strengthened with side-bonded CFRP sheets as opposed to that of soffit-bonded CFRP sheets. If a strength gain is actually observed, side-bonded sheets will overcome many difficulties faced practically with soffit bonded CFRP sheets. Double-T beams and inaccessible soffits of beams are examples as to why side-bonded CFRP sheets are of crucial importance to the construction industry.

Chapter 3: Experimental Program

The aim of this experimental program is to investigate the flexural capacity of RC beams externally strengthened by the use of side-bonded CFRP sheets. Twenty-five RC beams with varying flexural steel reinforcement ratio, ρ (%) were cast and strengthened with different CFRP alignments (soffit and side-bonded).

3.1. Test Specimens & Matrix

The 25 RC beam specimens were 150 mm wide, 300 mm deep, and 2000 mm long. A 25 mm cover was maintained across the specimens. Two 8 mm in diameter bars were used as top reinforcement and 10 mm diameter bars were used as shear reinforcement at 100 mm spacing. The average concrete strength (f'_c) and steel yield strength (f_y) were 47.2 and 550 MPa, respectively. The main reinforcement of the beams, orientation of the CFRP sheet and layers of CFRP were varied across the specimens. Table 2 displays the beam specimens, designations and cross-section detailing classifications that were used during the experimental program.

The beam specimens were designed according to the ACI318-14 [26] design guidelines, for f'_c = 47.2 MPa, and f_y = 550 MPa, balanced reinforcement ratio (ρ_b) = 2.71%, and minimum reinforcement ratio (ρ_{min}) = 0.312% [26]. A general elevation of the test specimens can be seen in Figure 4:
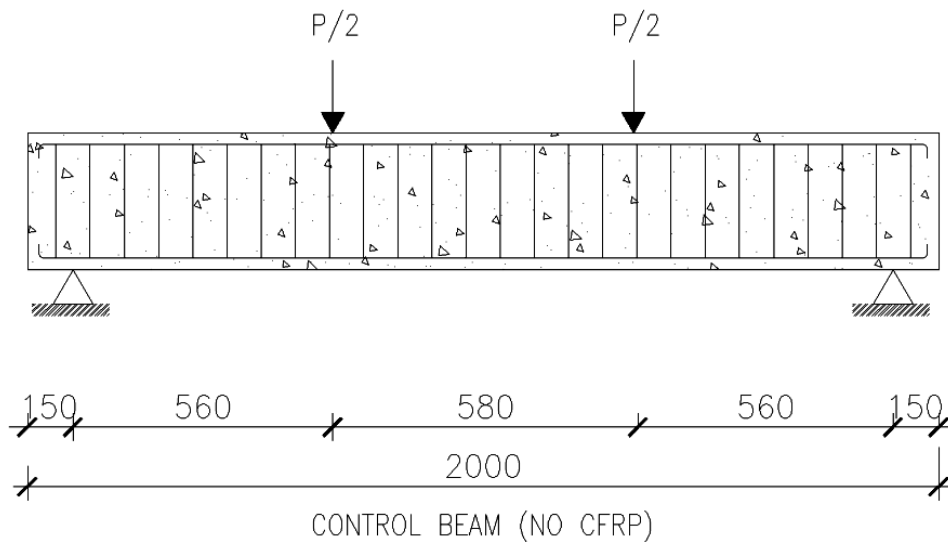
Figure 4: General elevation of the beam specimens

Table 2: Testing matrix according to the different reinforcement ratios
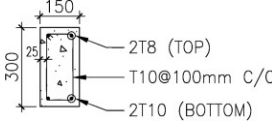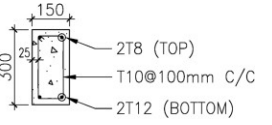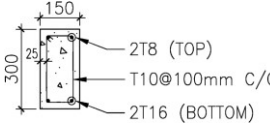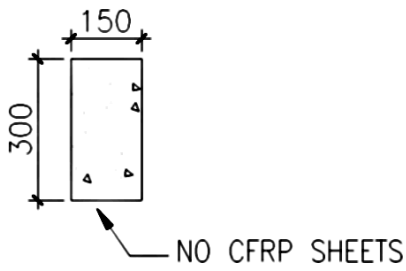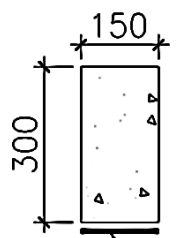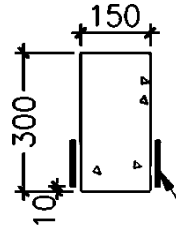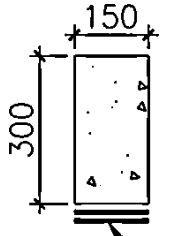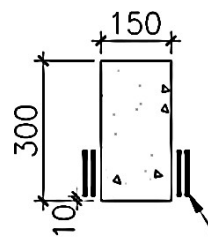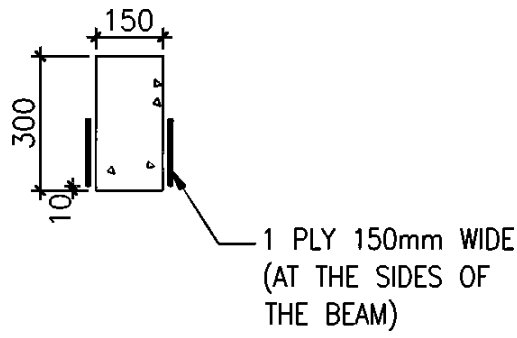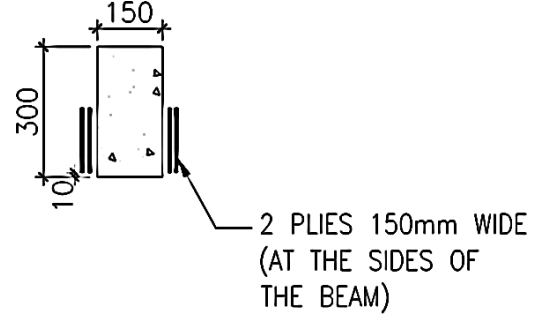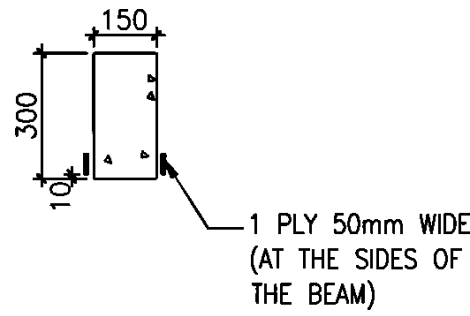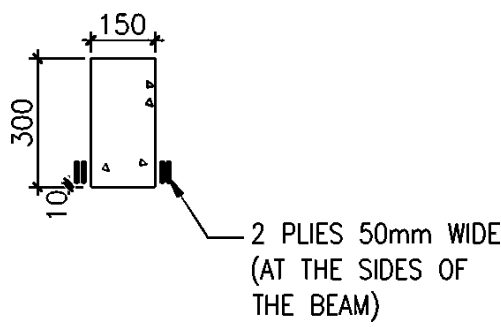
Group Designation:	Group A "GA"	Group B "GB"	Group C "GC"
Size (mm x mm)	150 x 300	150 x 300	150 x 300
ρ % (mm^2/mm^2)	0.3995 %	0.5773 %	1.035 %
ρ / ρ_b	0.1453	0.2099	0.3764
Quantity	7 x 2.0m Beams	11 x 2.0m Beams	7 x 2.0m Beams
Section Detail:			
f'_c (MPa)	47.2 MPa	47.2 MPa	47.2 MPa
f_y (MPa)	550 MPa	550 MPa	550 MPa

Table 3, shows the testing matrix. It displays the different parameters that were varied in the experimental program to aid us in a better understanding of the behavior of the beams,

Table 3: Testing matrix for different CFRP configuration

CFRP Designation	Group Designation	Quantity	Beam Detail
Control Beam, No CFRP "C"	GA-C	3	
	GB-C	3	
	GC-C	3	

Bottom Sheet, Single Ply "BS"	GA-BS	1	150 300 1 PLY 150mm WIDE (AT THE BOTTOM OF THE BEAM)
	GB-BS	1	
	GC-BS	1	
Side-Bonded Sheets, Single Ply "SS"	GA-SS	1	150 300 10 1 PLY 100mm WIDE (AT THE SIDES OF THE BEAM)
	GB-SS	1	
	GC-SS	1	
Bottom Sheet, Double Plies "BD"	GA-BD	1	150 300 2 PLIES 150mm WIDE (AT THE BOTTOM OF THE BEAM)
	GB-BD	1	
	GC-BD	1	
Side-Bonded Sheets, Double Plies "SD"	GA-SD	1	150 300 10 2 PLIES 100mm WIDE (AT THE SIDES OF THE BEAM)
	GB-SD	1	
	GC-SD	1	

31

Side-Bonded Sheets, Single Ply "SS2"	GB-SS2	1	150 / 300 / 10 / 1 PLY 150mm WIDE (AT THE SIDES OF THE BEAM)
Side-Bonded Sheets, Double Plies "SD2"	GB-SD2	1	150 / 300 / 10 / 2 PLIES 150mm WIDE (AT THE SIDES OF THE BEAM)
Side-Bonded Sheets, Single Ply "SS3"	GB-SS3	1	150 / 300 / 10 / 1 PLY 50mm WIDE (AT THE SIDES OF THE BEAM)
Side-Bonded Sheets, Double Plies "SS3"	GB-SD3	1	150 / 300 / 10 / 2 PLIES 50mm WIDE (AT THE SIDES OF THE BEAM)

The elevation of the strengthened RC beams can be seen in Figures 5 and 6:
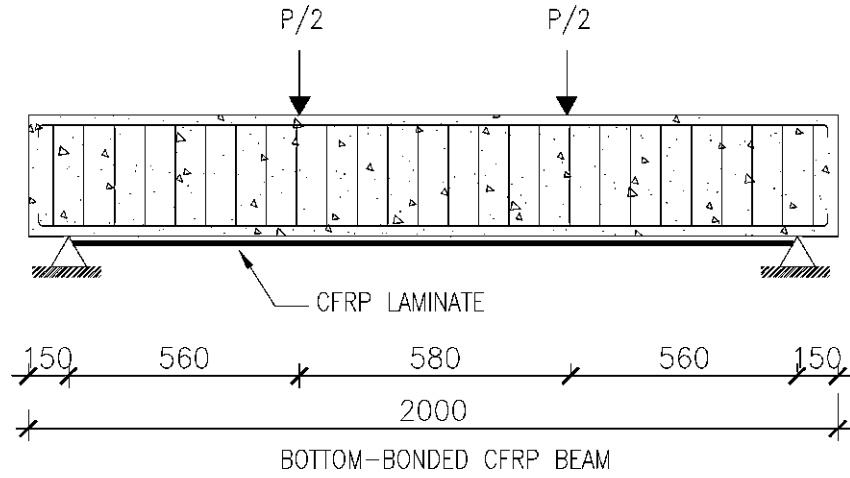
Figure 5: Elevation view for bottom-bonded strengthened specimens
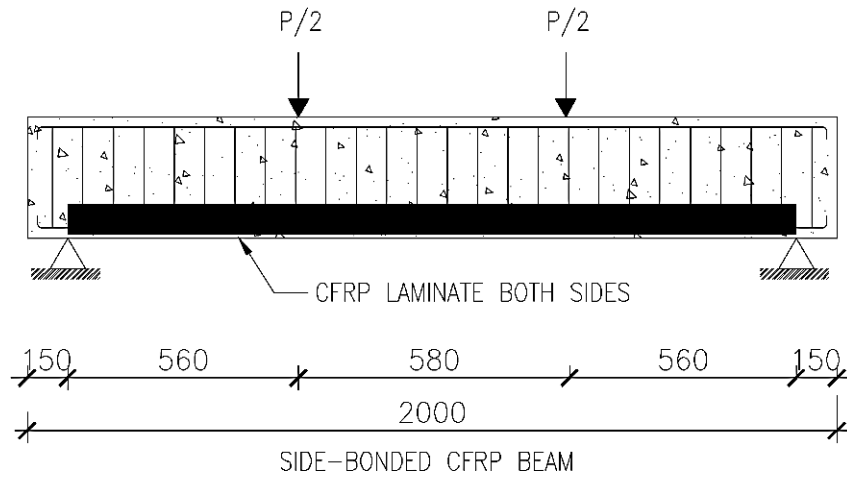
Figure 6: Elevation view for side-bonded strengthened specimens

3.2. Materials

3.2.1.   Concrete. The RC beams were cast using C50 concrete, which should have a minimum cubic compressive strength of 50MPa. The use of high-strength concrete was intended to enhance the shear capacity of the concrete as well as the tensile modulus. Those two mechanical properties of the concrete have a huge contribution in the mode of failures. The enhanced shear capacity will avoid developing flexural-shear cracks, and it will push the specimens to behave in pure flexural manner. The increased tensile modulus will reduce the possibility of the concrete cover delamination, which is a very common mode of failure for FRP. A

total of 8 cubes and 3 cylinders were cast for examining the concrete compressive strengths. The cubes were tested at 1, 3 and 28 days. The cylinders were tested on the 28 day mark only. The cylindrical and cubic compressive strengths results and averages values are respectively presented in Tables 4 and 5.

Table 4: Concrete compressive strength for the cylinders

Specimen	Cylinder 1	Cylinder 2	Cylinder 3	Average
Compressive Strength (N/mm^2)	47.1	46.4	48.2	**47.2**

Table 5: Concrete compressive strength for the cubes

Cube Ref.	Test Date	Test Age Days	Density (kg/m^3)	Load (kN)	Comp. Strength (N/mm^2)	Average (N/mm^2)
1	11-03-2015	1	2491	536	23.8	**23.3**
2	11-03-2015	1	2500	513	22.8	
3	13-03-2015	3	2523	1021	45.4	**46.1**
4	13-03-2015	3	2497	1054	46.8	
5	17-03-2015	7	2524	1195	53.1	**52.7**
6	17-03-2015	7	2526	1178	52.4	
7	07-04-2015	28	2517	1385	61.6	**61.9**
8	07-04-2015	28	2519	1400	62.2	

322. Steel rebar. The steel reinforcing bars, stirrups to be used in the beams are hot-rolled deformed bars BS4449 Grade 460 with a minimum yield and tensile strength of 460 and 550 MPa, respectively. The dimensions of the reinforcing steel are displayed in Table 6.

Table 6: Steel dimensions

Type	Table Designation	Diameter (mm)	Area (mm^2)
Longitudinal Rebar	T8,T10,T12,T16	8.000,9.525,12.000, 15.875	50.3,71,113, 200
Stirrups	T8	8.000	50.3

The uniaxial coupon tensile test was used to determine the tensile strengths of the reinforcing steel that was used (see Figure 7). Stress- strain curves of steel rebars were obtained from the test as shown in Figure 8. The tensile test results are summarized in Table 7.

Figure 7: Steel rebar tensile test
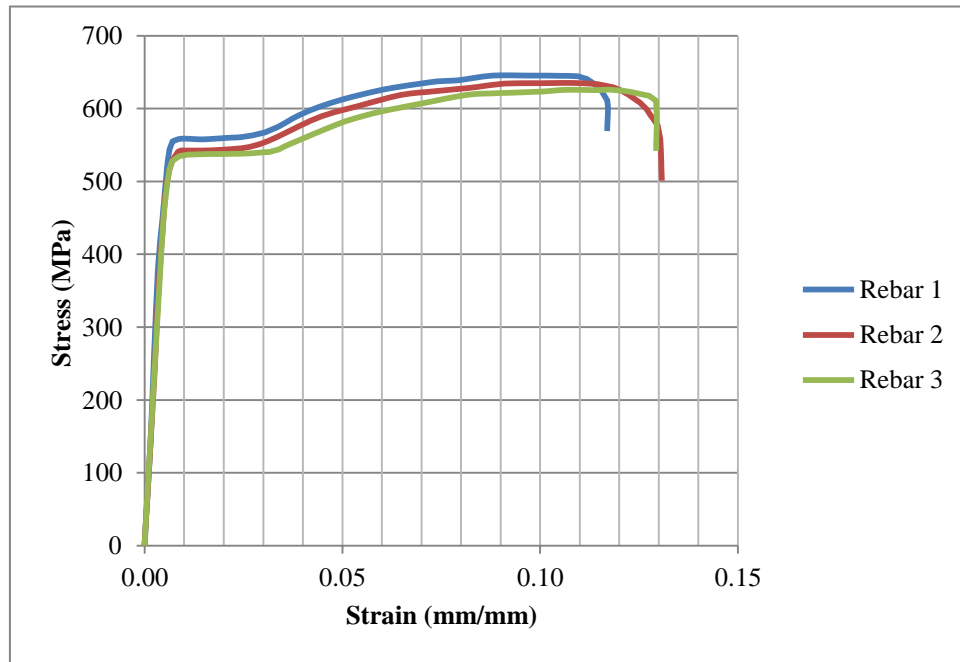
Figure 8: Stress- strain curves of tested steel rebars

Table 7: Coupon test results of steel

Specimen	Rebar 1	Rebar 2	Rebar 3	Average
Yield Strength (MPa)	558.35	548.78	547.28	**551.47**
Tensile Strength (MPa)	655.22	633.08	632.21	**640.17**
Modulus of Elasticity (GPa)	199.93	200.01	199.98	**199.97**

3.2.3. **Epoxy.** The V-wrap 700 [27] epoxy adhesive, shown in Figures 9 and 10, was used to help the CFRP bond to the prepared concrete surface. V-wrap 700 is a 2-part epoxy resin; 100% solids resin that allows for high elongation to optimize the properties of the V-wrap composite system. This epoxy can only be applied in temperatures between 4°C to 38°C, and it has an average of 15 minutes setting time. The physical properties of the epoxy are shown in Table 8 [27]:

Table 8: Mechanical properties of the epoxy adhesive [27]

Mechanical Property	Value
Tensile Strength (MPa)	72.4
Tensile Modulus (GPa)	3.18
Flexural Strength (MPa)	123.4
Flexural Modulus (MPa)	3120
Elongation (%)	5
Tg (Celcius)	82

Figure 9: V-wrap 700 - Epoxy resin

Figure 10: Mixing of Epoxy resin

3.2.4. **CFRP.** V-wrap C200H [19], that was used in this project, was manufactured by Structural Technologies. C200H is a unidirectional carbon fiber fabric with its fibers oriented in the zero degrees direction as shown in Figure 11. Tables 9 and 10 below display the dry and cured properties of the CFRP sheets which are used in this research.

Table 9: Fiber properties (dry)

Tensile Strength (MPa)	4830
Tensile Modulus (MPa)	227,500
Elongation (%)	2.1

Table 10: Cured laminate properties

	Average Value	Design Value
Tensile Strength (MPa)	1,240	1,034
Modulus of Elasticity (GPa)	73.77	73.77
Elongation at Break (%)	1.7	1.4
Thickness (mm)	1.02	1.02
Strength per Unit Width (kN/mm)	1.26	1.05

Figure 11: CFRP sheet

After the dry fibers are saturated with the resin, 5 witness panels were prepared to undergo a tensile test. The witness panels were prepared in accordance to ASTM D3039 [28] at a length of 254 mm and a nominal thickness of 1.02 mm. The testing was completed in accordance to ASTM D3039/D3039M-14 at a displacement load rate of 2mm/min and a grip pressure of 19.3 MPa. Figures 12 and 13 show a sample of the witness coupon panels that was produced.

Figure 12: FRP specimens

Figure 13: CFRP samples

The test was conducted along the direction of the fiber and was loaded at a head displacement rate of 2mm/min (constant strain rate of 0.01 min^{-1}), until the ultimate failure. The test set-up is shown in Figures 14-16.
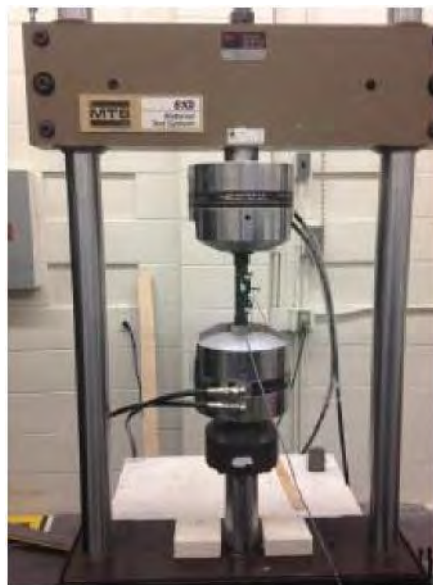
Figure 14: Schematic of the coupon test set-up

Figure 15: Coupon test set-up
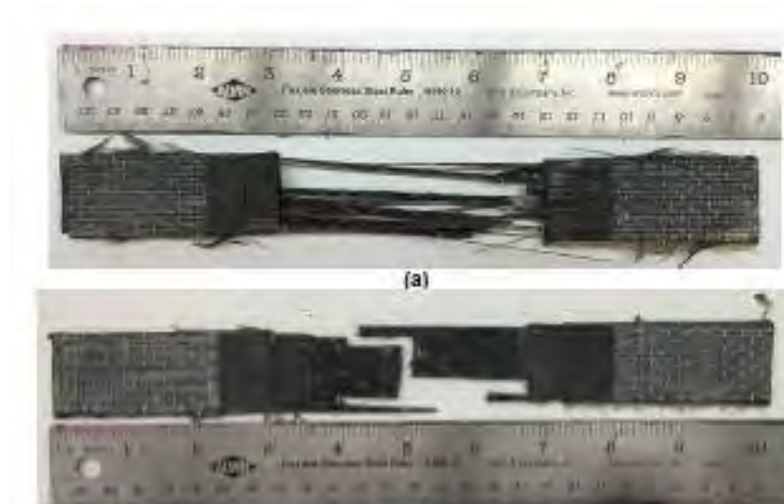
Figure 16: Tested CFRP specimen

The test report included the following for each tested sample as well as the average for all tested samples:

- o Sample thickness
- o Sample width
- o Section area
- o Tensile force at failure
- o Calculated tensile strength
- o Calculated tensile modulus
- o Tensile strain at failure
- o Mode of failure

All the mechanical properties mentioned previously are extremely important for the load-deflection analytical model. Moreover, those characteristics contribute significantly in the calculation of the cross-sections' ultimate capacity.

The results for the tested 5 witness coupon panels are provided in Table 11; the failure modes of the samples are reported in accordance to the designations mentioned by ASTM D3039. Figure 17 and Table 12 describe what each designation represents [29].

Table 11: FRP laminate coupon test results

Specimen ID	Width w	Area A	Peak load P_{max}	Strength F_{tu}	Modulus E_{chord}	Ultimate Strain ε_u	Failure Mode*
	mm	mm^2	kN	MPa	GPa	%	
TNS-W17_001	25.3	25.7	39.43	1533	66.6	2.3	AGM
TNS-W17_002	23.85	24.23	40.44	1668	70.6	2.36	LGM
TNS-W17_003	24.43	24.83	40.72	1639	69.2	2.37	AGM
TNS-W17_004	24.56	24.95	39.4	1578	75.9	2.08	AGM
TNS-W17_005	25.68	26.09	39.03	1495	72.2	2.07	AGM
AVERAGE	**24.77**	**25.16**	**39.81**	**1583**	**70.9**	**2.24**	
ST.DEV.	0.73	0.74	0.73	72	3.5	0.15	
C.O.V. (%)	2.9	2.9	1.8	4.5	4.9	6.7	
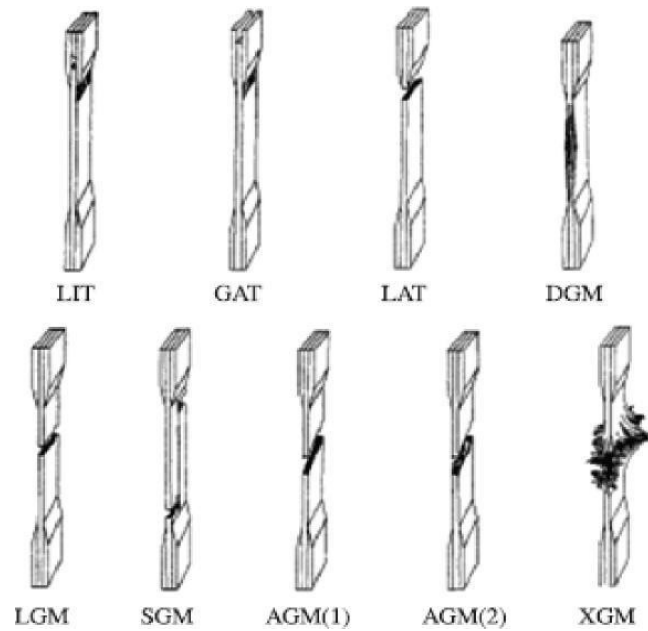
Figure 17: FRP failure modes [29]

Table 12: FRP failure modes explanation [29]

Failure Type	Code	Failure Area	Code	Failure Location	Code
Angled	A	Inside grip/tab	I	Bottom	B
Edge Delamination	D	At grip/tab	A	Top	T
Grip/tab	G	<1 W from grip/tab	W	Left	L
Lateral	L	Gage	G	Right	R
Multi-mode	M (xyz)	Multiple Areas	M	Middle	M
Long Splitting	S	Various	V	Various	V
Explosive	X	Unknown	U	Unknown	U
Other	O	-	-	-	-

3.3. Strengthening Procedure

Initially, the surface of the concrete should be prepared to ensure an open pore structure of the substrate including repair materials. The surface shall be prepared by using mechanical grinder with PCD cups. For CFRP application on beams, all the surfaces that will receive CFRP should be grinded, and then smoothened with V-wrap 700 epoxy with fume silica as putty filler. Moreover, for minor repairs such as bug holes and surface deviations, V-wrap 700 epoxy with fume silica can be used after priming the surface. Clean the prepared surface by using a standard vacuum to remove all the dust and loose particles. Surface preparation procedure is shown in Figures 18 and 19.

Figure 18: Concrete surface grinding

Figure 19: Smoothing the surface and filling all the bug holes with the patty

Afterwards, cut the CFRP sheets beforehand into prescribed lengths and widths as specified in the testing matrix. Mix resin components by using an electric

drill mixer low rpm in accordance with manufacturer's recommendations. Apply the primer coat of V-Wrap 700 epoxy to the prepared surface using a roller. Pre-saturate the appropriate length of V Wrap fabric with V Wrap epoxy. Install the CFRP sheet in the beams as per the requirement. Use a rib roller and roll in the direction of the fiber to remove all air pockets and ensure intimate contact with the surface. Then, allow the laminates to cure for three days. Attaching the CFRP procedure is shown in Figures 20 and 21.

| Figure 20: Saturating the cut CFRP sheets with the epoxy | Figure 21: Attaching the CFRP sheet on the prepared surface |

3.4. Instrumentation and Beam Test Set-up

The 25 RC beams were tested under two-point loading (four-point bending) until failure. INSTRON Universal Testing Machine (UTM), with a hydraulic actuator and a maximum capacity of 2500 kN, was used to apply monotonic load and simulate static loading condition. The beam specimens were also instrumented with strain gauges along a section taken at the mid-span of the specimens to measure the strain in the concrete at the top compressive surface, steel bars, and CFRP sheets, respectively, along the longitudinal axis of the beam specimens. Flexural tests were displacement controlled with a rate of 2 mm/min applied on the mid-span of the RC beam specimens. Figures 22 and 23 illustrate the four-point bending test set-up.
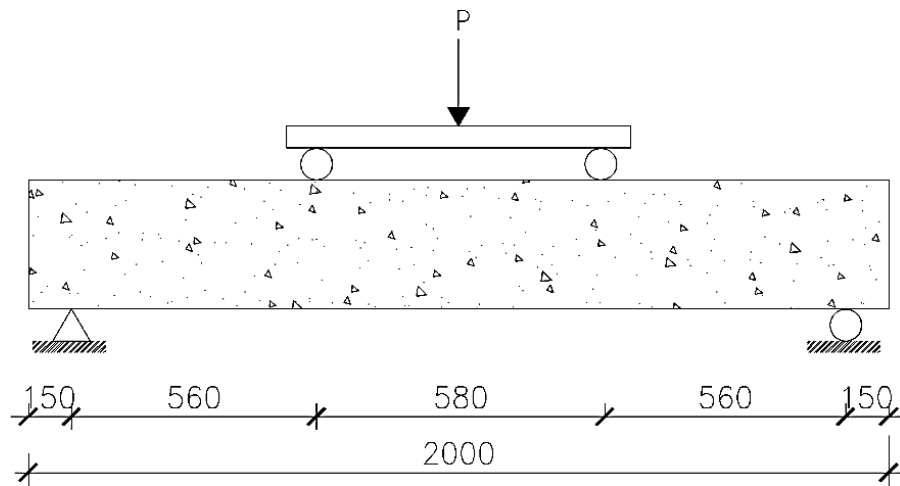
Figure 22: Schematic of flexural test set-up (mm)

Figure 23: Flexural test set-up

Chapter 4: Experimental Results and Discussions

This chapter includes testing results of the beams strengthened with soffit and side-bonded CFRP sheets with the fibers oriented parallel to the beam's longitudinal axis. The beams have been tested using two-point loading and both the applied force and mid-span deflection of the beam specimens were recorded. The results section shown below includes the obtained ultimate load-carrying capacity, the corresponding deflection at ultimate load, deflection at yield and the deflection at failure. In addition, strain graphs of the data recorded from the strain gauges (concrete, steel and FRP) are illustrated for each beam. Moreover, photos of the crushed beams are also provided to elaborate the different modes of failure.

The tested beams strengthened with bottom CFRP strengthening and side CFRP strengthening are compared with the control specimen, and the percentage increase of load-carrying capacity is included. Moreover, a comparison between side strengthening and bottom conventional strengthening is included with the percentage difference. Furthermore, the differences in deflections at failure of the beams have been included in the discussion section of each case.

The discussion section includes combined curves of load versus deflection, a comparison of load-carrying capacity, and a ductility study for each group of specimens. Finally, all the testing results and analyses have been summarized in a table at the end of this chapter.

4.1. Load versus Deflection Curves and Failure Modes

This section studies load versus mid-span deflection curves for all the tested specimens. The ultimate load at is recorded and denoted as (P_u), the corresponding deflection at ultimate load is represented with (δ_u), deflection at which the steel yields (δ_y), the failure load is assumed to be 80% of the ultimate load ($P_f = 0.8P_u$) and the corresponding deflection at failure is denoted as (δ_f). In addition, failure modes of the specimens are described and cross referenced to the figures of the crushed beams. It should be noted that the test setup and load versus deflection response curve for every tested specimen are provided in Appendix A. The strain gauges were installed at the top of the beam (concrete), top of steel bar, and at the middle of the CFRP laminate.

4.1.1   Group A:

4.1.1.1   Control beam (GA-C). The control specimen load versus strain curves of concrete and steel are shown in Figure 24. The control beam was cast with 2T10 main bottom reinforcement to compare the behavior of low reinforcement ratios with the behavior of conventionally strengthened and side strengthened members. The beam's ultimate load (P_u) is 97.3 kN with a corresponding deflection (δ_u) of 19.6 mm. The deflection at which the steel yielded (δ_y) was 6.2 mm and the failure deflection (δ_f) was 24.0 mm. The failure mode of the beam was the typical under-reinforced member behavior; steel yields then the concrete crushes as the neutral axis shifts up in the cracked section in a very ductile manner. Figure 25 shows the crush of the concrete at failure.
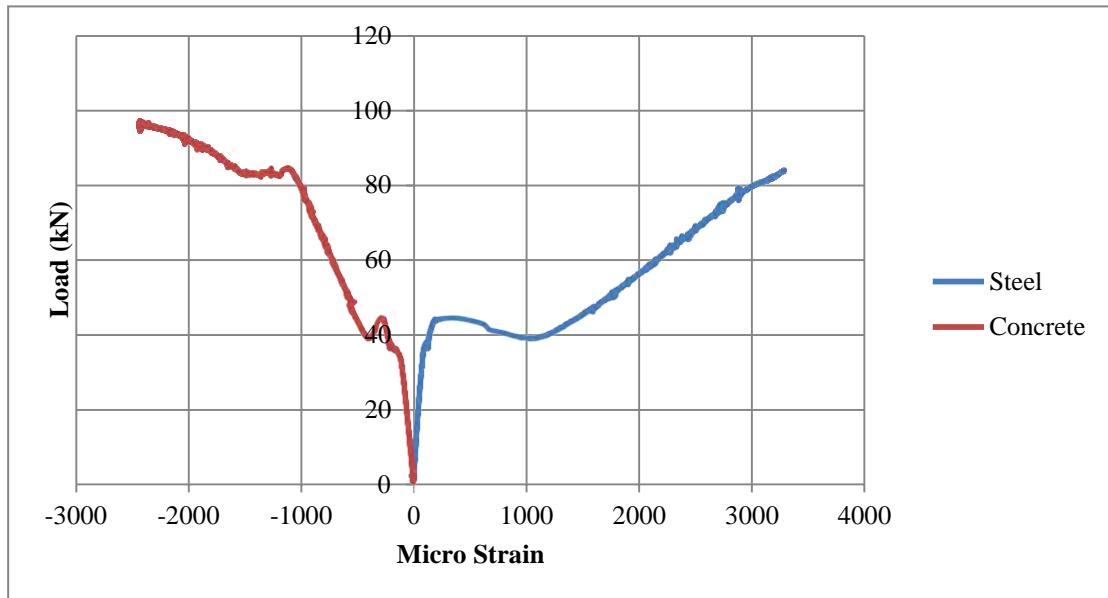
Figure 24: Load (kN) versus micro strain for beam (C)

4.1.1.2   Beam (GA-BS). Beam (BS) was strengthened conventionally for flexure (from the bottom) with one CFRP ply composite sheet. The load versus strain curves of the concrete, steel and CFRP are shown in Figure 26. Beam (BS) was cast mainly to study the relative effectiveness of side-bonded members to the bottom bonded ones. The beam sustained a maximum load (P_u) of 178.4 kN (83% increase over C beam) with a corresponding deflection (δ_u) of 19.0 mm. The deflection at which the steel yielded (δ_y) was 10.6 mm and the failure deflection (δ_f) was 19.3 mm. The failure mode of the beam was FRP debonding after steel yielding. Figure 27 shows the beam during steel yielding, and CFRP debonding at failure.

46

Figure 25: Control beam concrete crushes and beam failure
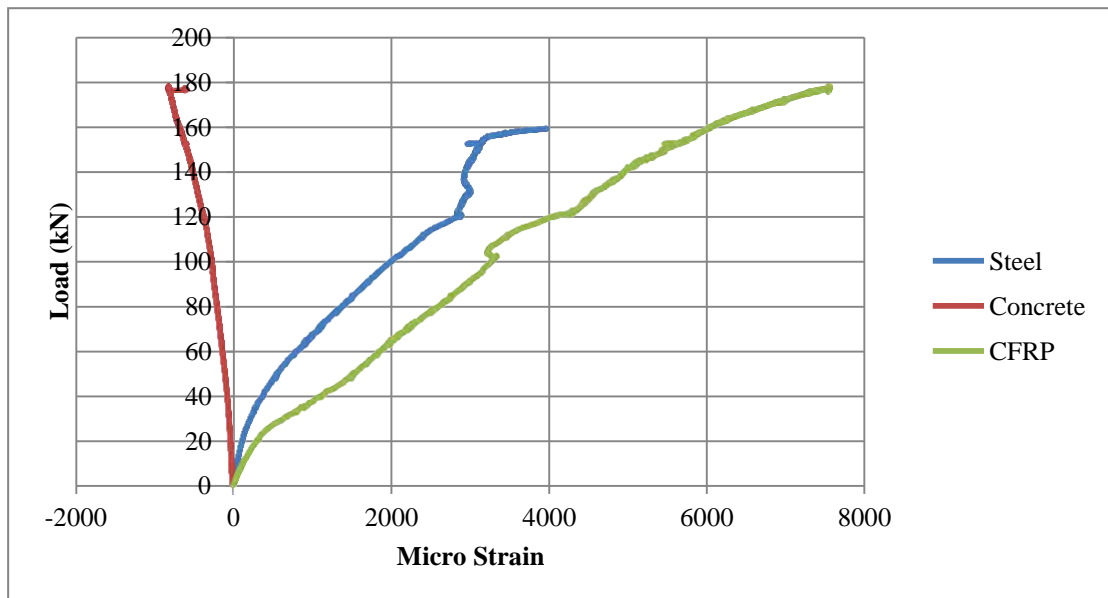
Figure 26: Load (kN) versus micro strain for beam (BS)

4.1.1.3 *Beam (GA-BD).* Beam (BD) was strengthened from the bottom with two plies of CFRP sheets. The load versus strain curves of the concrete, steel and CFRP are shown in Figure 28. Beam (BS) was cast mainly to study the relative effectiveness of double side-bonded members to the bottom bonded ones. The beam's ultimate load (P_u) was 189.8 kN (95% increase over C beam) with a corresponding deflection (δ_u) of 12.1 mm. The deflection at which the steel yielded (δ_y) was 7.1 mm and the failure deflection (δ_f) was 12.3 mm. The failure mode of the beam was steel yielding followed with FRP delamination and concrete crushing. Figure 29 shows the beam during steel yielding and concrete crushing at failure.

Figure 27: Beam (BS) failure and FRP debonding
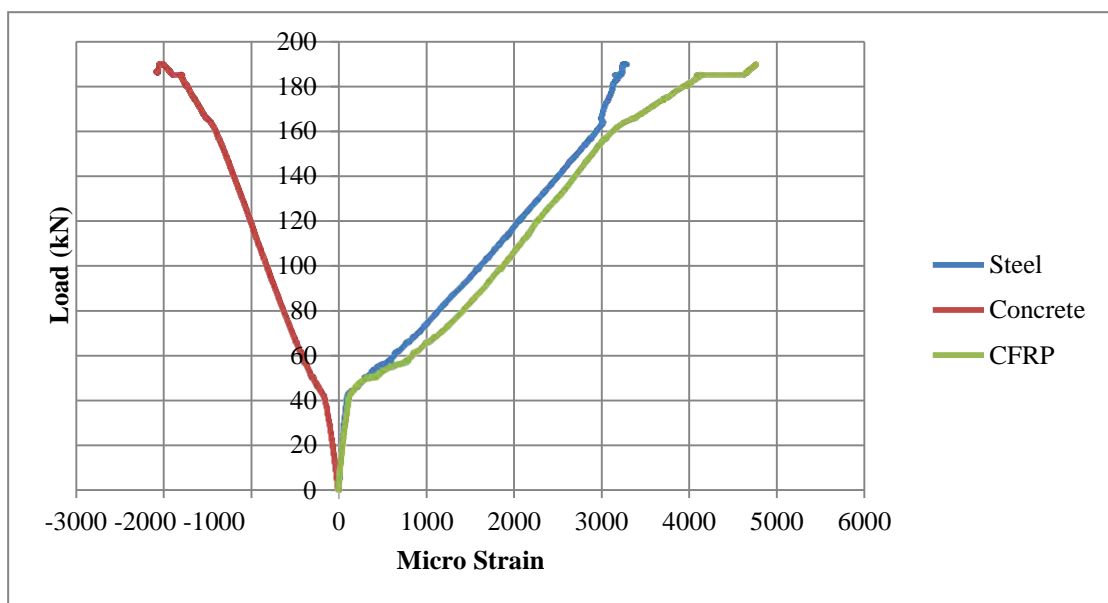
Figure 28: Load (kN) versus micro strain for beam (BD)

Figure 29: Beam (BD) complete failure

4.1.1.4 Beam (GA-SS). Beam (SS) was strengthened from both sides with one CFRP ply sheet, while having the fiber texture along the length of the beam. The load versus strain curves of the concrete, steel and CFRP are shown in Figure 30. Beam (SS) was cast to examine the performance of the side-bonded strengthening of flexural members while having a low reinforcement ratio. The beam resisted ultimately a load (P_u) of 157.9 kN (62% increase over C beam) with a corresponding deflection (δ_u) of 13.0 mm. The deflection at which the steel yielded (δ_y) was 5.6 mm and the failure deflection (δ_f) was 13.0 mm. The failure mode of the beam was yielding of the steel, debonding of the CFRP followed with concrete crushing, which is relatively a ductile mode of failure. Figure 31 shows the beam during steel yielding then the crush of the concrete at failure.

4.1.1.5 Beam (GA-SD). Beam (SD) was strengthened with two plies of CFRP sheets on each side of the beam while orienting the texture along the length of the beam. The load versus strain curves of the concrete, steel and CFRP are shown in Figures 32. Beam (SD) was cast to understand the performance of multiple plies strengthening on the sides for flexural members with low reinforcement ratio. The beam's maximum load (P_u) was 188.2 kN (93% increase over C beam) with a corresponding deflection (δ_u) of 12.0 mm. The deflection at which the steel yielded (δ_y) was 7.5 mm and the failure deflection (δ_f) was 12.5 mm. The failure mode of the beam was yielding of the steel, debonding of the CFRP before concrete crushing, which indicates a relatively brittle failure of the section. Figure 33 shows the debonding of the CFRP sheets at failure.

4.1.2 Group B:

4.1.2.1 Control beam (GB-C). The control beam has 2T12 as the main bottom reinforcement; the load versus strain curves of the concrete and steel are shown in Figure 34. The control beam was cast mainly to compare the behavior of moderate reinforcement ratios with the behavior of conventionally strengthened members as well as side-bonded strengthened members. The beam crushed at a load (P_u) of 117.4 kN with a corresponding deflection (δ_u) of 13.9 mm. The deflection at which the steel yielded (δ_y) was 5.0 mm and the failure deflection (δ_f) was 20.1 mm. The failure mode of the beam was the typical under-reinforced member with a ductile behavior; steel yields then the concrete crushes as the neutral axis shifted up in the cracked section.

Figure 35 shows the beam during steel yielding, and then the crush of the concrete at failure.

4.1.2.2   Beam (GB-BS). Beam (BS) was strengthened conventionally for flexure (from the bottom) with one ply of CFRP sheet; the load versus strain curves of the concrete, steel and CFRP are shown in Figure 36. Beam (BS) was tested mainly to compare its performance with the behavior of side-bonded strengthened members. The beam failed at a load (P_u) of 190.2 kN (62% increase over C beam) with a corresponding deflection (δ_u) of 18.3 mm. The deflection at which the steel yielded (δ_y) was 8.0 mm and the failure deflection (δ_f) was 18.4 mm. The failure mode of the beam was the FRP debonding with a minor concrete crushing. Figure 37 shows the beam at failure.

4.1.2.3   Beam (GB-BD). Beam (BD) was strengthened from the bottom with two CFRP plies; the load versus strain curves of the concrete, steel and CFRP are shown in Figure 38. Beam (BD) was tested mainly to study the relative effectiveness of side strengthened flexural members. The beam's critical load (P_u) was 178.5 kN (92% increase over C beam) with a corresponding deflection (δ_u) of 15.3 mm. The deflection at which the steel yielded (δ_y) was 8.7 mm and the failure deflection (δ_f) was 15.3 mm. The failure mode of the beam has started with steel yielding followed the CFRP debonding without concrete crushing. Figure 39 shows the beam at failure.
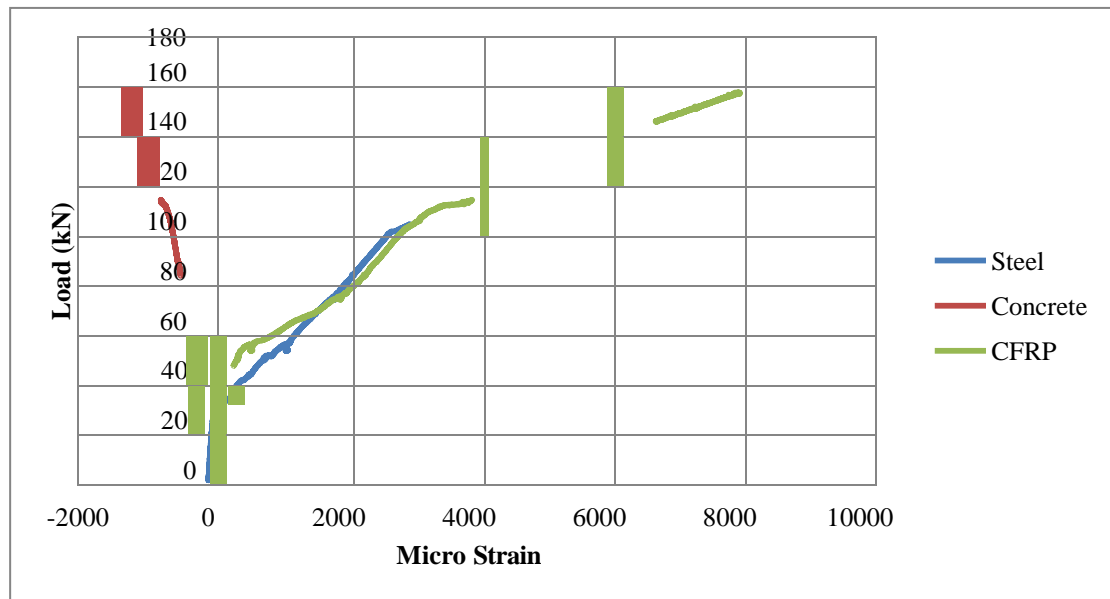
Figure 30: Load (kN) versus micro strain for beam (SS)
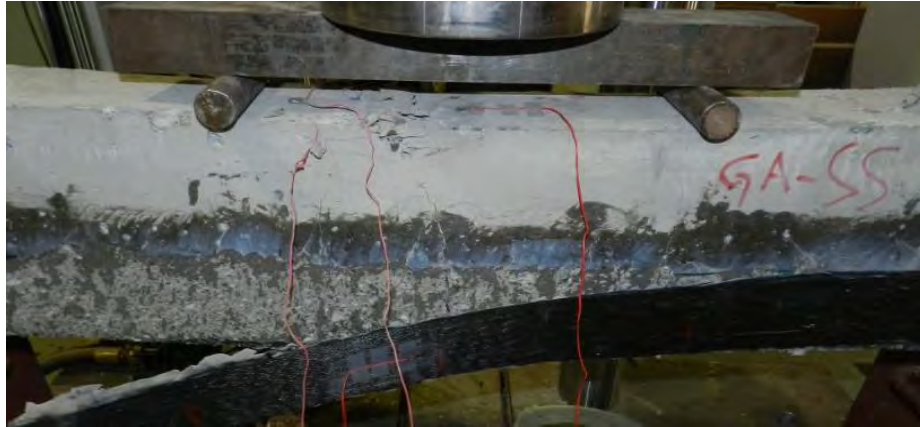
Figure 31: Beam (SS) final failure
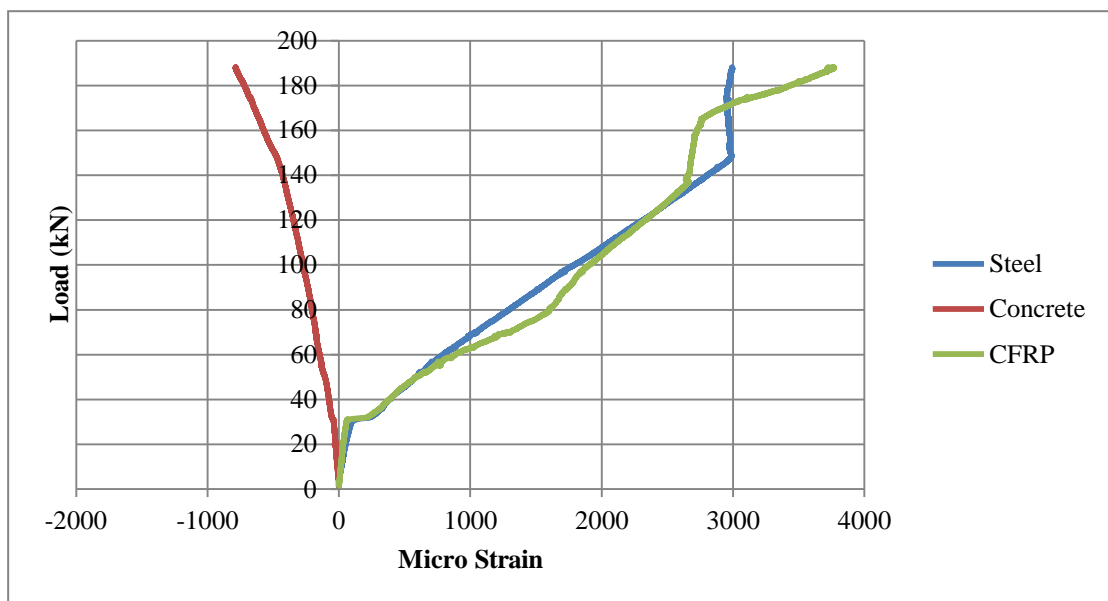
Figure 32: Load (kN) versus micro strain for beam (SD)

Figure 33: Beam (SD) final failure
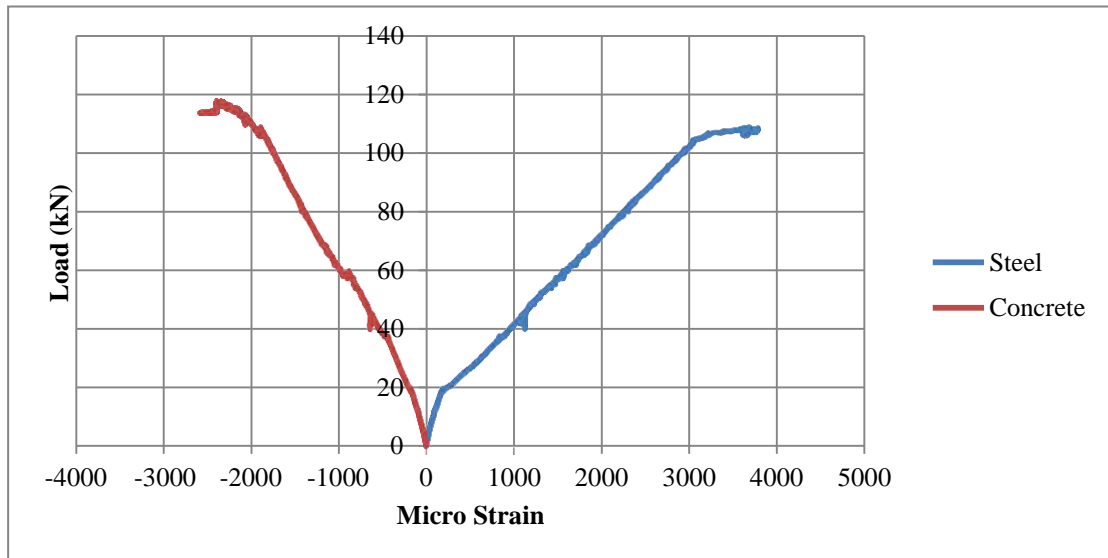
Figure 34: Load (kN) versus micro strain for beam (C)

Figure 35: Control beam at failure
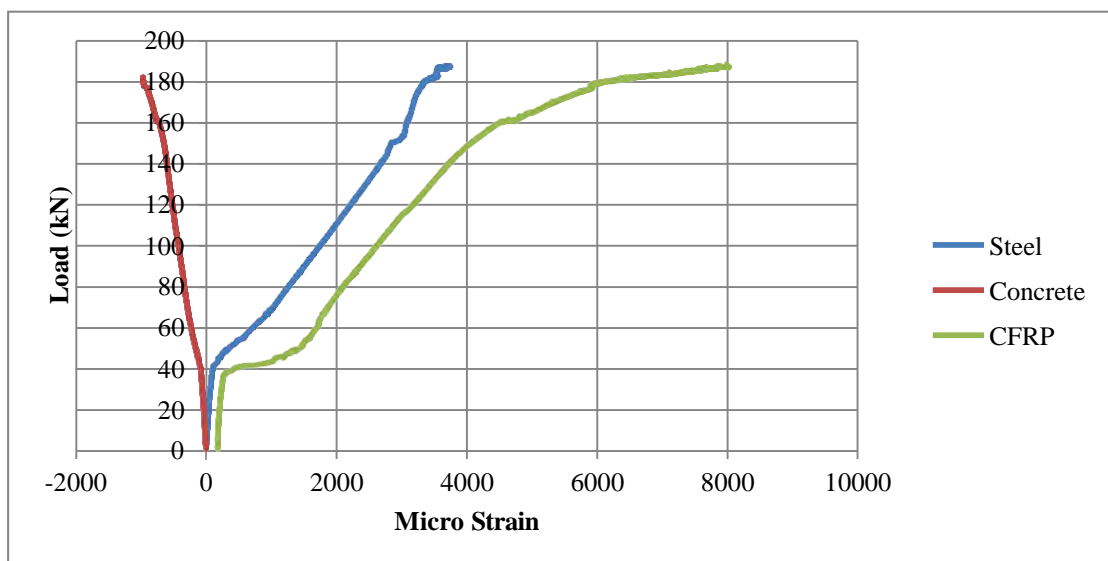
Figure 36: Load (kN) versus micro strain for beam (BS)

Figure 37: Beam (BS) complete failure
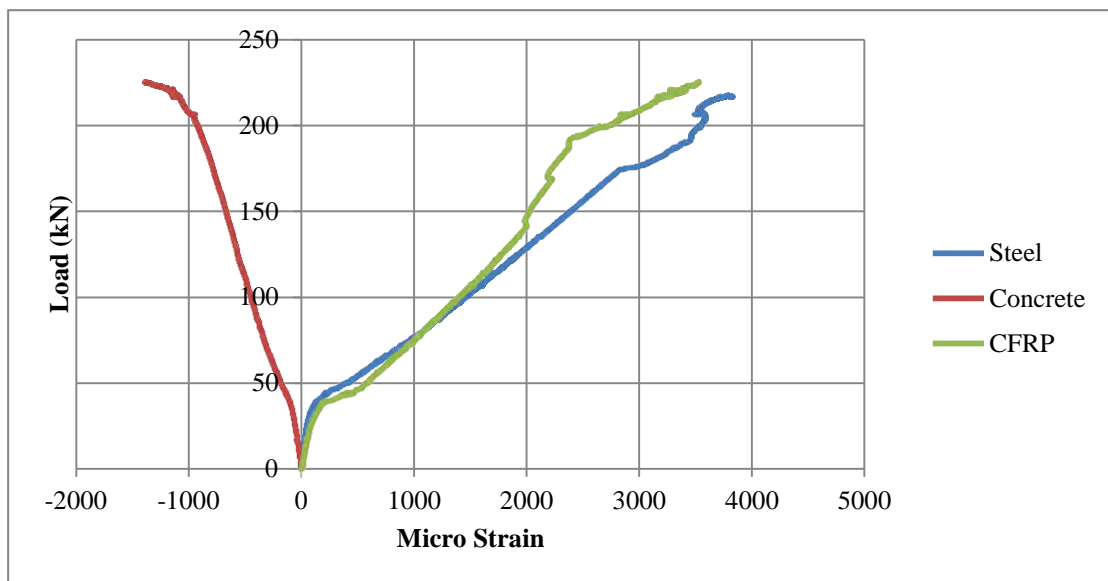
Figure 38: Load (kN) versus micro strain for beam (BD)

Figure 39: Beam (BD) final failure

4.1.2.4 ***Beam (GB-SS-1).*** Beam (SS-1) was strengthened from the sides with one CFRP ply with orienting the fibers along the length of the beam; the load versus strain curves of the concrete, steel and CFRP are shown in Figure 40. Beam (SS-1) was cast to know the performance of strengthened beam with side-bonded 100 mm CFRP sheets in flexure while having a moderate reinforcement ratio. The beam sustained a load (P_u) of 194.9 kN (66% increase over C beam) with a corresponding deflection (δ_u) of 14.7 mm. The deflection at which the steel yielded (δ_y) was 7.0 mm and the failure deflection (δ_f) was 15.2 mm. The failure mode of the beam was the crushing of the concrete prior to CFRP sheet debonding. Figure 41 shows the CFRP debonding at failure.
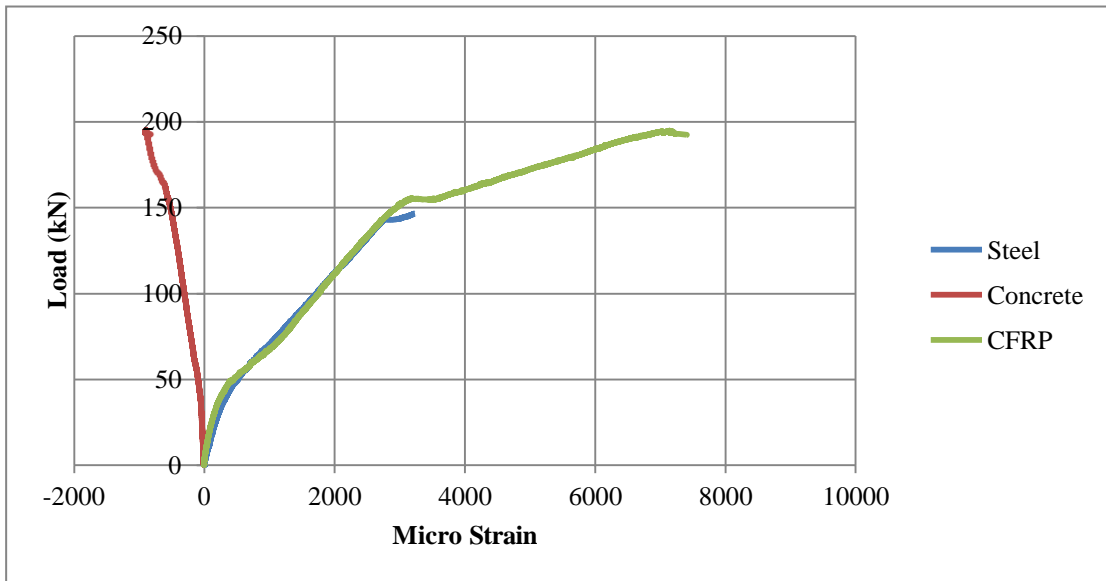
Figure 40: Load (kN) versus micro strain for (SS-1) beam

Figure 41: Beam (SS-1) failure and FRP debonding

4.1.2.5   Beam (GB-SS-2). Beam (SS-2) was strengthened from the sides with one CFRP 150 mm ply sheet which has larger depth of CFRP than SS-1; the load versus strain curves of the concrete, steel and CFRP are shown in Figure 42. Beam (SS-2) was cast to understand the performance of the side strengthening of flexural members with different sheets widths. The beam failed at a load (P_u) of 219.8 kN (87% increase over C beam) with a corresponding deflection (δ_u) of 16.5 mm. The deflection at which the steel yielded (δ_y) was 9.8 mm and the failure deflection (δ_f) was 16.8 mm. The failure mode of the beam was the crushing of the concrete and debonding of the CFRP sheet after the steel had yielded. Figure 43 shows the debonding of CFRP and the concrete crushing at failure.

4.1.2.6   Beam (GB-SS-3). Beam (SS-3) was strengthened from the sides with one CFRP 50mm ply which is smaller depth of CFRP than SS-1; the load versus strain versus curves of the concrete, steel and CFRP are shown in Figure 44. Beam (SS-3) was cast to know the performance of the side strengthening of flexural members while having a moderate reinforcement ratio. The beam resisted a maximum load (P_u) of 164 kN (40% increase over C beam) with a corresponding deflection (δ_u) of 14.4 mm. The deflection at which the steel yielded (δ_y) was 7.6 mm and the failure deflection (δ_f) was 15.2 mm. The failure mode of the beam was steel yielding followed by concrete crushing prior to CFRP sheet debonding. Figure 45 shows the beam during steel yielding, and then the crush of the concrete at failure.

Figure 42: Load (kN) versus micro strain for beam (SS-2)

55

Figure 43: (SS-2) beam concrete crushing and beam failure

Figure 44: Load (kN) versus micro strain for beam (SS-3)

Figure 45: Beam (SS-3) concrete crushing and beam failure

4.1.2.7 Beam (GB-SD-1). Beam (SD-1) was strengthened from the sides with two plies of CFRP sheets with angling the texture along the length of the beam; the load versus strain curves of the concrete, steel and CFRP are shown in Figure 46. Beam (SD-1) was cast to study the behavior of multiple plies side strengthening of flexural members while having a moderate reinforcement ratio. The beam has reached a maximum load (P_u) of 188.2 kN (84% increase over C beam) with a corresponding deflection (δ_u) of 12.9 mm. The deflection at which the steel yielded (δ_y) was 8.8 mm and the failure deflection (δ_f) was 13.1 mm. The failure mode of the beam was yielding of the steel, debonding of the CFRP, followed with concrete crushing. Figure 47 shows the crush of the concrete at failure.
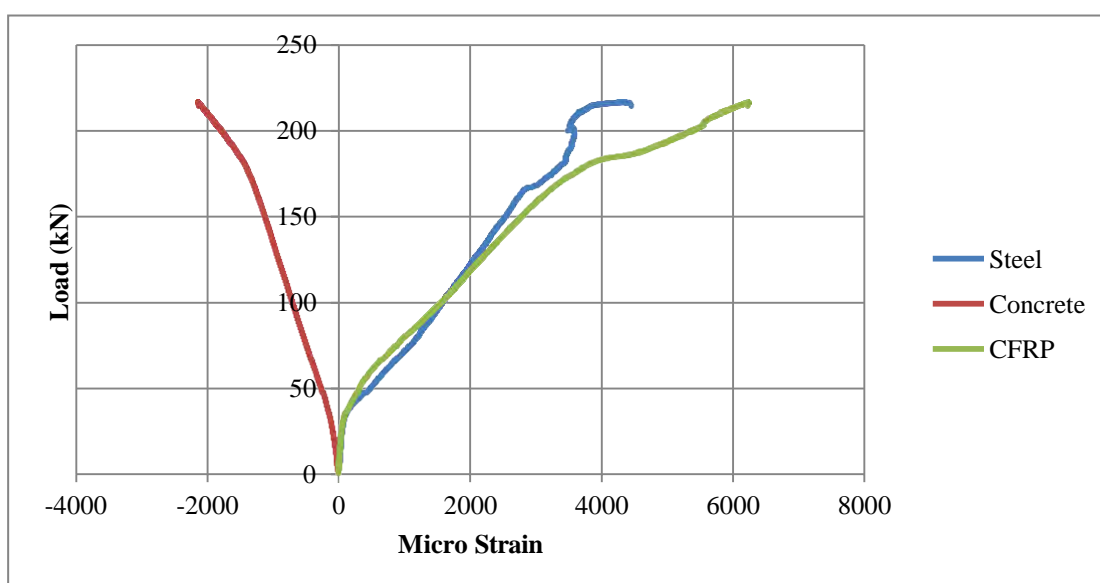
Figure 46: Load (kN) versus micro strain for beam (SD-1)

Figure 47: (SD-1) beam concrete crushing and beam failure

4.1.2.8 Beam (GB-SD-2). Beam (SD-2) was strengthened from the sides with two plies of 150mm CFRP sheets, which is wider than what has been tested in (SD-1); the load versus strain curves of the concrete, steel and CFRP are shown in Figure 48. Beam (SD-2) was cast to distinguish the performance of deeper side strengthening of flexural members while having a moderate reinforcement ratio. The beam resisted a load (P_u) of 227.1 kN (93% increase over C beam) with a corresponding deflection (δ_u) of 15.1 mm. The deflection at which the steel yielded (δ_y) was 8.9 mm and the failure deflection (δ_f) was 15.9 mm. The failure mode of the beam was yielding of the steel, debonding of the CFRP before crushing of the concrete. Figure 49 shows the debonding of CFRP sheets and the crush of the concrete at failure.
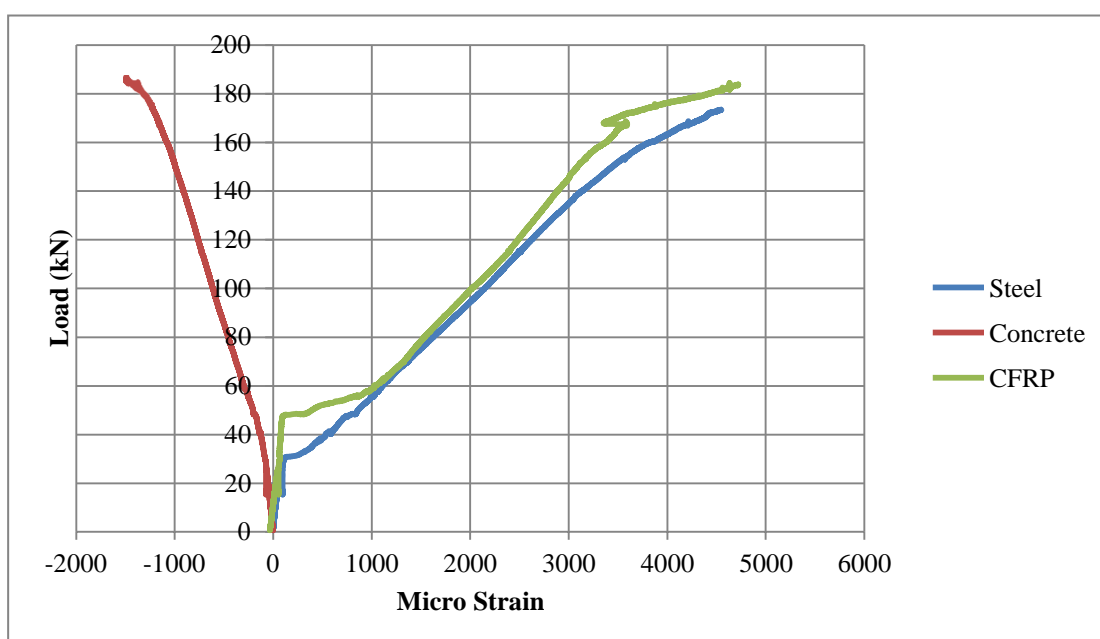
Figure 48: Load (kN) versus micro strain for beam (SD-2)

Figure 49: Beam (SD-2) concrete crushing and beam failure

4.1.2.9 Beam (GB-SD-3). Beam (SD-3) was strengthened from the sides with two plies of 50 mm width CFRP sheets, which is smaller than (SD-1); the load versus strain curves of the concrete, steel and CFRP are shown in Figure 50. Beam (SD-3) was tested to comprehend the performance of different multiple plies depths in a moderate reinforced concrete flexural elements. The beam's maximum load (P_u) was 186 kN (59% increase over C beam) with a corresponding deflection (δ_u) of 13.1 mm. The deflection at which the steel yielded (δ_y) was 7.6 mm and the failure deflection (δ_f) was 13.3 mm. The failure mode of the beam was yielding of the steel, debonding of the CFRP prior to minor concrete crushing initiation at failure. Figure 51 shows the beam during steel yielding, and CFRP debonding at failure.
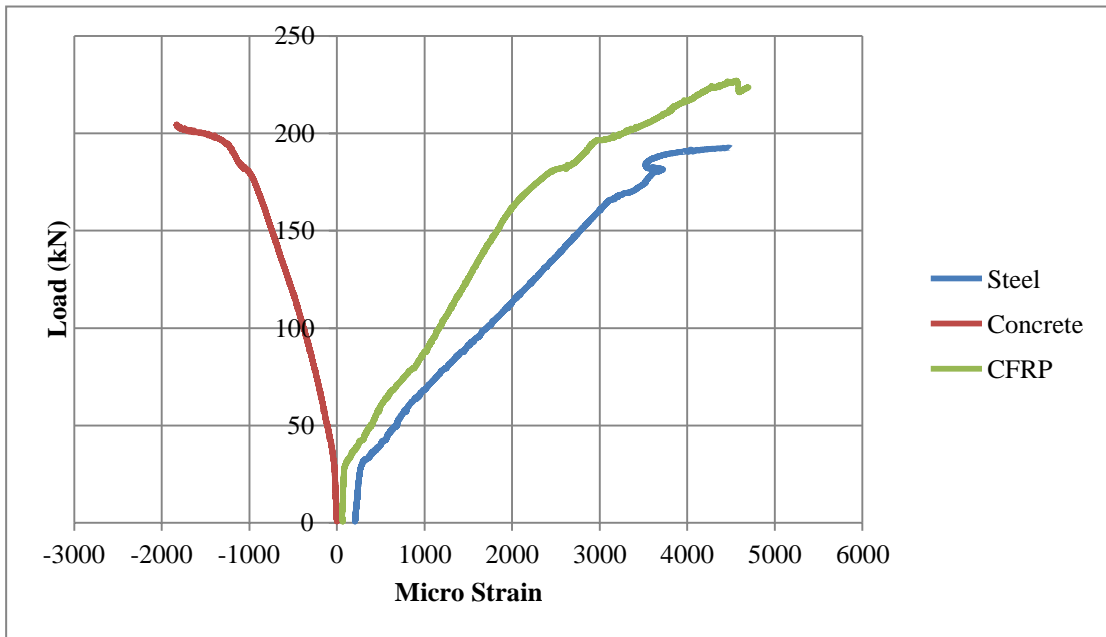
Figure 50: Load (kN) versus micro strain for beam (SD-3)
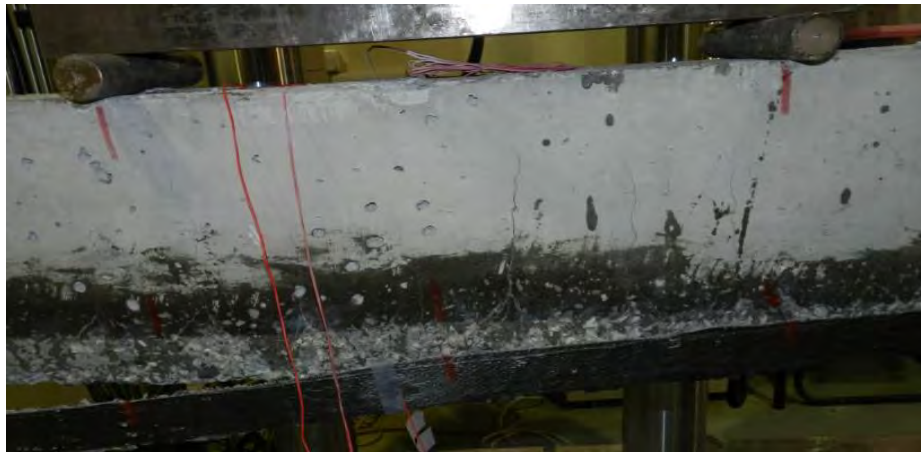
Figure 51: Beam (SD-3) failure and FRP debonding

59

4.1.3   Group C:

4.1.3.1   Control beam (GC-C). The control beam specimen has 2T16 main reinforcement; the load versus strain curves of the concrete and steel are shown in Figure 51. The control beam was tested mainly to compare the behavior of a relatively higher reinforcement ratio with the behavior of conventionally strengthened members as well as side strengthened members. The beam has reached an ultimate load (P_u) of 179.9 kN with a corresponding deflection (δ_u) of 10.1 mm. The deflection at which the steel yielded (δ_y) was 5.2 mm and the failure deflection (δ_f) was 20.0 mm. The failure mode of the beam was the typical under-reinforced member behavior with lower ductility mechanism compared to the control beams of group A and B; steel yields then the concrete crushes as the neutral axis shifted up in the cracked section. Figure 53 shows the crush of the concrete at failure.

4.1.3.2   Beam (GC-BS). Beam (BS) was strengthened conventionally for flexure (from the bottom) with one 150 mm CFRP ply; the strain versus load curves of the concrete, steel and CFRP are shown in Figure 54. Beam (BS) was cast mainly to monitor the behavior of conventional FRP flexural strengthening and to compare it to the behavior of side strengthened members. The beam sustained a load (P_u) of 247.4 kN (38% increase over C beam) with a corresponding deflection (δ_u) of 12.0 mm. The deflection at which the steel yielded (δ_y) was 12.6 mm and the failure deflection (δ_f) was 7.2 mm. The failure mode of the beam was CFRP debonding with minor concrete crushing. Figure 55 shows the CFRP debonding at failure.

4.1.3.3   Beam (GC-BD). Beam (BD) was strengthened from the bottom with two 150mm plies of CFRP sheets; the load versus strain curves of the concrete, steel and CFRP are shown in Figure 56. Beam (BD) was cast mainly to compare its behavior with the behavior of side strengthened members, with multiple plies of FRP. The beam resisted at an ultimate load (P_u) of 282.2 kN (57% increase over C beam) with a corresponding deflection (δ_u) of 12.6 mm. The deflection at which the steel yielded (δ_y) was 8.3 mm and the failure deflection (δ_f) was 15.8 mm. The failure mechanism has started with steel yielding, then CFRP debonding occurred before concrete crushing. Figure 57 shows the beam during steel yielding, and then CFRP debonding followed by crush of the concrete at failure.
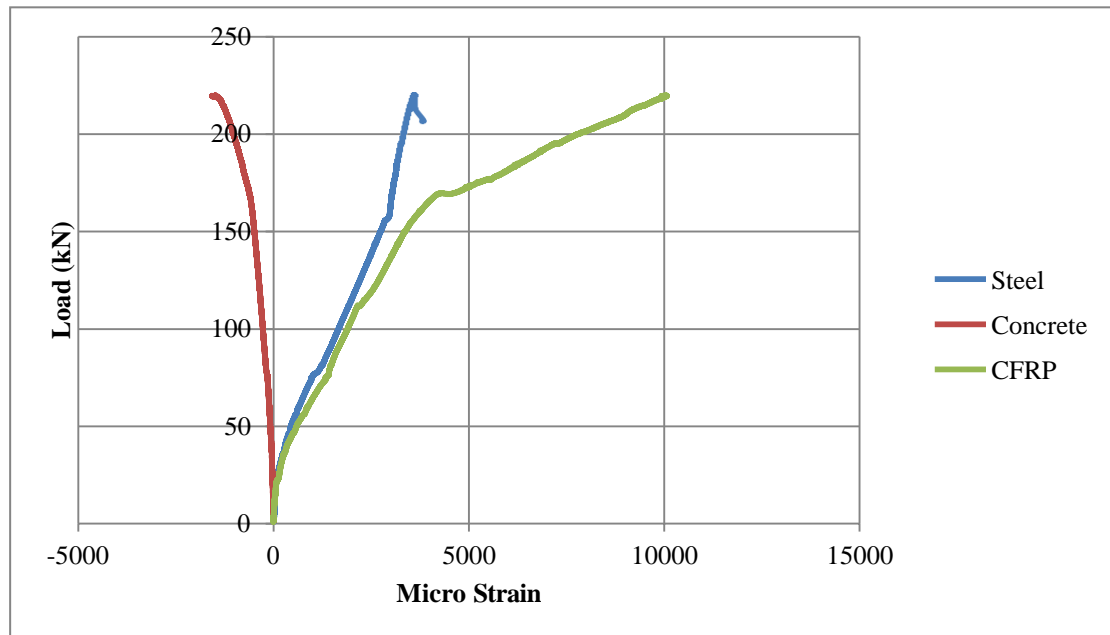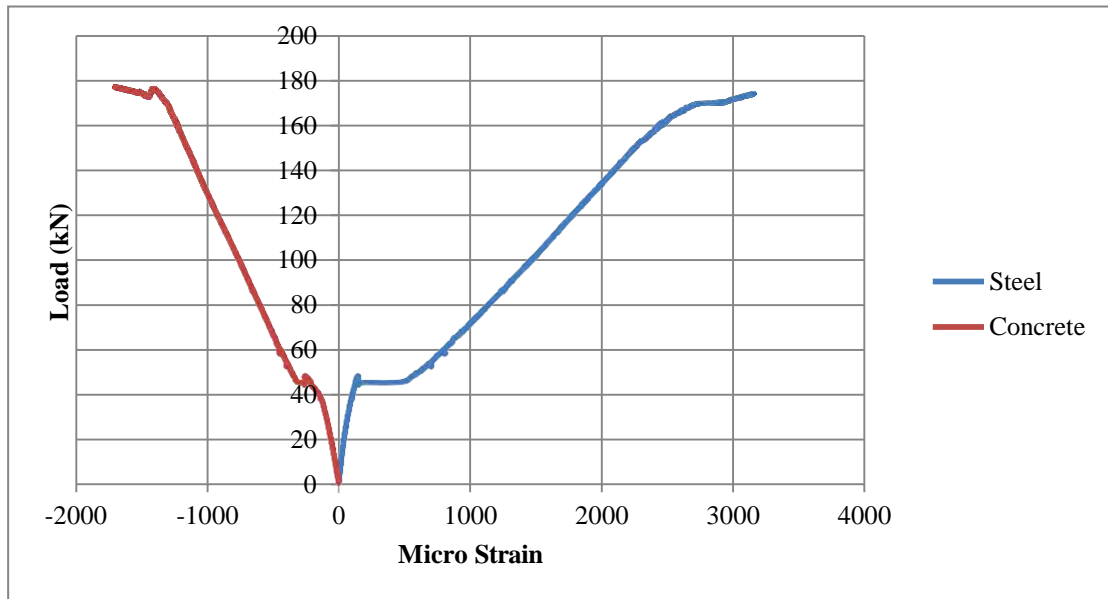
Figure 52: Load (kN) versus micro strain for beam (C)

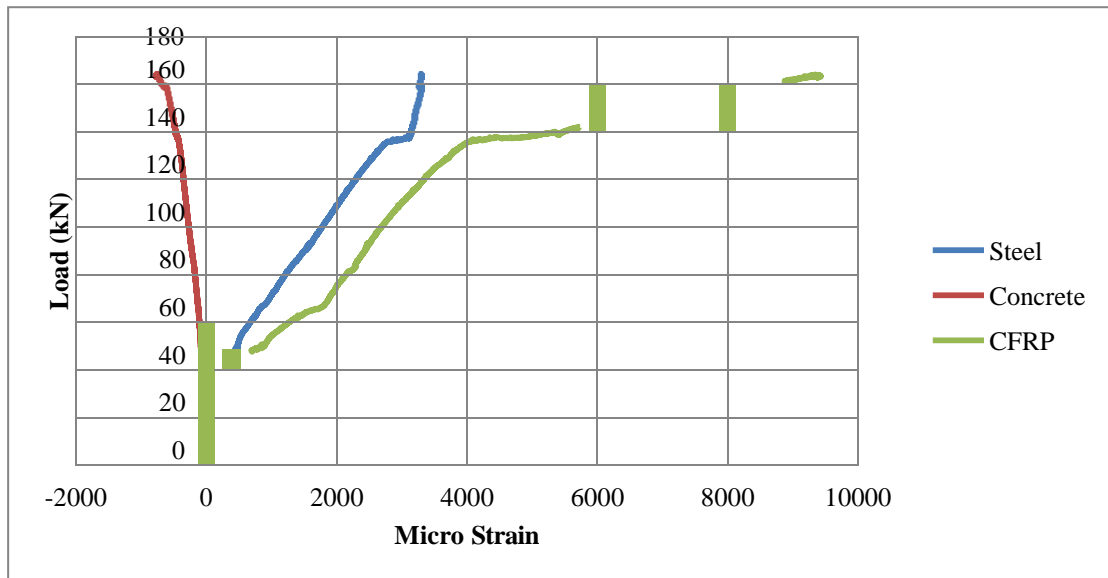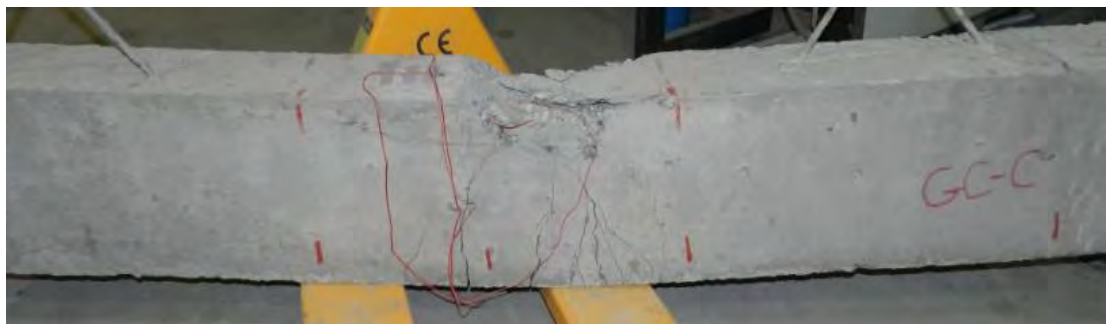
Figure 53: Control beam concrete crushing and beam failure

Figure 54: Load (kN) versus micro strain for beam (BS)

61
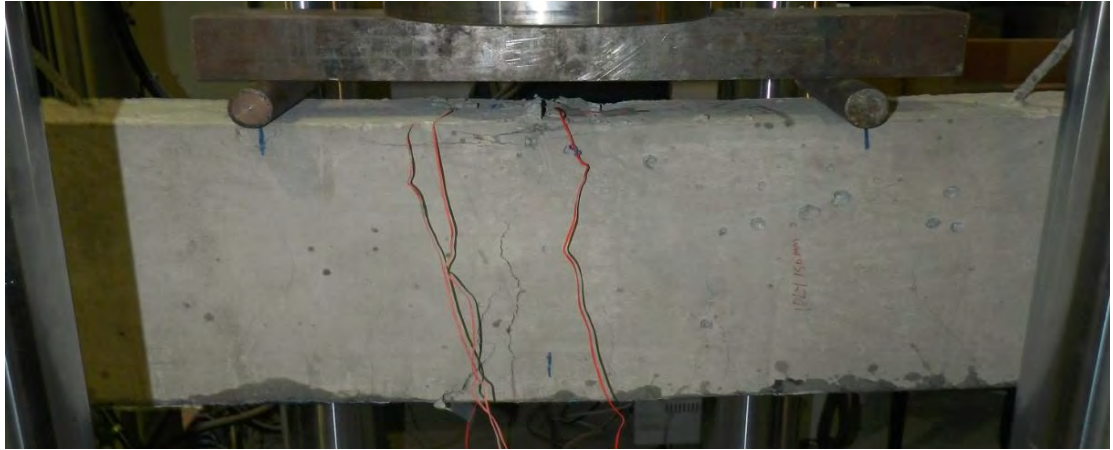
Figure 55: Beam (BS) concrete crushing, FRP debonding and beam failure
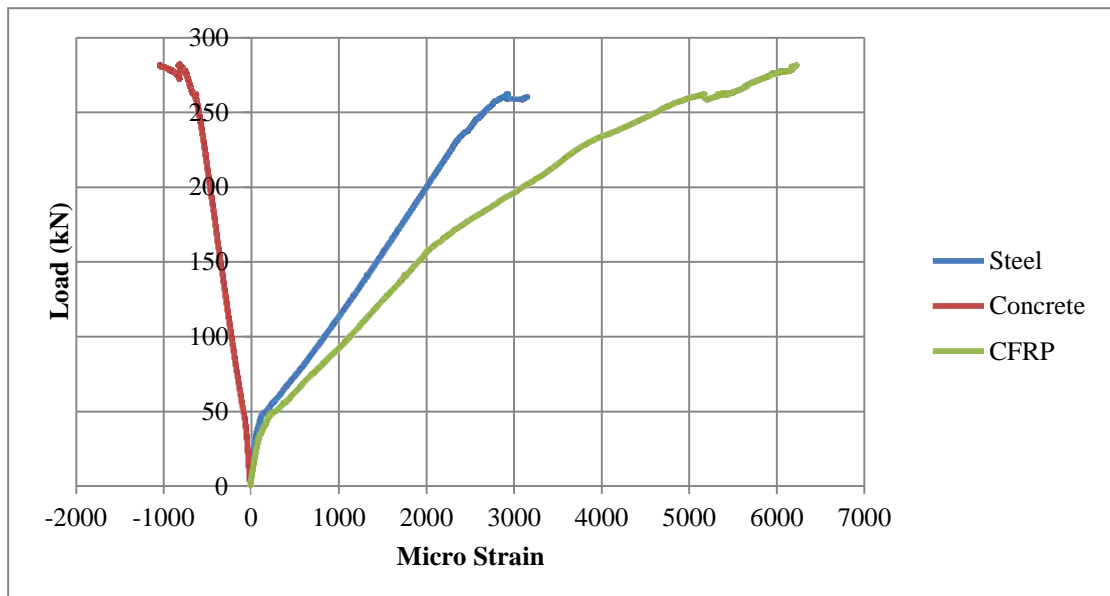
Figure 56: Load (kN) versus micro strain for beam (BD)

Figure 57: Beam concrete crushing, FRP debonding and beam failure

4.1.3.4 Beam (GC-SS). Beam (SS) was strengthened from the sides with one 100m CFRP ply while having the texture along the length of the beam; the test load versus mid-span deflection curve, and the load versus strain curves of the concrete, steel and CFRP are shown in Figure 58. Beam (SS) was tested to study the performance of the side strengthening of flexural members with a relatively higher reinforcement ratio. The beam sustained a load (P_u) of 244.3 kN (36% increase over C beam) with a corresponding deflection (δ_u) of 12.5 mm. The deflection at which the steel yielded (δ_y) was 8.1 mm and the failure deflection (δ_f) was 16.2 mm. The beam's failure has begun with steel yielding, concrete crushing initiation, and then followed by CFRP debonding. Figure 59 shows the beam during steel yielding, then the crush of the concrete and CFRP debonding at failure.
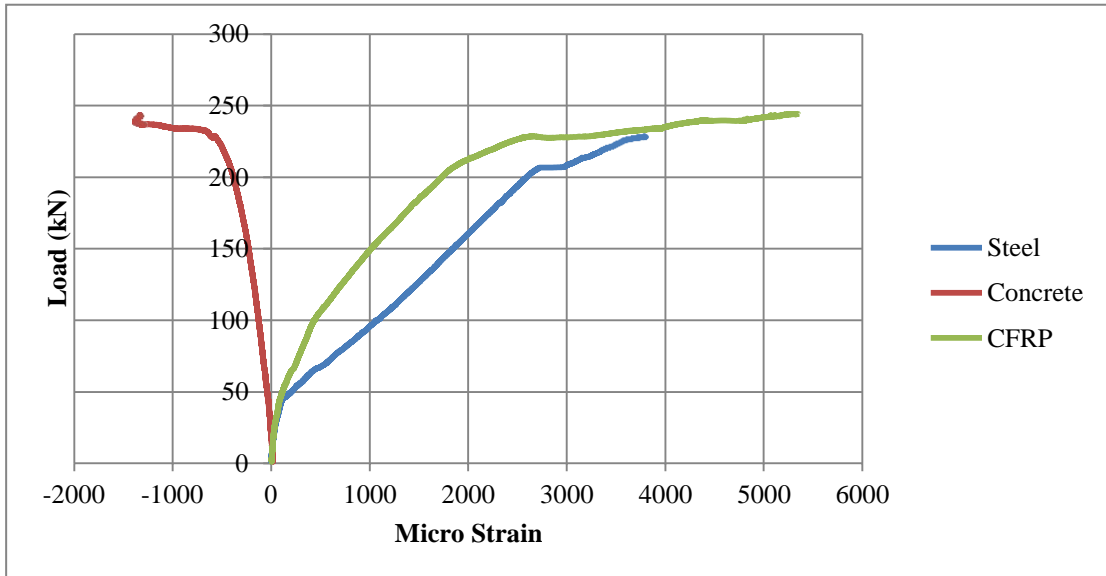
Figure 58: Load (kN) versus micro strain for beam (SS)

Figure 59: (SS) beam concrete crushing and beam failure

63

4.1.3.5   Beam (GC-SD). Beam (SD) was strengthened from the sides with two 100mm plies while angling the texture along the length of the beam; the test load versus mid-span deflection curve, and the load versus strain curves of the concrete, steel and CFRP are shown in Figure 60. Beam (SD) was cast to examine the performance of multiple plies side strengthening of flexural members with a relatively higher reinforcement ratio. The beam's ultimate load (P_u) was 269.6 kN (49% increase over C beam) with a corresponding deflection (δ_u) of 13.3 mm. The deflection at which the steel yielded (δ_y) was 8.7 mm and the failure deflection (δ_f) was 13.8 mm. The failure mode of the beam was yielding of the steel, debonding of the CFRP, and then followed by concrete crushing. Figure 61 shows the crush of the concrete at failure.
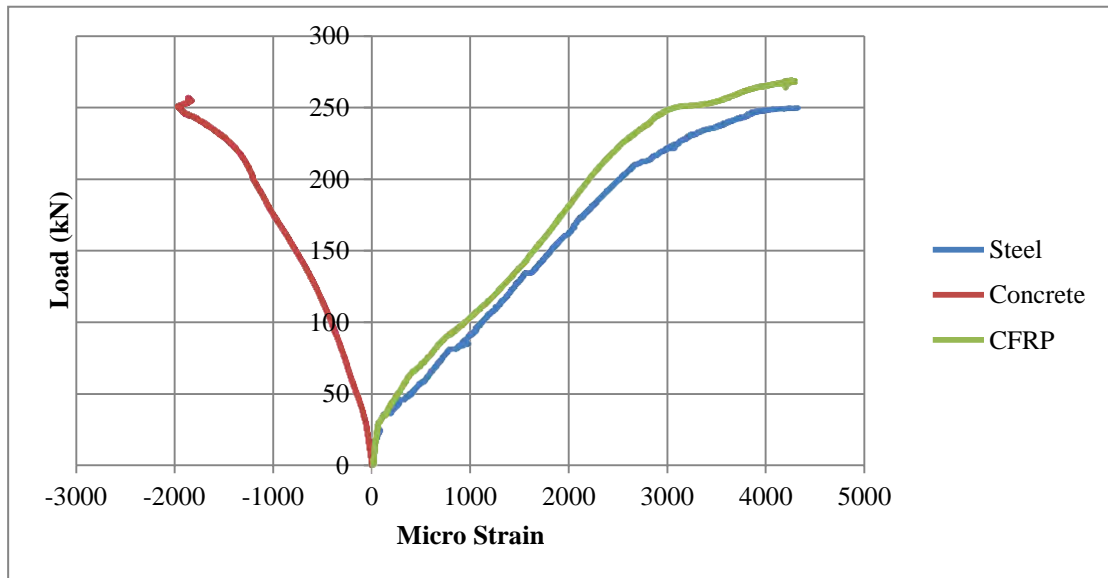
Figure 60: Load (kN) versus micro strain for beam (SD)

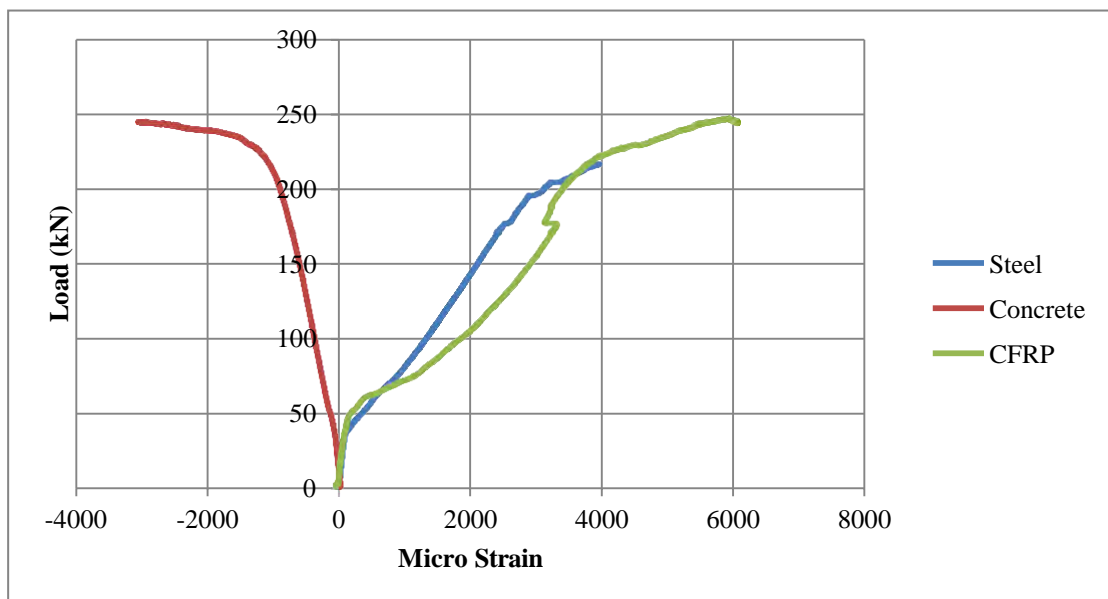Figure 61: (SD) beam minor concrete crushing and beam failure

4.2. Summary of the Results Obtained

This section presents a summary table that has all the data for the tested beams. Table 13 summarizes the yielding force (P_y), beam's stiffness ($K = P_y / \delta_y$), percentage increase over control beams of each group, and ultimate load (P_u), and percentage increase for each specimen over the control beams of each group. The data shown in table 14 are the deflection at steel yielding (δ_y), the deflection at the ultimate strength of the beam (δ_u), the deflection at failure (δ_f), and the mode of failure. The mode of failure is denoted by a sequence of letters (S: steel yielding, C: concrete crushing, and F: FRP debonding). As such, (SC) represents steel yielding followed by concrete crushing, (SF) means steel yielding followed by CFRP debonding, and (SCF) is denoted for steel yielding followed by concrete crushing and CFRP debonding. A comprehensive discussion of the obtained results is provided in the subsequent chapter of this thesis.

Table 13: Summary of loads data

Group	Specimen	P_y (kN)	K (kN/mm)	% Increase	P_u (kN)	% P_u increase
GA	C	79.6	12.8	-	97.3	-
	BS	155.6	14.7	15.1%	178.4	83.3%
	BD	151.2	21.3	66.4%	189.8	95.0%
	SS	102.6	18.4	43.7%	157.9	62.2%
	SD	145.4	19.3	50.6%	188.2	93.3%
GB	C	90.0	17.8	-	117.4	-
	BS	149.8	18.7	4.9%	190.2	62.0%
	BD	178.5	20.6	15.4%	225.4	92.0%
	SS-1	137.1	19.5	9.7%	194.9	66.0%
	SS-2	201.3	20.5	15.0%	219.8	87.2%
	SS-3	135.1	17.7	-0.7%	164.0	39.7%
	SD-1	172.1	19.6	10.0%	216.6	84.4%
	SD-2	211.7	23.6	32.7%	227.1	93.4%
	SD-3	130.8	17.3	-3.0%	186.4	58.8%
GC	C	114.9	22.0	-	179.9	-
	BS	195.4	27.1	23.3%	247.4	37.5%
	BD	259.0	31.3	42.3%	282.2	56.8%
	SS	211.9	26.2	19.3%	244.3	35.8%
	SD	238.1	27.3	24.1%	268.6	49.3%

Table 14: Summary of deflection data

Group	Specimen	δ_y (mm)	δ_u (mm)	δ_f (mm)	Failure Mode
GA	C	6.2	19.6	24.0	SC
	BS	10.6	19.0	19.3	SF
	BD	7.1	12.1	12.3	SCF
	SS	5.6	13.0	13.3	SCF
	SD	7.5	12.0	12.5	SF
GB	C	5.0	13.9	20.1	SC
	BS	8.0	18.3	18.4	SCF
	BD	8.7	15.3	15.3	SF
	SS-1	7.0	14.7	15.2	SCF
	SS-2	9.8	16.5	16.8	SCF
	SS-3	7.6	14.4	15.2	SCF
	SD-1	8.8	12.9	13.1	SCF
	SD-2	8.9	15.1	15.9	SCF
	SD-3	7.6	13.1	13.3	SF
GC	C	5.2	10.1	20.0	SC
	BS	7.2	12.0	12.6	SCF
	BD	8.3	12.6	15.8	SCF
	SS	8.1	12.5	16.2	SCF
	SD	8.7	13.3	13.8	SCF

Chapter 5: Discussion of Results

In this chapter, each group of specimens will be discussed separately. A combined load versus deflection curve is illustrated to study the behavior of each single beam compared to the control specimen. The bases of comparison are the ultimate flexural strength (P_u), the deflection at failure (δ_f) and the ductility of the beams. The ductility of the specimens is measured using the following indices: ultimate index ($I_u = \delta_u / \delta_y$), and failure index ($I_f = \delta_f / \delta_y$). Furthermore, the chapter includes a strain response section to discuss the strain levels of the steel and CFRP reinforcement at failure.

5.1   Group (A)

5.1.1   Load-deflection and ultimate performance

This group has a lower reinforcement ratio than the other groups, and thus has lower ultimate flexural capacity. The reinforcement of this group consists of 2T10 as main bottom tension reinforcement. Figure 62 shows a combination of the load versus mid-span deflection curves for all the specimens in group A.
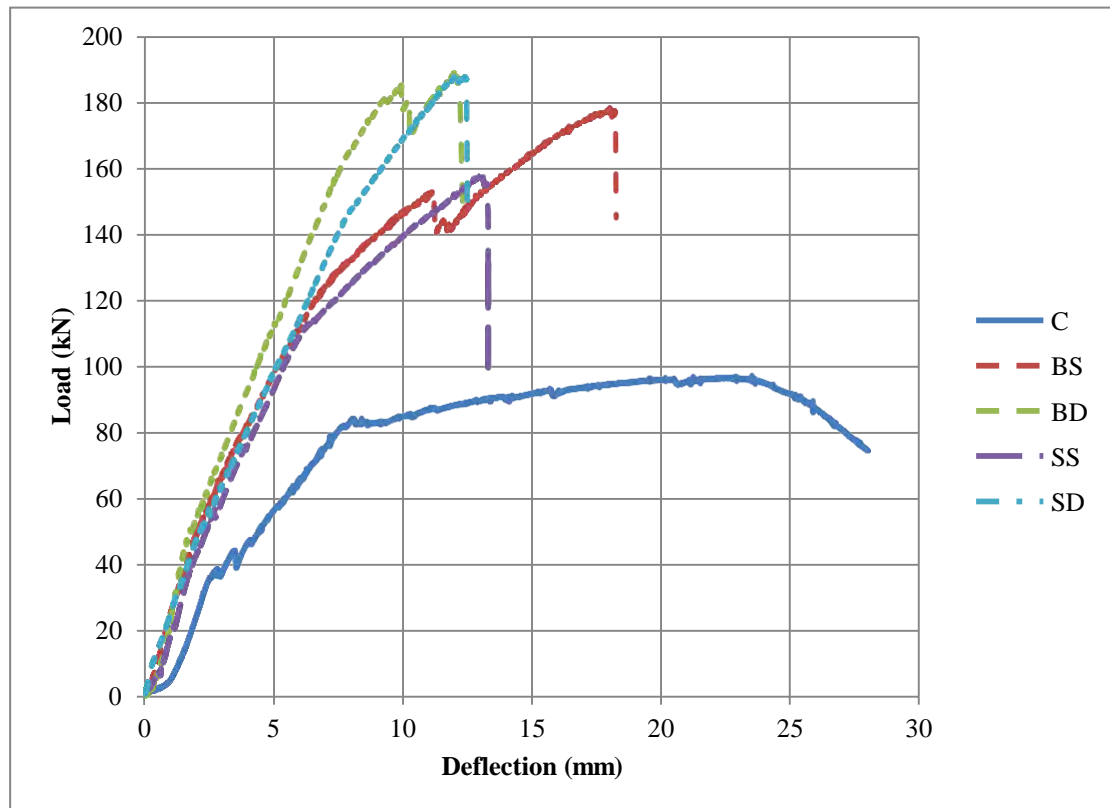
Figure 62: Group A - load (kN) versus deflection (mm)

Typically, the control beam has a higher deflection than the other beams with a lower ultimate capacity. This behavior is very predicted for conventional reinforced concrete beams without any CFRP reinforcement. However, the ductility of the beams will reduce as we increase the effective tension reinforcement due to increase in the cracked stiffness of the composite section. Figures 63 and 64 are bar charts that illustrate the ultimate load and the ductility indices change percentages compared to the control specimen.
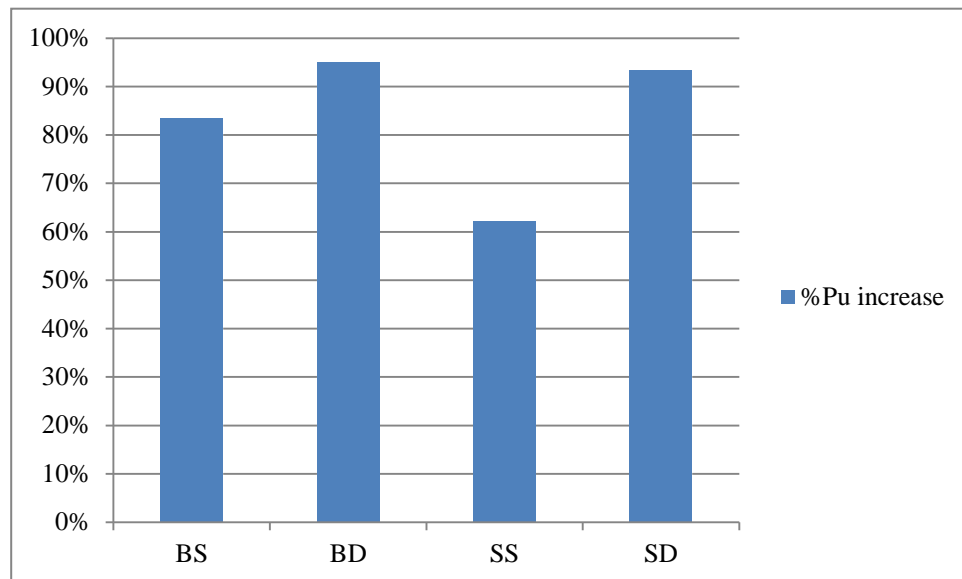
Figure 63: Ultimate load increase compared to the control specimen for Group A
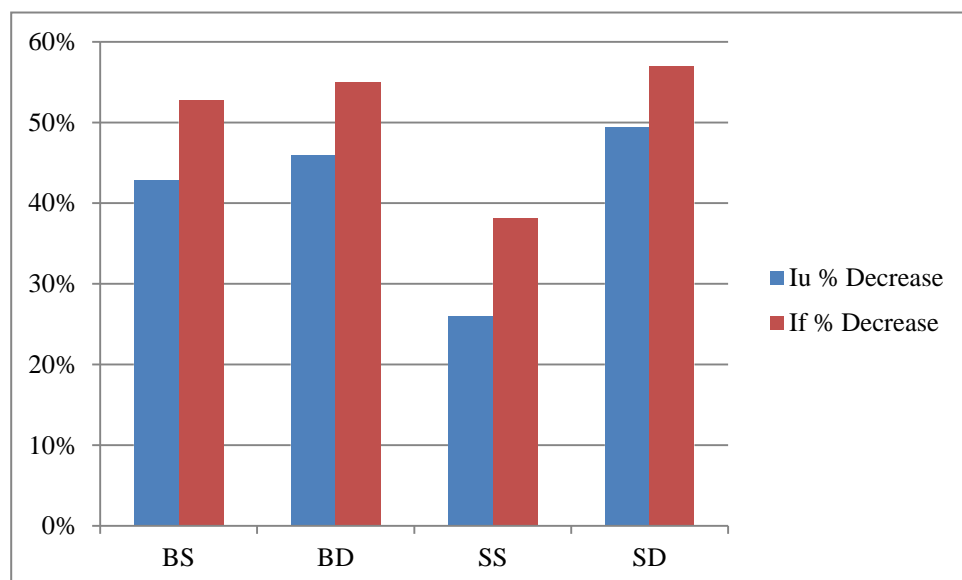
Figure 64: Ductility indices decrease compared to the control specimen for Group A

The beams (BS) and (SS) are strengthened with one ply from the bottom and the sides respectively. Beam (BS) has a higher ultimate capacity and a higher deflection at failure although it has lower CFRP ratio. The percentage difference in ultimate capacity is 12.2% and the difference in deflection at failure is 4.96 mm which is significant; this indicates the effectiveness of the one ply bottom CFRP strengthening compared to the one ply side-bonded technique.

Beams (BD) and (SD) have double plies applied to the bottom and the sides respectively. The results of both specimens indicate similar ultimate capacities and deflections at failure. Beam (BD) has a higher ultimate capacity as the percentage difference in ultimate capacity is 1.5% and the deflection at failure difference is 0.37 mm despite the difference in the FRP ratio. Those results propose that multiple side-bonded-ply of FRP is more effective. In other words, with higher effective reinforcement ratios, the utilization of side-bonded FRP gets closer to the conventional bottom-bonded competence.

Ultimately, the strengthened specimens have recorded a significant load increase compared to the control beam specimen. The bottom bonded FRP has enhanced the capacity by 83% and 95% for single and double plies, respectively. Moreover, the side-bonded FRP has also improved the capacity by 62% and 93% for single and double plies, respectively. This indicates the improvement in the side-bonded performance with the higher CFRP fiber ratios.

5.1.2   Strain response

This section discusses the strain response of the steel as well as the CFRP reinforcement for group A, as shown in Figures 65 and 66, respectively. The yield strain of the steel reinforcement in those specimens is 0.00275 mm/mm (2,750 micro-strain); and the ultimate rupture strain for the CFRP sheets used in the experimental program is 0.017 mm/mm (17,000 micro-strain) as mentioned in Chapter 3.

Initially, the steel strain response shown in Figure 65 exhibited similar levels in the uncracked region, but afterwards the strain trends took different slopes according to the different CFRP configurations. The steel in the control beam as well as the single ply specimens (SS and BS) has reached the yield strain, and continued in yielding until the ultimate failure. Nonetheless, the steel in those specimens (C, SS and BS) has reached yielding on different working loads (80 kN, 105 kN and 155 kN,

respectively), which indicates the increased contribution of CFRP laminates. On the other hand, specimens SD and BD reached the yielding strain at the ultimate loads (approximately 185 kN for both) without additional strains in the plastic region of the steel; this justifies the brittle global failure of those two specimens.
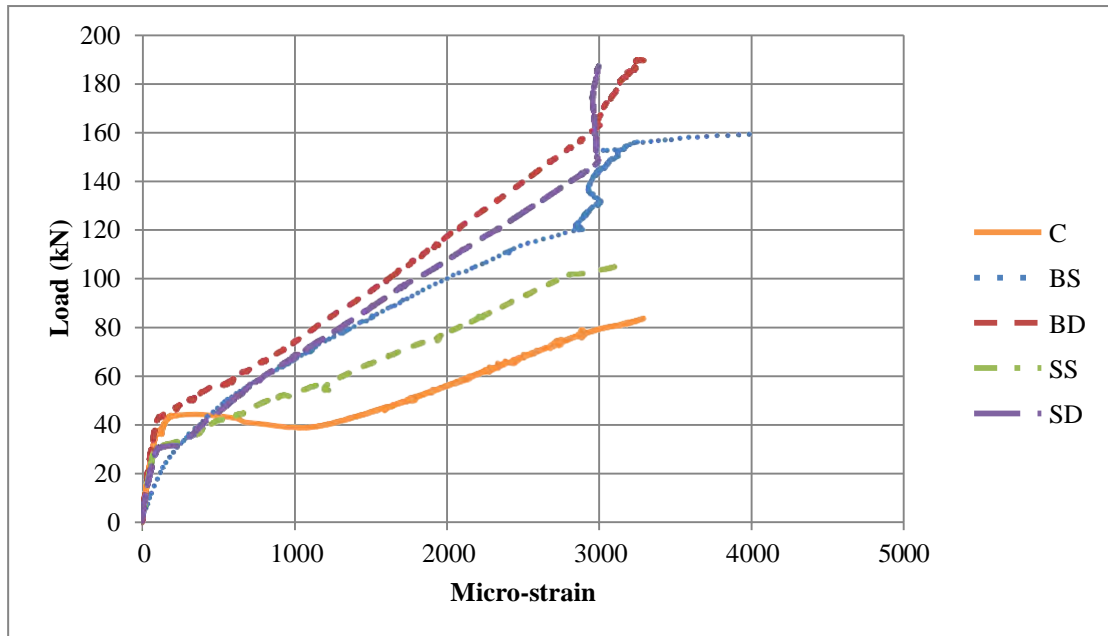
Figure 65: Steel strain response for Group A
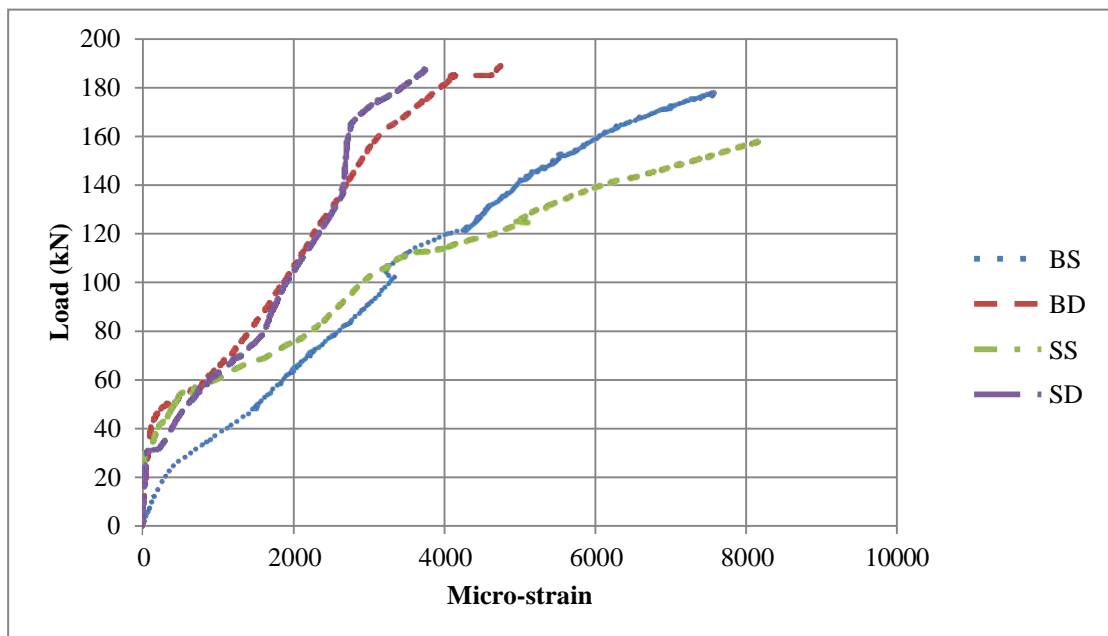
Figure 66: FRP strain response for Group A

For the CFRP strain response, the graph in Figure 66 shows that none of the specimens has reached the ultimate rupture strain. The single ply specimens (SS and

BS) have the maximum utilization of the FRP materials with 7,500 and 8,100 micro-strain levels. However, beam BS has reached a higher ultimate load of 180 kN compared to the 160 kN load for SS specimen; which is justified if we consider the fibers moment arm difference between the side-bonded and the bottom-bonded configurations. On the other hand, the double-ply specimens (SD and BD) have recorded micro-strain levels of 3,600 and 4,600 with a similar corresponding ultimate load of 185 kN. Those two specimens exhibited equivalent ultimate behavior, but the SD specimen has roughly 33% more fibers with 25% less moment arm; which indicates the lower efficiency of the side-bonded FRP.

5.2   Group (B)

5.2.1   Load-deflection and ultimate performance

This group of specimens has a moderate steel reinforcement ratio that consisted of 2T12 bottom tension mild steel. Three different widths of FRP sheets are applied on the sides to study the behavior of the side-bonded FRP sheets with different depths. Figure 67 shows the combined load versus deflection curves for all the beams in group B.
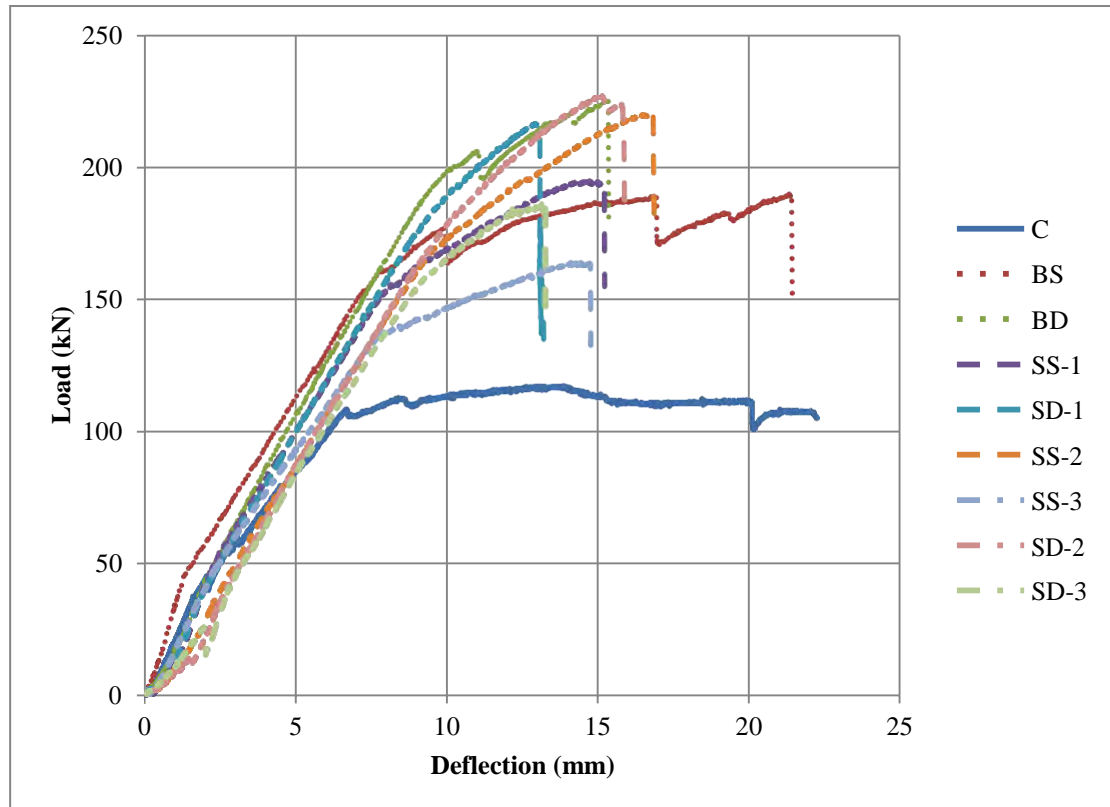
Figure 67: Group B - load (kN) versus deflection (mm)

71

Figures 68 and 69 are bar charts that illustrate the ultimate load and the ductility indices change percentages compared to the control specimen.
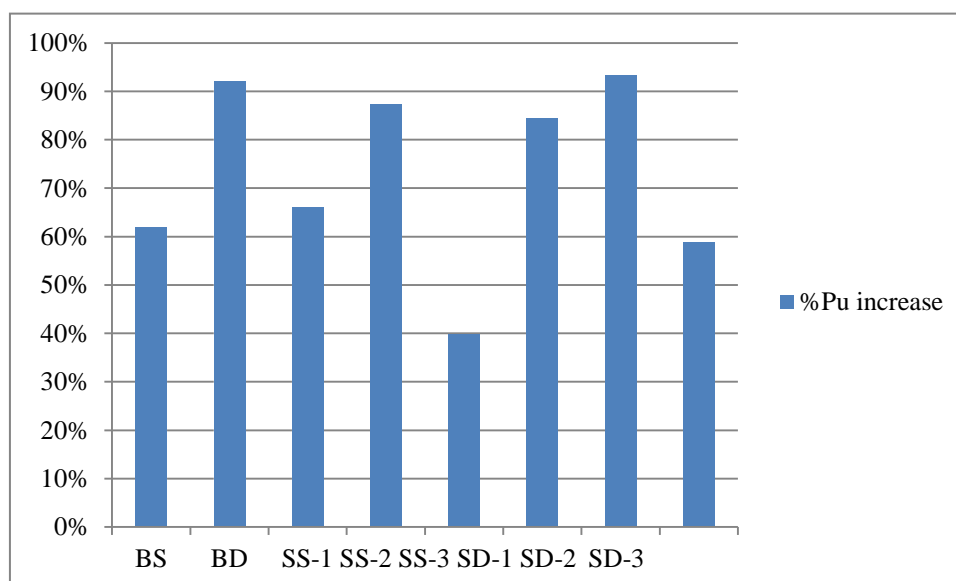
Figure 68: Ultimate load increase compared to the control specimen for Group B
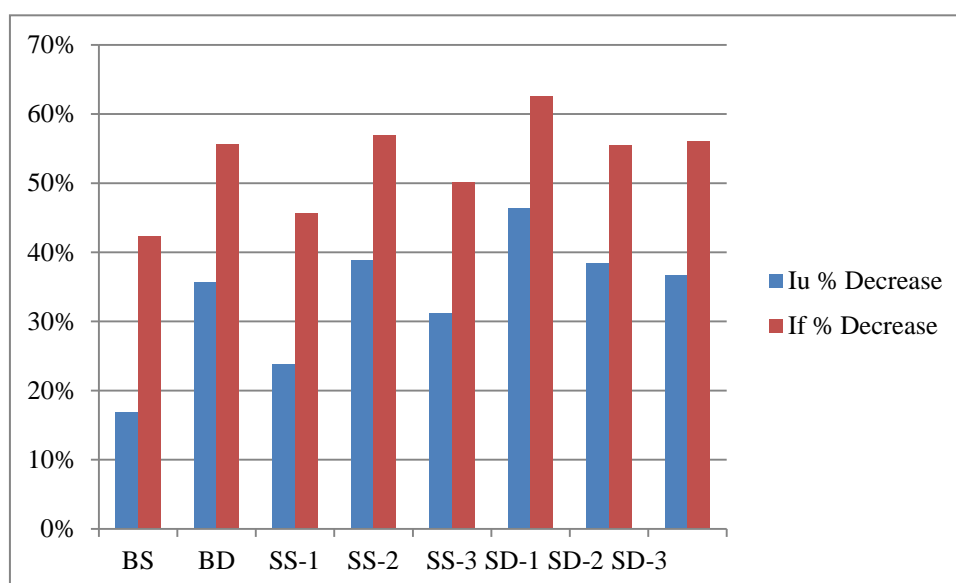
Figure 69: Ductility indices decrease compared to the control specimen for Group B

5.2.2   Group (B) side versus bottom strengthening comparison

Similarly, a combined graph is provided to study the effect of side strengthening to bottom strengthening in flexure. The load versus deflection curve for beams (C, BS, BD, SS-1 and SD-1) are shown in Figure 70.
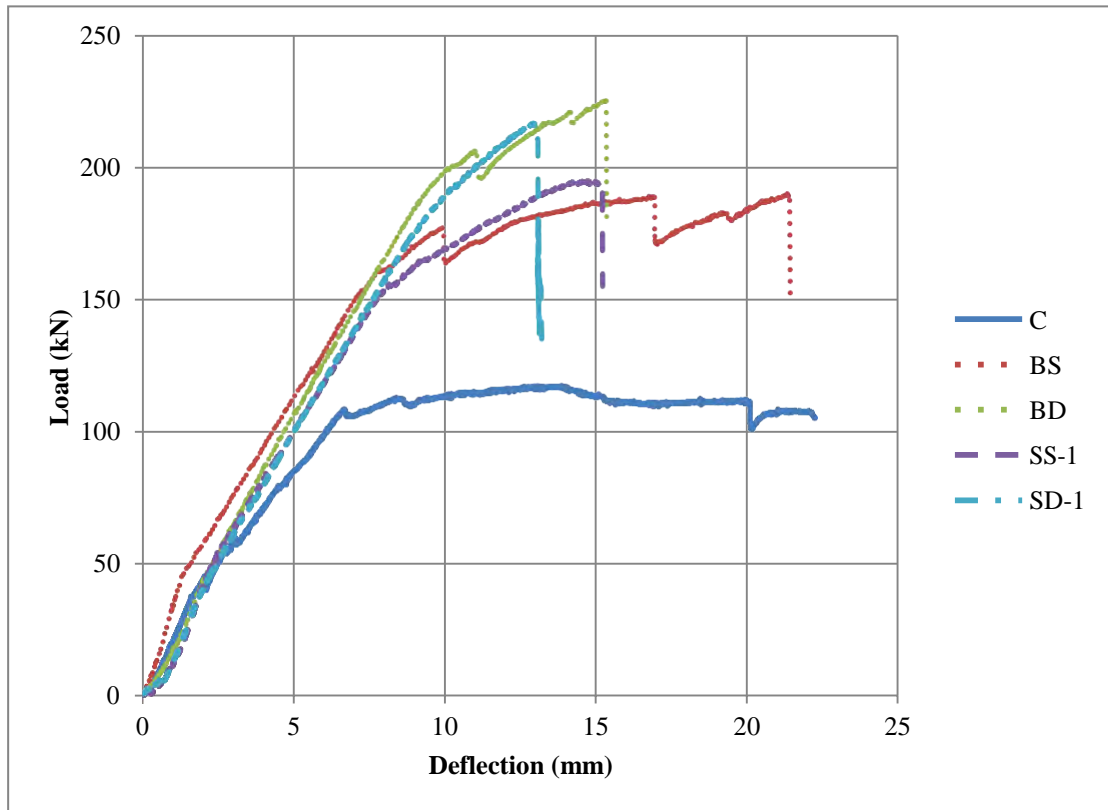
Figure 70: Group B - side vs. bottom strengthening

The control beam has the highest deflection of all the beams, which is typical for under-reinforced concrete flexural elements. Furthermore, the control beam has the lowest ultimate attained load of all, since it has the lowest equivalent reinforcement ratio in the group.

The beams (BS) and (SS-1) are both strengthened with one ply from the bottom and the sides, respectively. Beam (SS-1) resisted a higher ultimate load, yet both beams have close values, while beam BS exhibited higher ductility at failure. The percentage difference between the ultimate capacities is 2.43% and the deflection at failure difference is equal to 3.21 mm.

Beams (BD) and (SD-1) have double plies applied to the bottom and the sides respectively. The results of both specimens are almost the same in ultimate load, but beam (BD) has a higher deflection at failure. Beam (BD) has a higher ultimate capacity as the percentage difference in ultimate capacity is equivalent to 4.01% and the deflection at failure difference is 2.26 mm.

73

Furthermore, the previous comparison of single and double plies strengthening reinforces the conclusion that as the effective tension reinforcement ratio increases, the behavior of both technologies (bottom and side-bonded FRP) at ultimate get analogous characteristics.

5.2.3   Beams (SS-1), (SS-2) and (SS-3) comparison:

Beams (SS-1), (SS-2) and (SS-3) have one ply of CFRP bonded from the sides of each specimen. Beam (SS-1) has a medium sized sheet (width = 100 mm), while beam (SS-2) has a wider sheet (width = 150 mm), and (SS-3) is strengthened with a narrower sheet of 50 mm. This section will mainly discuss the change in behavior of different FRP depths with a single ply side-bonded system. The graph below shows a combined load versus deflection curve for the beams.
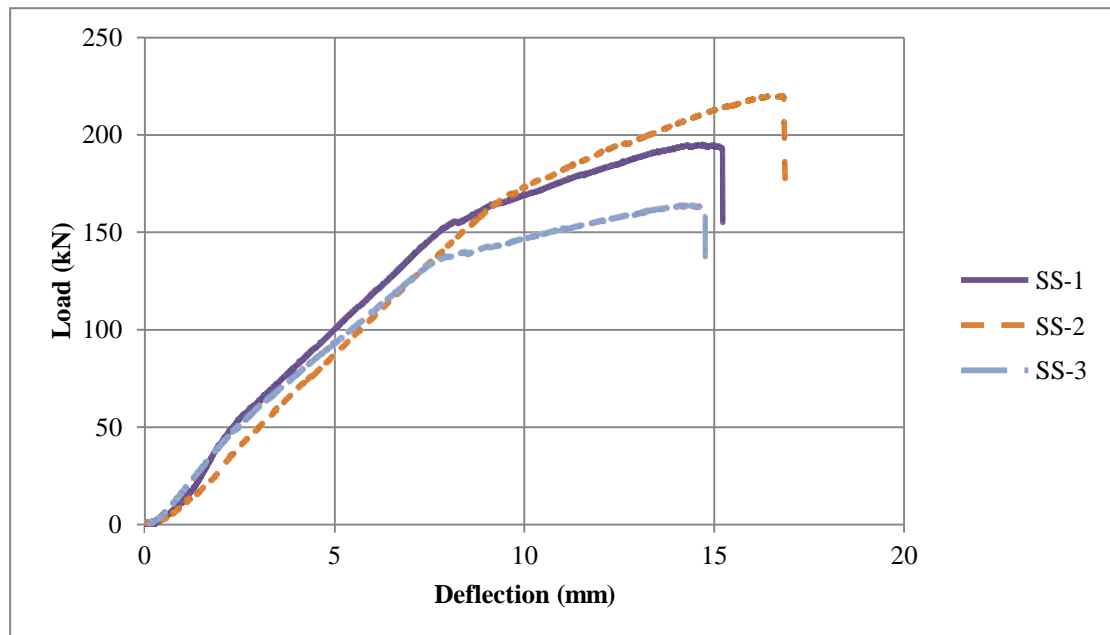
Figure 71: Group B - Single ply side-bonded specimens

As shown in Figure 71, the beam with wider sheets (SS-2) has the highest load-carrying capacity and highest deflection at ultimate. On the hand, (SS-3) resisted the lowest ultimate load with a considerable ductility due to the low CFRP ratio. Specimen (SS-2) has 50% more side-bonded CFRP compared to (SS-1), yet the increase in ultimate load was only 12%, yet (SS-3) has incurred more deflection prior to failure. Moreover, decreasing the FRP width in beam (SS-3) by 50% relative to (SS-1) has reduced the capacity of the beam by 17.2%. Typically, as the specimen has wider CFRP sheets, it will sustain a higher load which is also relative to the depth of

the fibers' centroid. However, the wider the FRP attached on sides of the beams, the more ductile the behavior is at failure, which is not the case for bottom bonded CFRP specimens.

5.2.4 Beams (SD-1), (SD-2) and (SD-3) comparison:

Beams (SD-1), (SD-2) and (SD-3) have two plies of CFRP sheets bonded to the sides of each sample. These three double-ply specimens have similar FRP widths configuration to the (GB-SS) specimens. The graph in Figure 72 shows a combined load versus mid-span deflection curves for the beams.
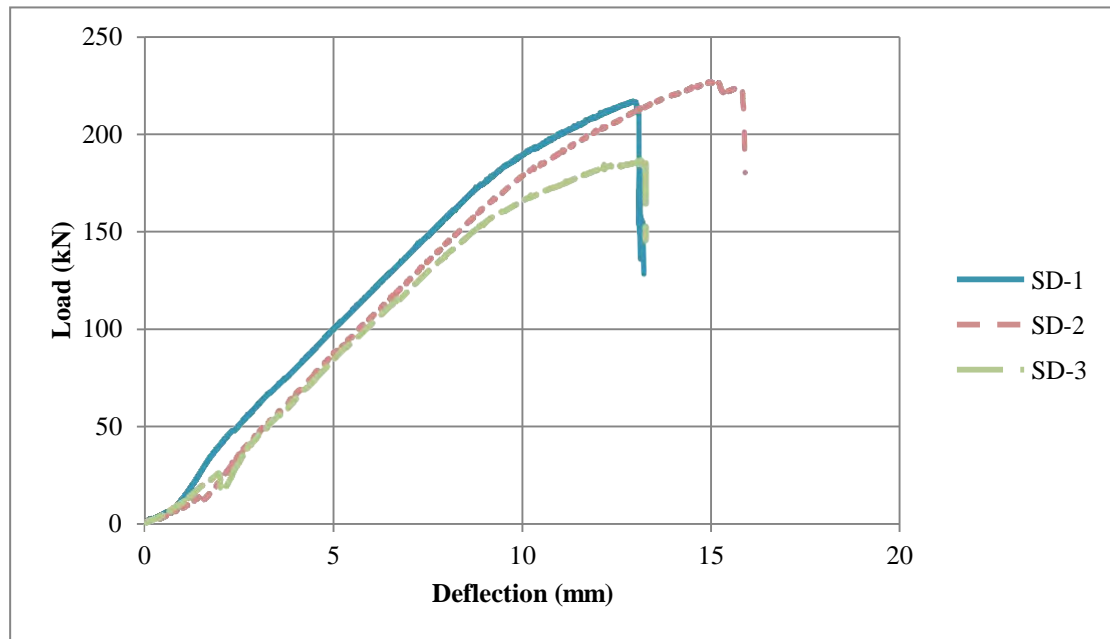
Figure 72: Group B - double plies side-bonded specimens

Similarly, (GB-SD) specimens have followed the expected behavior achieved in the single-ply sample. The difference in ultimate load among (SD-2) and (SD-1) is 4.72%, which does not reflect the 50% increase in fibers. Nonetheless, (SD-3) which has narrower sheets has recorded a 15% reduction in ultimate compared to (SD-1). Eventually, ductility improvement has been noted when wider side-bonded FRP are used compared to the narrower ones, yet the ultimate capacity increase is minor because the centroid of the sheets gets closer to the center of the cracked composite section.

Generally, CFRP technology has limitations when it comes to strength improvement. Group B includes six side-bonded specimens with six different fiber

ratios. Figure 73 plots the ultimate load improvement versus the FRP reinforcement ratio ($\rho_{FRP} = A_{FRP} / bd_f$) for the same steel reinforcement ratio. The graph shows that the load-carrying is logarithmically proportional to ρ_{FRP}. In other words, the strength improvement rate decreases as the FRP reinforcement ratio increases.
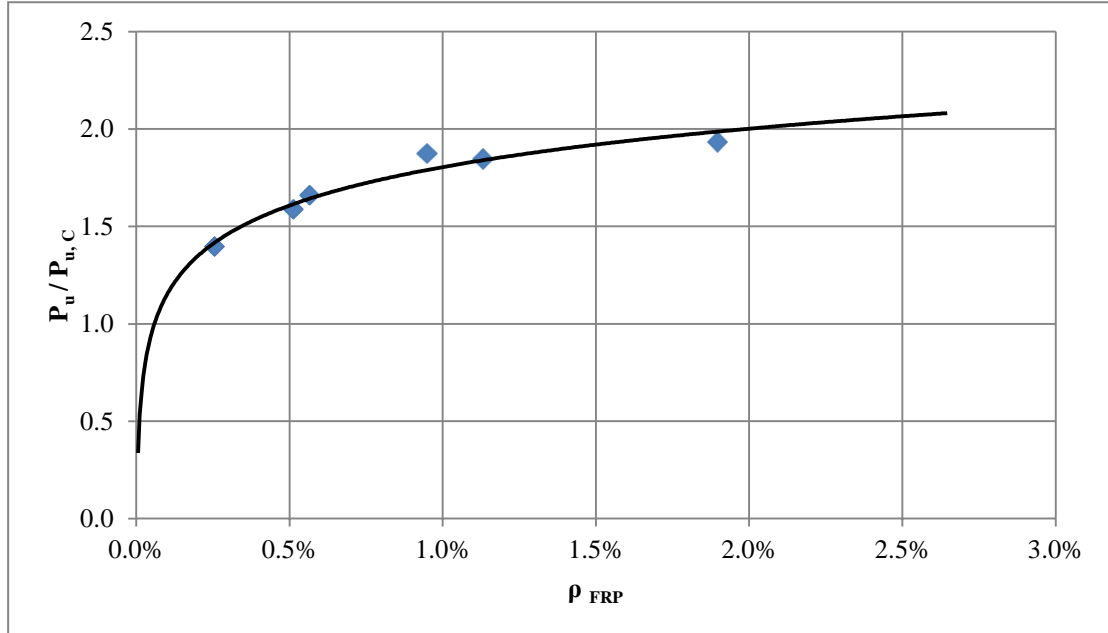
Figure 73: $P_u / P_{u,C}$ vs. CFRP ratio for Group B

5.2.5   Strain response

This section discusses the strain response of the steel as well as the CFRP reinforcement for group B, shown in Figures 74 and 75, respectively. The yield strain of the steel used as reinforcement in those specimens is 0.00275 mm/mm (2,750 micro-strain); and the ultimate rupture strain for the CFRP sheets used in the experimental program is 0.017 mm/mm (17,000 micro-strain) as mentioned in Chapter 3.

Initially, the steel strain response showed in Figure 74 shows that all the specimens have reached the yielding stage. The steel in the single ply specimens (BS and SS) has reached the yield strain, and continued in yielding until the ultimate failure at loads of 187 kN and 155 kN. Nonetheless, the steel in the double-ply specimens (BS and SD) has reached yielding on similar working load of 215 kN, which indicates the lower efficiency of the side-bonded scheme.
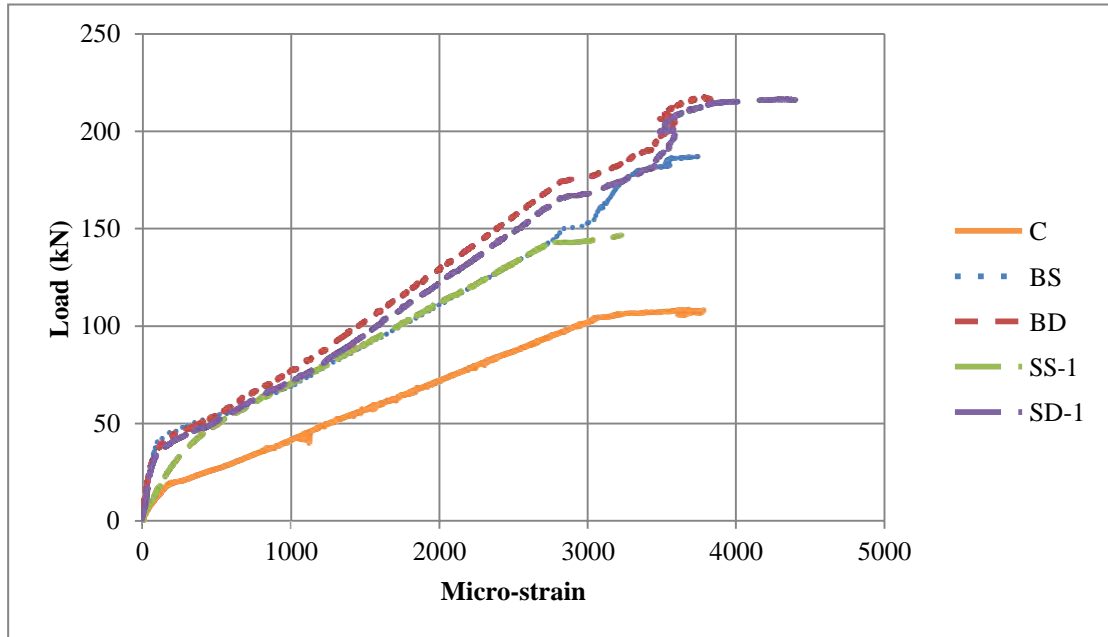
Figure 74: Steel strain response for Group B
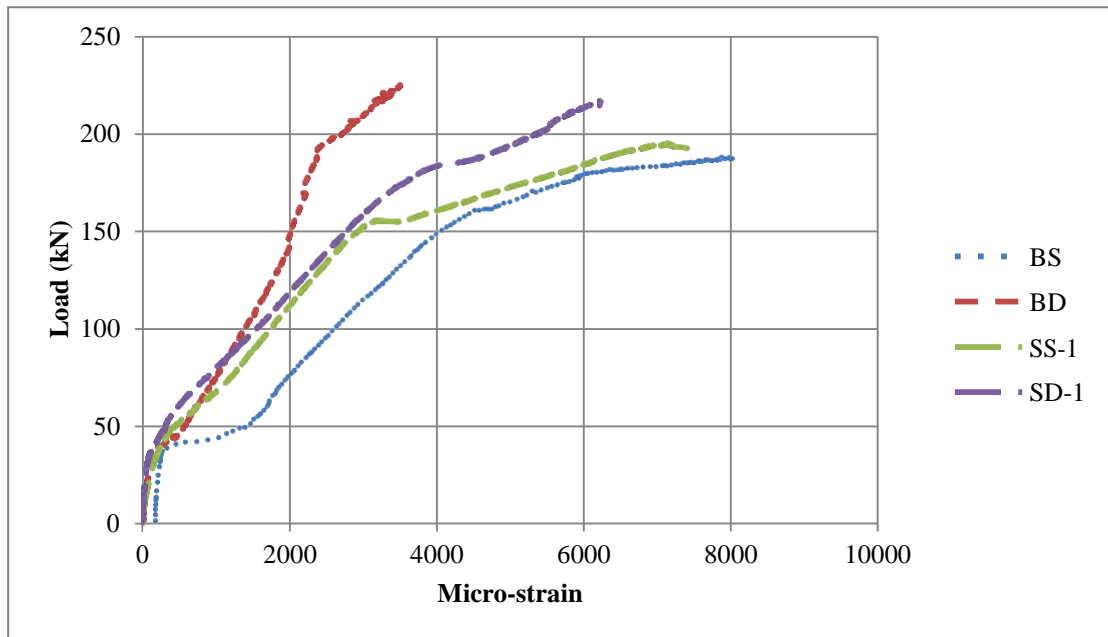
Figure 75: FRP strain response for Group B

For the CFRP strain response, the graph in Figure 75 shows that none of the specimens has reached the ultimate rupture strain. The single ply specimens (BS and SS) have the maximum utilization of the FRP materials with 8,000 and 7,400 micro-strain levels. However, beam BS has recorded a slightly lower ultimate load of 186 kN compared to the 194 kN load for (SS) specimen; which is justified if we consider the fibers moment arm difference between the side-bonded and the bottom-bonded configurations. On the other hand, the double-ply specimens (BD and SD) have

77

recorded micro-strain levels of 3,400 and 6,100 with a similar corresponding ultimate load of 220 kN. Those two specimens exhibited equivalent ultimate behavior, but the (SD) specimen has approximately 33% more fibers with 25% less moment arm; which indicates the lower efficiency of the side-bonded FRP compared to the bottom-bonded ones. Moreover, the strain difference between (BD) and (SD) specimens indicates a more ductile failure.

5.3   Group (C)

5.3.1   Load-deflection and ultimate performance

This group of RC beams has 2T16 as tension reinforcement which is higher than the other groups and thus a higher ultimate flexural capacity. The purpose of investigating this group is to study the performance of side-bonded FRP strengthening with higher reinforcement ratios. Figure 76 shows a combination of the load versus deflection curves for all the beams in group C.
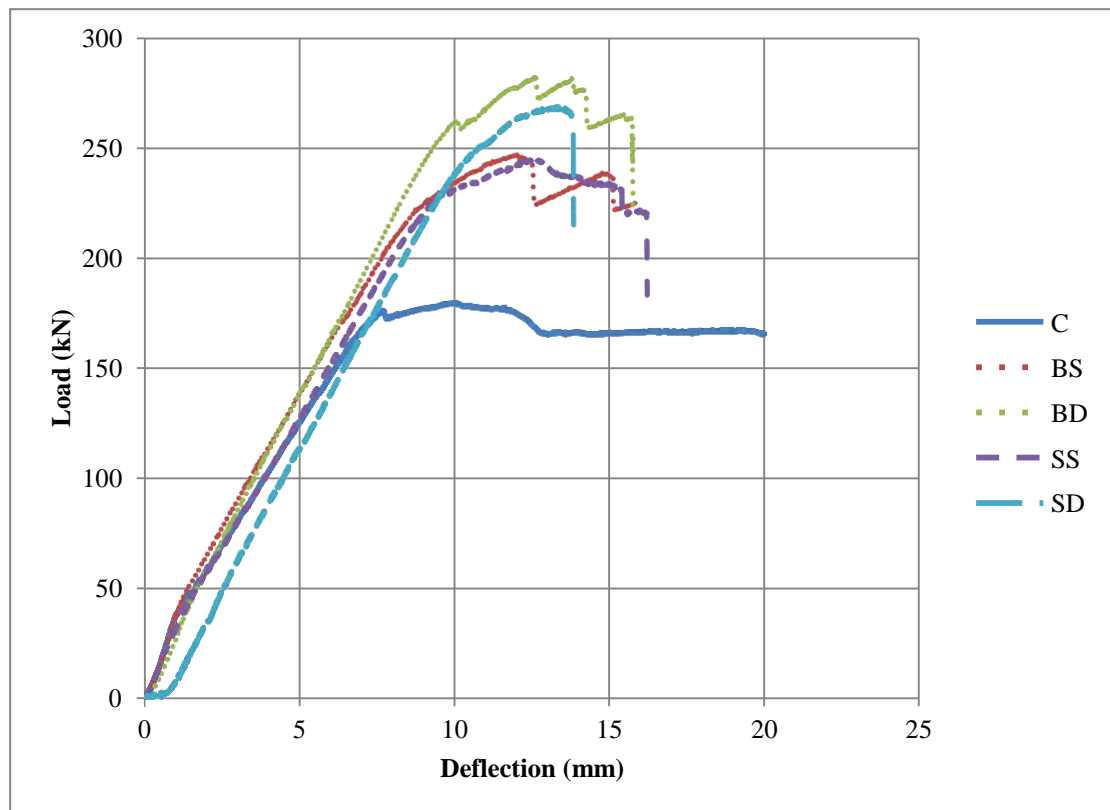
Figure 76: Group C - load (kN) versus deflection (mm)

Comparing all the beams together, the control beam has the highest deflection at failure whereas beam (BD) has the highest ultimate flexural capacity.

78

Figures 77 and 78 are bar charts that illustrate the ultimate load and the ductility indices change percentages compared to the control specimen.

The beams (BS) and (SS) are both strengthened with one ply from the bottom and the sides respectively. Beams (BS) and (SS) behaved similarly in both ultimate load and deflection. Beam (BS) has a higher capacity as the percentage difference in ultimate capacity is 1.24%. Beam (SS) has the advantage in deflection at failure as the difference is 1.93 mm.
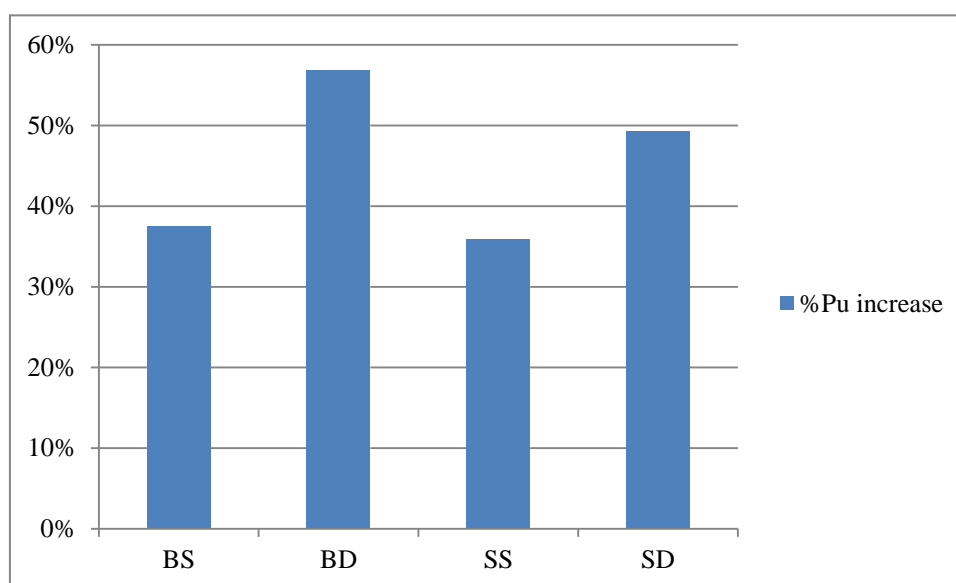
Figure 77: Ultimate load increase compared to the control specimen for Group C
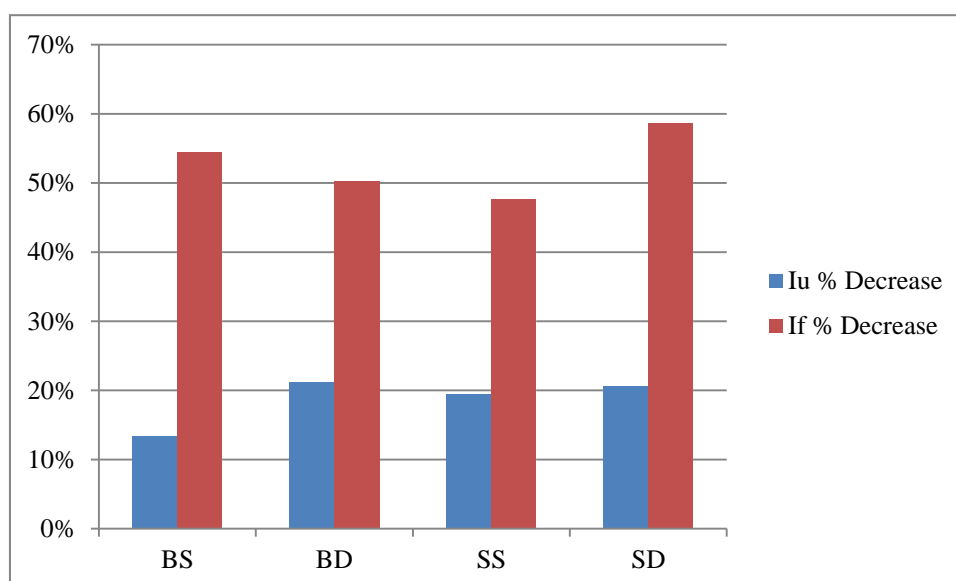
Figure 78: Ductility indices decrease compared to the control specimen for Group C

Beams (BD) and (SD) have double plies attached to the bottom and the sides respectively. Following the single ply specimens, the ultimate performance of (BD) and (SD) are close with a more ductile failure for the bottom-bonded beam. The percentage difference in ultimate capacity is equal to 4.91% while the deflection at failure difference is 3.61 mm.

Ultimately, the strengthened specimens have recorded a significant load increase compared to the control beam. The bottom bonded FRP has enhanced the capacity by 38% and 57% for single and double plies, respectively. Moreover, the side-bonded FRP has also improved the capacity by 36% and 49% for single and double plies respectively. This indicates the development in the side-bonded performance with the higher reinforcement ratios. However, the CFRP strengthening technology becomes less efficient as in group A (with lower steel reinforcement ratio), where the improvement in the flexural capacity has reached 95%.

5.3.2 Strain response

This section discusses the strain response of the steel as well as the CFRP reinforcement for group C, shown below in Figures 79 and 80. The yield strain of the steel used as reinforcement in those specimens is 0.00275 mm/mm (2,750 micro-strain); and the ultimate rupture strain for the FRP sheets used in the experimental program is 0.017 mm/mm (17,000 micro-strain) as mentioned in Chapter 3.
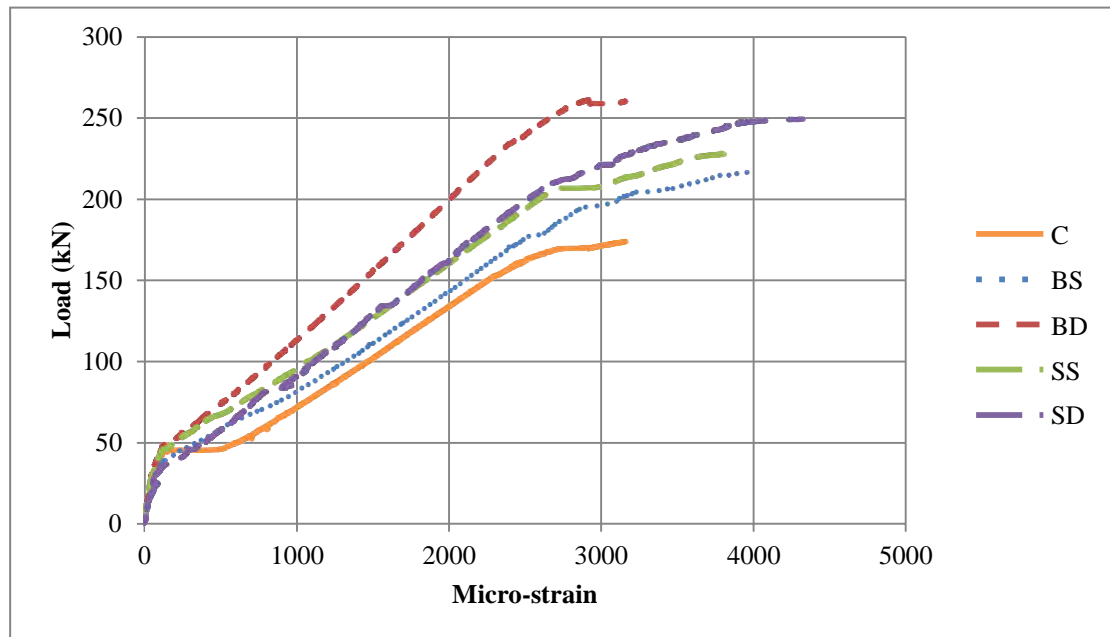
Figure 79: Steel strain response for Group C

Initially, the steel strain response showed in Figure 79 exhibited similar levels in the uncracked region, but afterwards the strain trends took different slopes according to the different CFRP configurations. The steel in the single ply specimens (BS and SS) reached the yield strain, and continued in yielding until the failure at corresponding ultimate load of 230 kN approximately. Despite the fact that (SS) has 33% more fibers over (BS), both specimens behaved similarly because of the high reinforcement ratio. In the same way, specimens (SD) and (BD) reached the yielding strain at the ultimate loads (approximately 260 kN for both) with additional strains in the plastic region of the steel.
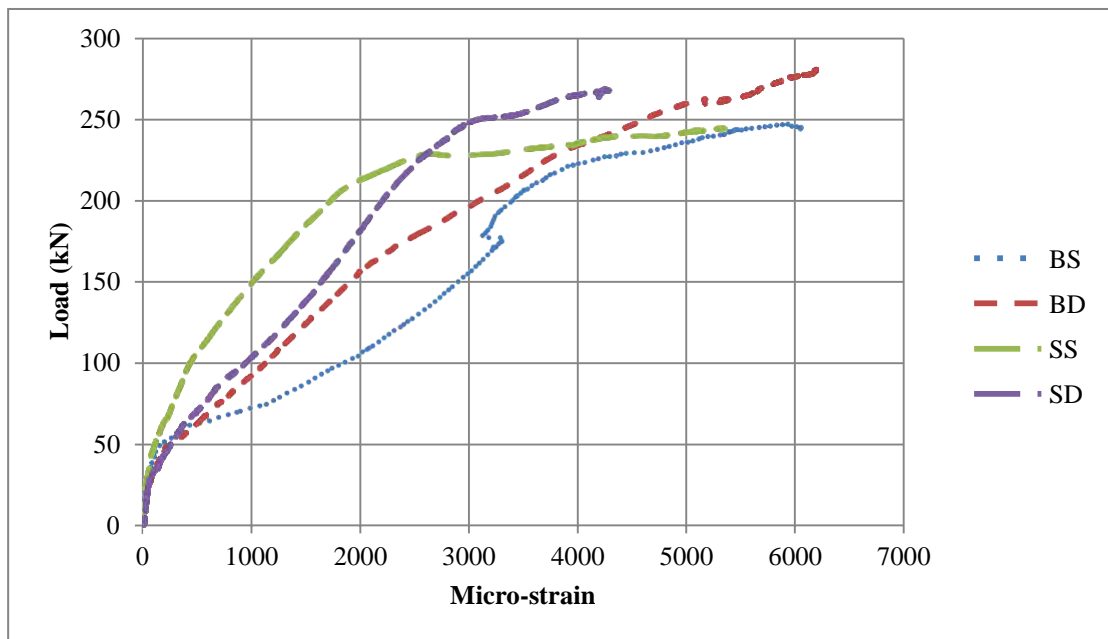
Figure 80: FRP strain response for Group A

For the CFRP strain response, the graph in Figure 80 shows that none of the specimens has reached the ultimate rupture strain. The bottom-bonded specimens (BS and BD) have the maximum utilization of the FRP materials with 6,000 and 6,200 micro-strain levels. However, beam (BD) has reached a higher ultimate load of 280 kN compared to the 245 kN load for (BS) specimen; which is technically logical considering that (BD) beam has double the amount of fibers. On the other hand, the side-bonded specimens (SS and SD) have recorded micro-strain levels of 5,300 and 4,300 with corresponding ultimate loads of 245 kN and 267 kN respectively. The previous strain levels for the FRP indicate that at higher reinforcement ratios, the bottom-bonded scheme is more efficient and more economical.

5.4 Conclusions

The first part of this section includes a general discussion on side strengthening and bottom strengthening as the reinforcement ratio increases in groups A, B and C. The second part discusses the depth of the side-bonded FRP and its effect on the overall performance of the beam specimens.

5.4.1 Groups A, B and C:

As explained before, the reinforcement increases from group A to C. This section summarizes the conclusions regarding side strengthening compared to bottom strengthening for both one sheet and double plies as the reinforcement ratio increases.

For single sheet strengthening, it is observed in group A that beam (BS) has a higher ultimate capacity and a higher deflection at failure compared to beam (SS). The percentage difference between them is 12% and deflection difference is 4.96 mm. This performance difference indicates that bottom-bonded strengthening is more effective than the side-bonded technique when the mild steel reinforcement ratio is relatively low. As we increase the reinforcement ratio in group B, beam (SS-1) has a higher strength. The percentage difference between both beams wasn't significant. It is equal to 2.43%. Beam (BS) still has the advantage over beam (SS-1) in deflection at failure with a difference of 3.21 mm. Consequently, with moderate reinforcement ratios, the strength performance of side-bonded FRP gets improved with less ductile failure. In group C, beam (BS) has a higher capacity but not significantly as the difference is equal to 1.24%. Beam (SS) has the advantage deflection as the difference is 3.61 mm. Therefore, the results of group C support the outcomes of group B, as the side-bonded specimen's strength has increased compared to the ductility behavior.

On the other hand, the case of two plies strengthening can be monitored in group A considering that beam (BD) has a slightly higher ultimate capacity compared to beam (SD). In addition, both specimens have a similar behavior in deflection at failure, which means close ductility factors. The percentage difference between them is 1.5% and deflection difference is 0.37 mm. As we increase the reinforcement ratio in group B, beam (BD) has a higher strength with 4.01% only. Beam (BD) also has the advantage over beam (SD-1) in deflection at failure with a difference of 2.26 mm. Similarly in group C, beam (BD) has a marginally higher capacity with 4.91% difference. Beam (SD) has the advantage deflection as the difference is 1.93 mm. The

results for groups A, B and C are converging to the idea that as the FRP ratio increases, the performance of side-bonded technique gets enhanced and relatively close to the bottom bonded strengthening.

The previous findings indicate the effectiveness of side-bonded FRP in flexure as the strength differences are in the range from 1% to 12%. Nonetheless, the behavior and performance differences are occurring due to many factors; the first factor is that the moment arm of bottom FRP is higher than the side-bonded ones. In other words, the FRP depth (d_f) is higher in bottom strengthening than in side strengthening which creates a higher moment arm resisting the applied moment.

As a result, the engineer had to use 100 mm FRP sheets on the sides to provide an equivalent amount of force to the 150 mm bottom-bonded FRP; which expresses heavily towards the material efficiency in bottom strengthening technique. Another important factor for the performance differences is the FRP force distribution. The side-bonded FRP has a trapezoidal force distribution compared to the uniformly distributed force in the bottom sheets. The inconsistency of the force distribution in the side-bonded sheets will allow the extreme bottom fibers to reach the debonding strain before the higher ones. This dominos mechanism will permit the global sheet failure even if the higher fibers have not reached their debonding strain. In other words, when the side strengthened beams are tested; the sheets will start to debond from the bottom, and continue to debond fully faster than the bottom strengthened beams. The rapid debonding happens because the strain level is not constant over the FRP side-bonded sheets, whereas it is maximized in bottom strengthened beams.

5.4.2   Side-bonded FRP depths effects:

This section will show the increase in ultimate capacity due to the increase in FRP width on the sides. For single ply side-bonded FRP, group B has three different side-strengthening using one layer of fiber, which are beams (SS-1), (SS-2) and (SS-3). The graph in Figure 81 below shows the difference in ultimate capacities as the width of the sheet increases for one ply. The trend of the graph is logarithmic, which means that as the side-bonded FRP width increases, the additional incremental load gets smaller.
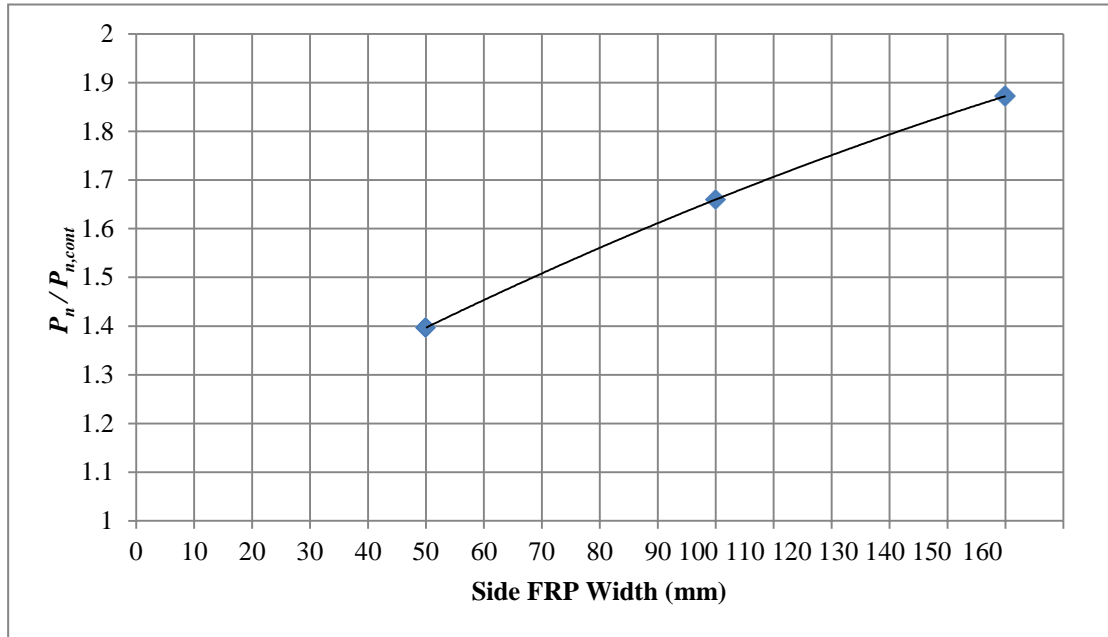
Figure 81: Ultimate load comparison between single ply side-bonded strengthening

The difference in strength between 50 mm sheets and 100 mm sheets is 17.2% while it is equal to 12% among 100 mm and 150 mm FRP sheets. This indicates the effectiveness of increasing the depth of the FRP sheets, yet as the sheet gets closer to the neutral axis of the section, the efficiency of the fibers reduces. In other words, as we increase the depth of FRP, the contribution of the sheets in enhancing the ultimate capacity decreases, which leads to wasting more materials.

The second case is comparing double plies side strengthening in group B, which are (SD-1), (SD-2) and (SD-3) specimens. The graph in Figure 82 shows the difference in enhancing the ultimate capacity as the width of the sheet increases for double plies. Similarly, the trend of the curve is logarithmic even more that the single-ply case. This indicates the lower efficiency for multiple CFRP plies considering wider sheets.

The strength difference from the 50 mm sheets to 100 mm ones is 15.3%, while it is equal to only 4.5% when the sheets increase from 100 mm to 150 mm. This corroborates the previous conclusion which is that increasing the width of the FRP on the sides will decrease the effectiveness of the sheets in enhancing the ultimate strength of RC beams. Moreover, the depth increase has a more severe effect, as the double plies improved only by 4.5% compared to the single ply case.
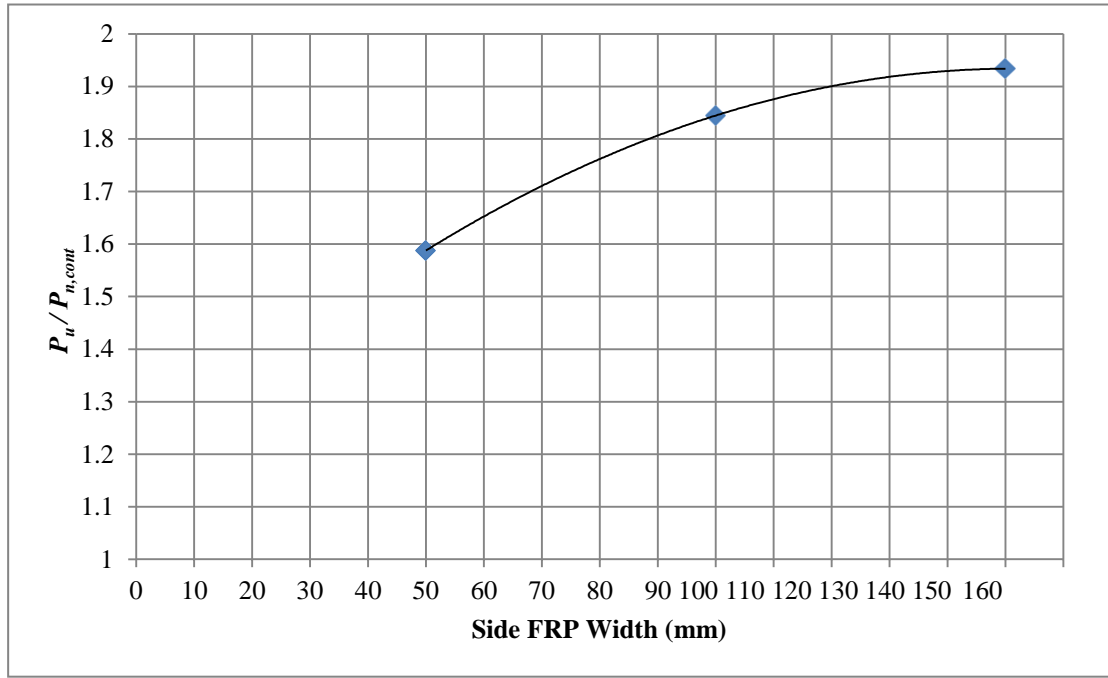
84

Figure 82: Ultimate load comparison between double plies side-bonded strengthening

5.4.3 Side-bonded FRP effectiveness with different steel reinforcement ratios:

Technically, external CFRP reinforcement improves the strength of structural elements to a certain extend. The main steel flexural reinforcement affects the contribution of the CFRP in the global strength performance. Groups A, B and C have different steel reinforcement ratios, and each group has two side-bonded specimens. Figure 83 plots the ultimate load improvement for the side-bonded specimens (SS and SD) versus the steel reinforcement ratio ($\rho_{steel} = A_s / bd$).

The graph shows that as the steel reinforcement ratio increases, the capacity improvement ($P_u / P_{u, C}$) reduces. In other words, as the steel reinforcement ratio rises, the contribution of the CFRP shrinks because the steel elastic modulus is three times higher than that of the CFRP. Therefore, the steel is stiffer material which will absorb more load than CFRP at any elastic strain level, which leads to reduce the contribution of the CFRP with higher reinforcement within a section. Accordingly, RC beam specimens with higher reinforcement ratios will fail in a brittle mode by concrete crushing or CFRP debonding upon yielding of the steel reinforcement.
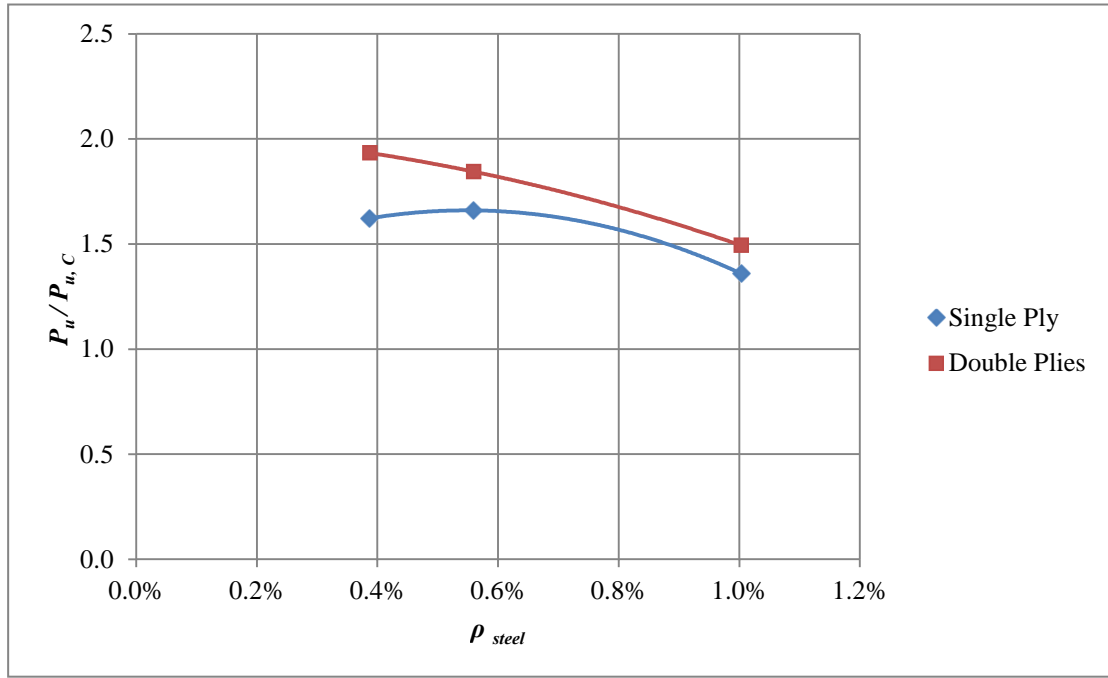
Figure 83: P_u / $P_{u, C}$ vs. Steel ratio

All the previous results and findings are emphasizing the effectiveness of the side-bonded FRP strengthening. However, it has proven that the bottom-bonded technique is more efficient and more economical due to the deeper moment arm and the consistency of the strain level in the fibers. Generally, the side-bonded FRP is more effective with moderate steel reinforcement ratios, as the global performance develops similar behavior to the bottom-bonded beams in strength as well as ductility. Nevertheless, as the side-bonded sheets depth gets closer to the neutral axis of the composite section, the overall FRP contribution decreases. Consequently, it is recommended in further studies to cut the sheets to smaller ones with the same total width; the purpose of this technique is to avoid the global FRP failure when the extreme lower fibers reach the debonding strain.

5.5   Experimental Program Data Summary

Table 15 in section 5.5 summarizes all the specimens' data, results, and changes in strength and ductility. The ductility of a specimen is measured by ultimate ductility index ($I_u = \delta_u / \delta_y$) and failure ductility index ($I_f = \delta_f / \delta_y$).

Table 15: Summary of data

Group	Specimen	δ_y (mm)	δ_u (mm)	δ_f (mm)	Failure Mode	$I_u = \delta_u / \delta_y$	$I_u / I_{u,C}$	% Decrease	$I_f = \delta_f / \delta_y$	$I_f / I_{f,C}$	% Decrease
GA	C	6.2	19.6	24.0	SC	3.15	1.00	-	3.85	1.00	-
	BS	10.6	19.0	19.3	SF	1.80	0.57	42.8%	1.82	0.47	52.7%
	BD	7.1	12.1	12.3	SCF	1.70	0.54	45.9%	1.74	0.45	55.0%
	SS	5.6	13.0	13.3	SCF	2.33	0.74	26.0%	2.39	0.62	38.1%
	SD	7.5	12.0	12.5	SF	1.59	0.51	49.4%	1.66	0.43	57.0%
GB	C	5.0	13.9	20.1	SC	2.74	1.00	-	3.98	1.00	-
	BS	8.0	18.3	18.4	SCF	2.28	0.83	16.8%	2.30	0.58	42.3%
	BD	8.7	15.3	15.3	SF	1.77	0.64	35.6%	1.77	0.44	55.6%
	SS-1	7.0	14.7	15.2	SCF	2.09	0.76	23.8%	2.17	0.54	45.5%
	SS-2	9.8	16.5	16.8	SCF	1.68	0.61	38.8%	1.72	0.43	56.9%
	SS-3	7.6	14.4	15.2	SCF	1.89	0.69	31.1%	1.99	0.50	50.1%
	SD-1	8.8	12.9	13.1	SCF	1.47	0.54	46.4%	1.49	0.37	62.5%
	SD-2	8.9	15.1	15.9	SCF	1.69	0.62	38.4%	1.77	0.45	55.5%
	SD-3	7.6	13.1	13.3	SF	1.74	0.63	36.7%	1.75	0.44	56.0%
GC	C	5.2	10.1	20.0	SC	1.93	1.00	-	3.84	1.00	-
	BS	7.2	12.0	12.6	SCF	1.67	0.87	13.4%	1.75	0.46	54.5%
	BD	8.3	12.6	15.8	SCF	1.52	0.79	21.1%	1.91	0.50	50.3%
	SS	8.1	12.5	16.2	SCF	1.55	0.81	19.5%	2.01	0.52	47.7%
	SD	8.7	13.3	13.8	SCF	1.53	0.79	20.6%	1.59	0.41	58.6%

Chapter 6: Analytical Models

This chapter will discuss the experimental results validation using two technical concepts to create analytical models that predict the behavior of the tested specimens. The first concept is the effective flexibility of cracked reinforced concrete section. This model was used to predict the load-deflection behavior of the specimens. The second concept is strain compatibility within the composite section which is used to estimate the ultimate load carrying capacity and mode of failure using ACI-440.2R-08 design guidelines.

6.1. Flexibility Model for Cracked Sections

Flexibility in general is the reciprocal of the stiffness of the structural element. Flexibility and stiffness are mechanical properties of a cross-section, which is used to predict the deflection of structural elements under loadings. The flexibility of flexural reinforced concrete elements needs a combination of theoretical and empirical approaches, as they crack under the loading due to the low concrete modulus of rupture. Stiffness and flexibility are well-developed for conventional concrete members. However, flexural elements strengthened with FRP composites have more complications due to the differences in the mechanical properties between FRP and mild steel. The flexibility of the FRP strengthened members in flexure can be calculated using the semi-empirical equations presented in the ACI-440.2R-08.

The equation used to find the effective flexibility is [30]:

$$\frac{1}{E_c I_{eff}} = \frac{1}{E_c I_{cr}} [1 + \frac{\omega}{1 + \omega}] \le \frac{1}{E_c I_g} , \qquad for\ M \ge M_{cr} \tag{1}$$

where:

$$\omega = (\frac{M_{cr}}{M})^3 \beta_d \frac{I_g}{I_{cr}} - 1) \tag{2}$$

and,

$$\beta_d = \alpha_b (\frac{E_f}{E_s} + 1) , \alpha_b = 0.5 \tag{3}$$

The terms used in the equations are:

E_c = Modulus of elasticity of concrete (MPa)

E_f = Modulus of elasticity of CFRP sheets (MPa)

E_s = Modulus of elasticity of steel (MPa)

M = The applied bending moment on the element (N-mm)

M_{cr} = The cracking moment of reinforced concrete (N-mm)

I_g = Gross moment of inertia (mm^4)

I_{cr} = Cracked moment of inertia (mm^4)

α_b = FRP balancing factor.

These equations are used to calculate the flexibility of the tested beams under the loading. ACI-440.2R-08 flexibility model assumes a gross moment of inertia of the section before reaching the cracking moment of a section. The cracking moment is calculated according to the concrete gross area without any reinforcement. Afterwards, the model uses an empirical combination of the gross moment of inertia and the fully cracked one to estimate the instant flexibility of the section according to the applied load at that specific instant. Therefore, as the applied load increases, the stiffness of the section reduces, since the concrete will crack more and the neutral axis will change for each single load increment. Afterwards, the flexibility is used to calculate the mid-span deflection of the section at any time increment according to the following equation:

$$\Delta_{max} = \frac{Pa}{24} \left(\frac{1}{E_c I_{eff}} \right) (3l^2 - 4a^2) \qquad (4)$$

where:

P = The applied load (N)

a = The shear span of the point load from the support in the two-point loading configuration (mm)

E_c = Modulus of elasticity of concrete (MPa)

I_{eff} = Effective moment of inertia (mm^4)

l = The total beam's span (mm)

Moreover, the load-deflection response curves for Group B have been plotted with two different cracking moments. The first is the conventional cracking moment calculated using the concrete gross area only to resist the tension before the first crack. The second approach is to calculate the cracking moment using the transitional section with the CFRP; as the fibers are substituted with an equivalent concrete section, and the cracking moment is calculated according to the new section. The modified cracking moment is calculated to examine the effect of CFRP in the load-deflection response at the pre-cracking stage.

The specimens' actual load-deflection data are compared with the predicted curves developed by the analytical model. The solid line represents the actual data, the dashed line represents the predicted curves with the conventional cracking moment, and the dotted curves in group B are the predicted response with the modified cracking moment using the transitional section.

6.2. Beams Graphs and Predicted Curves

Figures 84-102 show the predicted load-deflection curves for all the specimens with comparison to the actual curves imported from the testing data.
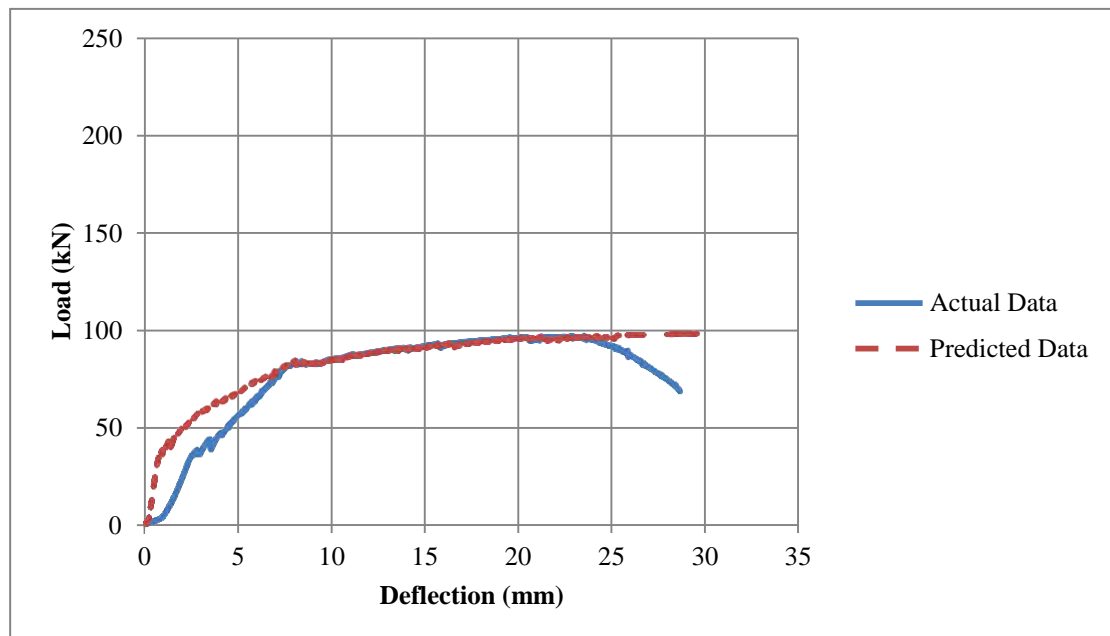
6.2.1 Group A

Figure 84: Beam (GA-C) actual and predicted load-deflection curves
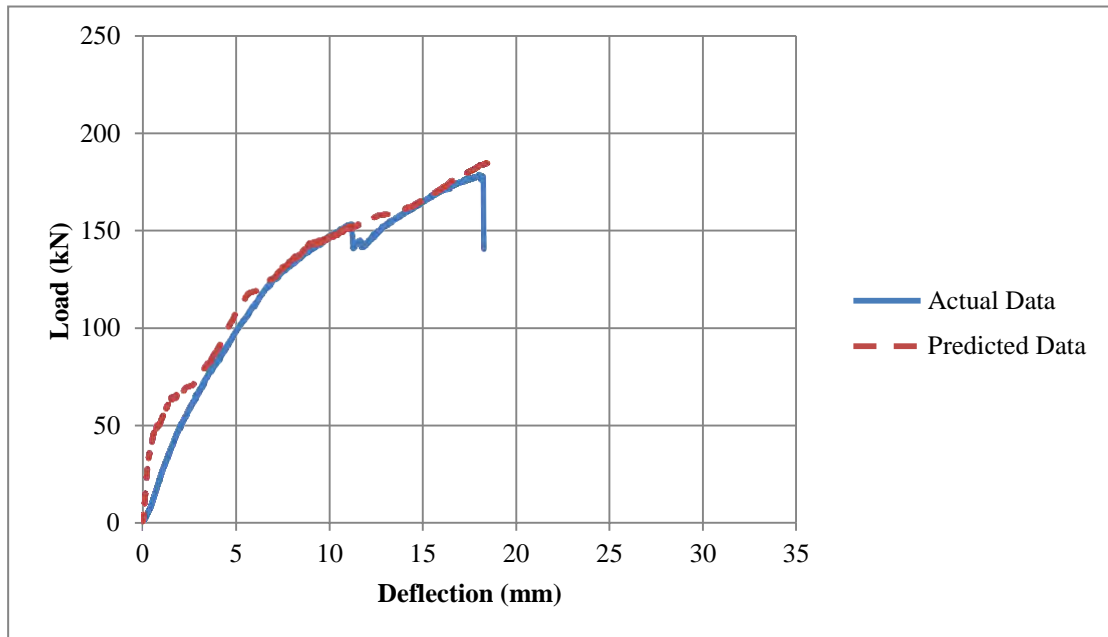
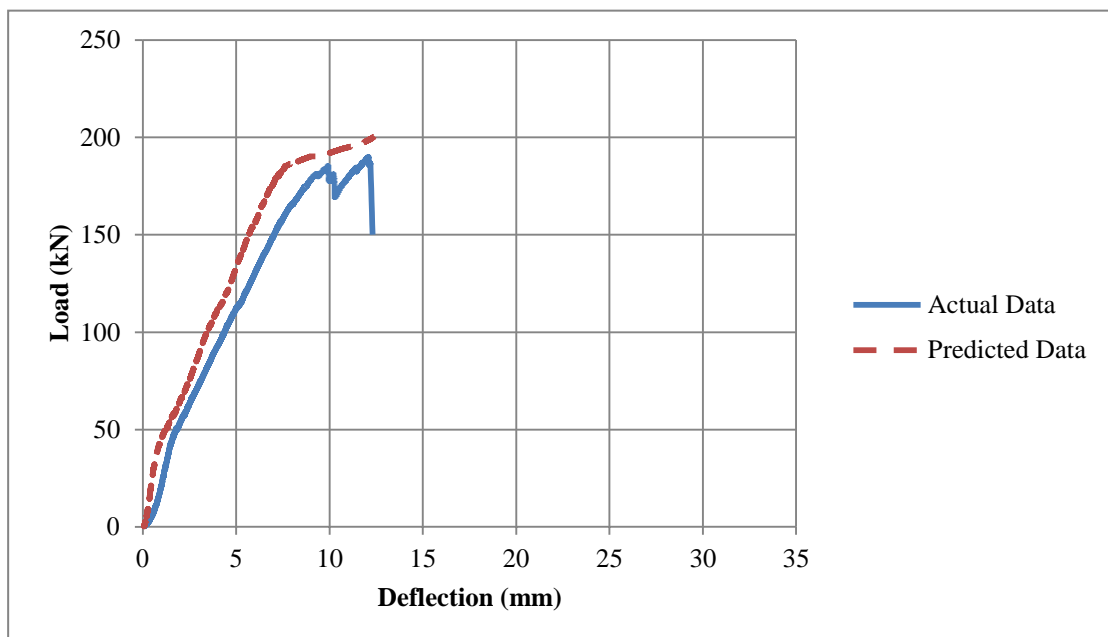Figure 85: Beam (GA-BS) actual and predicted load-deflection curves

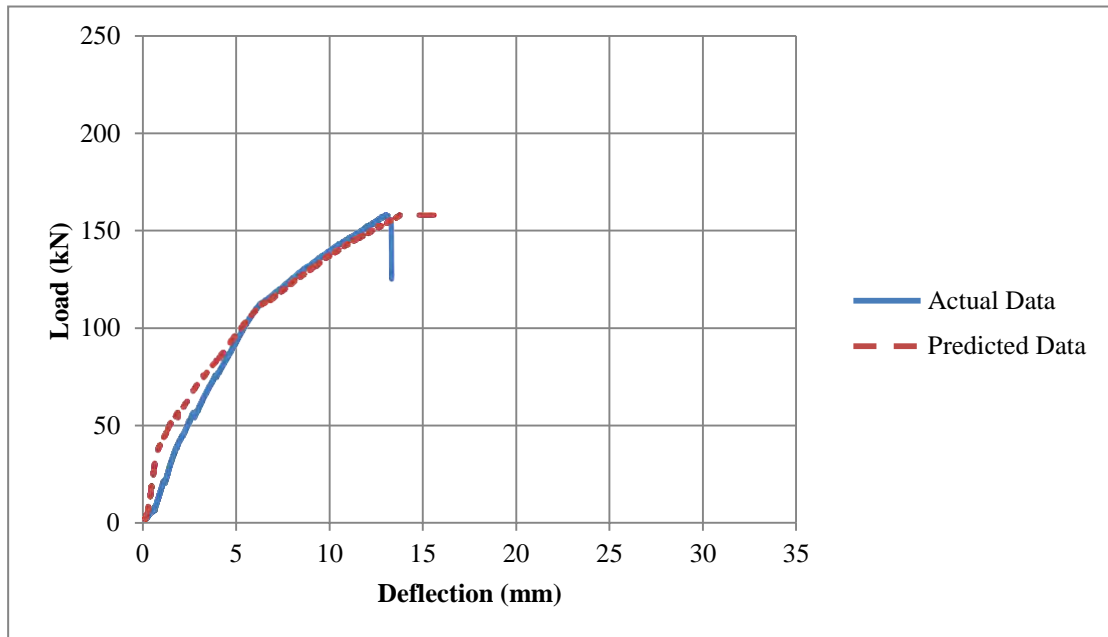Figure 86: Beam (GA-BD) actual and predicted load-deflection curves

91

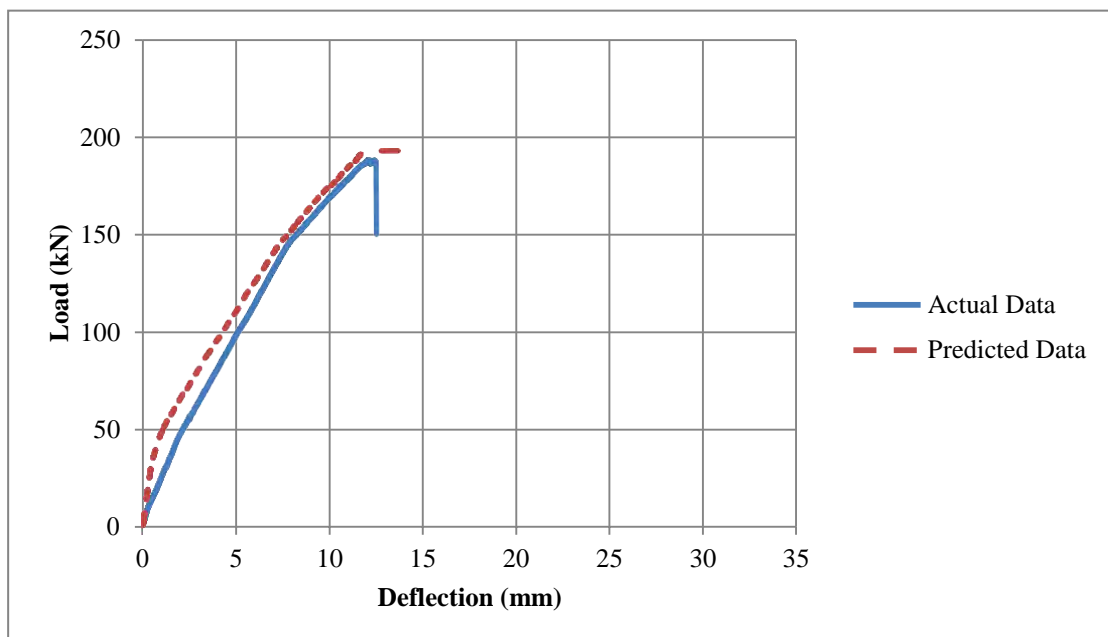Figure 87: Beam (GA-SS) actual and predicted load-deflection curves

Figure 88: Beam (GA-SD) actual and predicted load-deflection curves
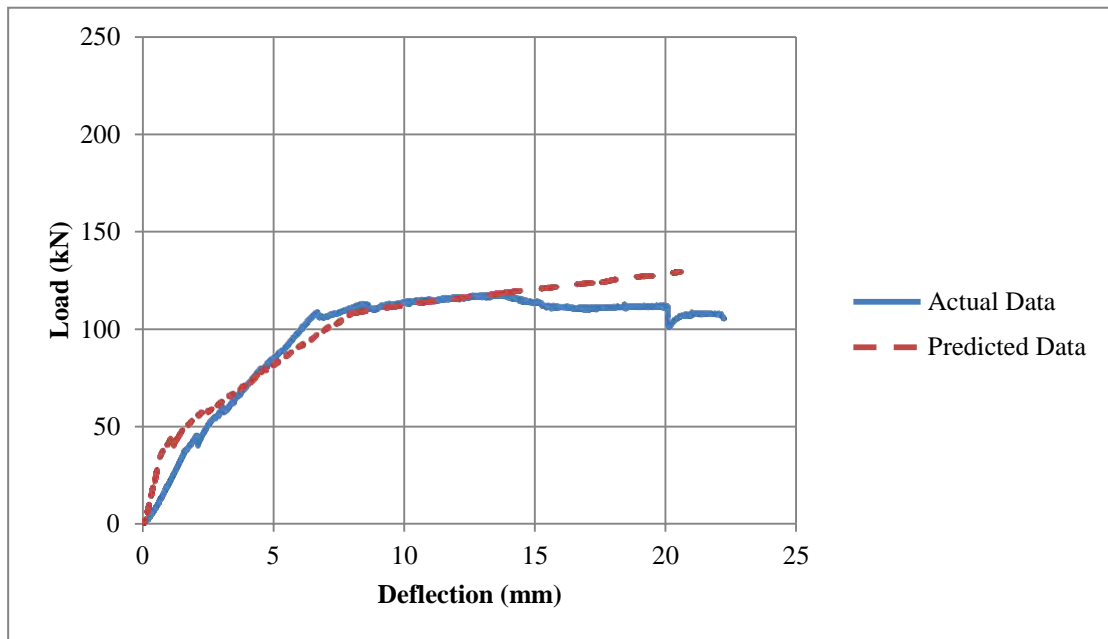
6.2.2   Group B

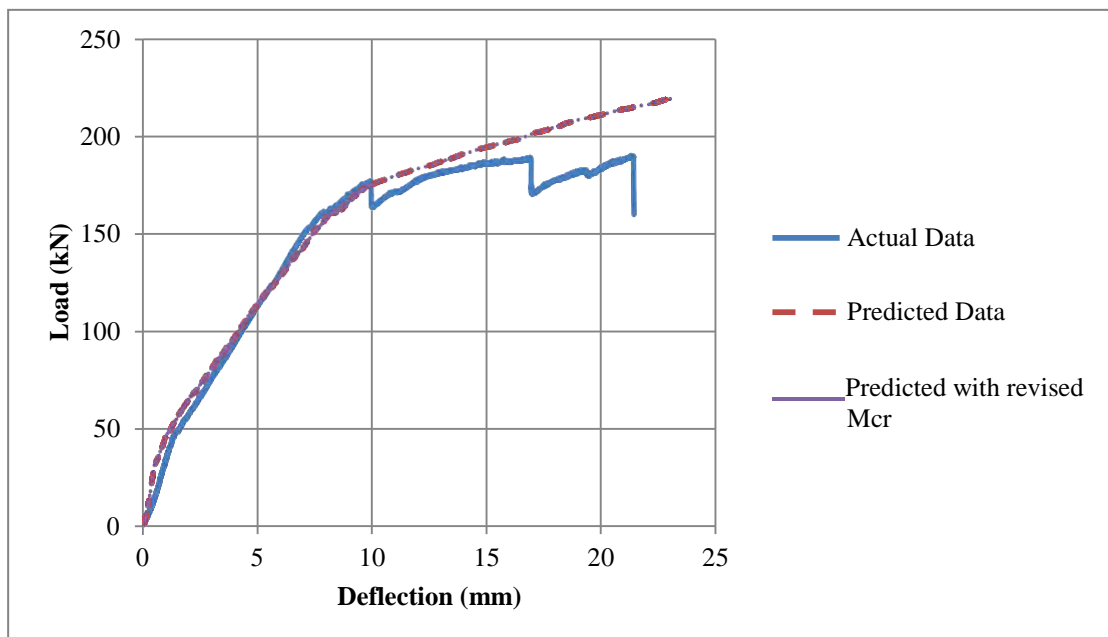Figure 89: Beam (GB-C) actual and predicted load-deflection curves

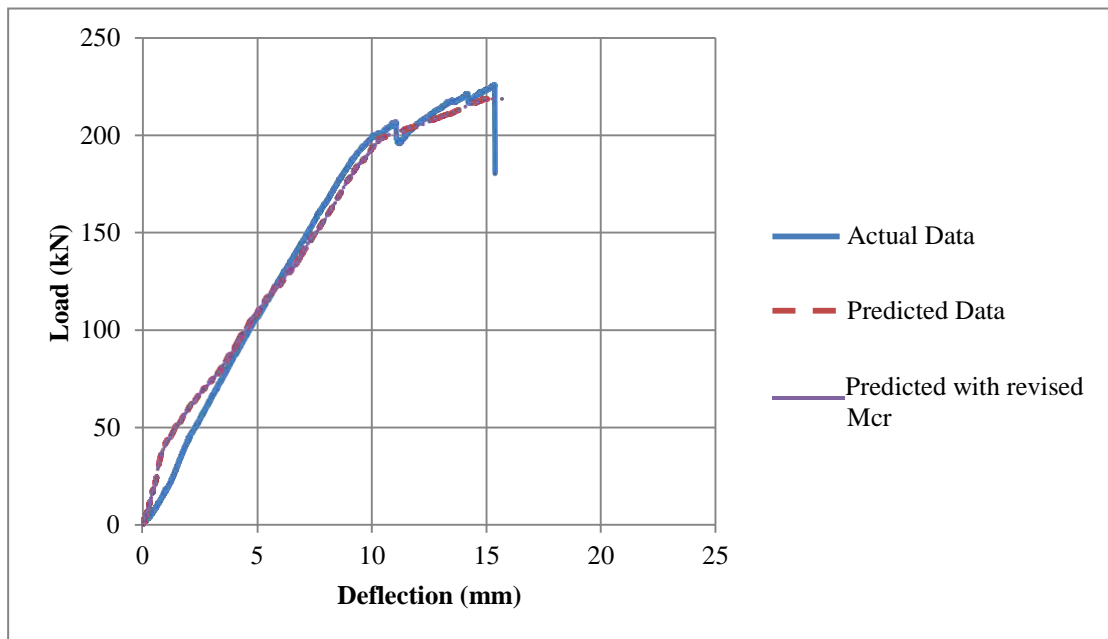Figure 90: Beam (GB-BS) actual and predicted load-deflection curves

Figure 91: Beam (GB-BD) actual and predicted load-deflection curves

Figure 92: Beam (GB-SS-1) actual and predicted load-deflection curves

Figure 93: Beam (GB-SS-2) actual and predicted load-deflection curves

Figure 94: Beam (GB-SS-3) actual and predicted load-deflection curves
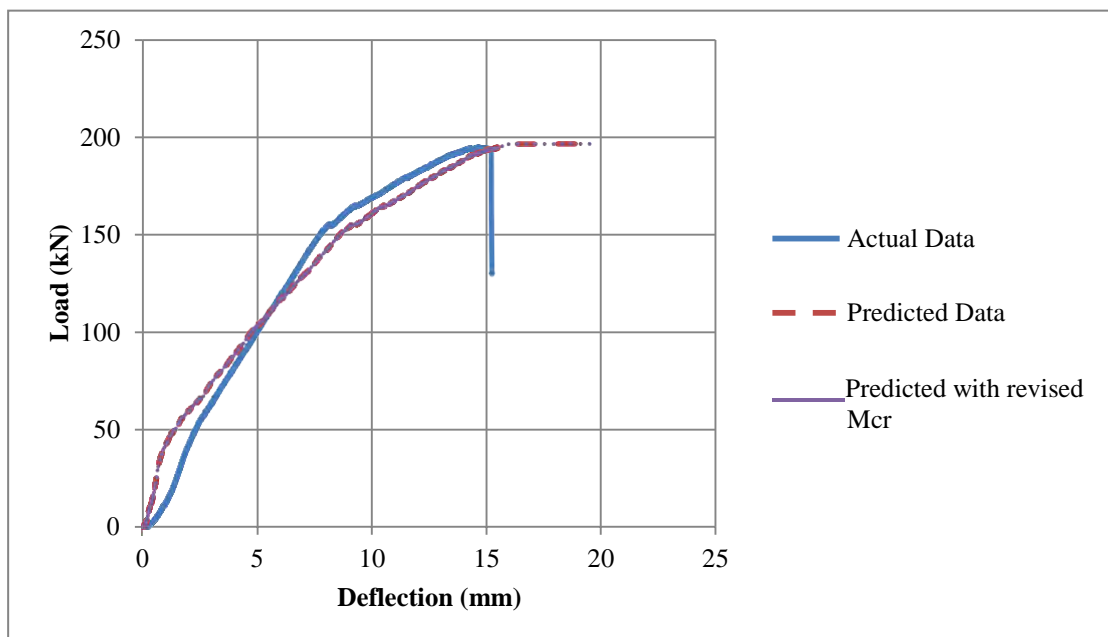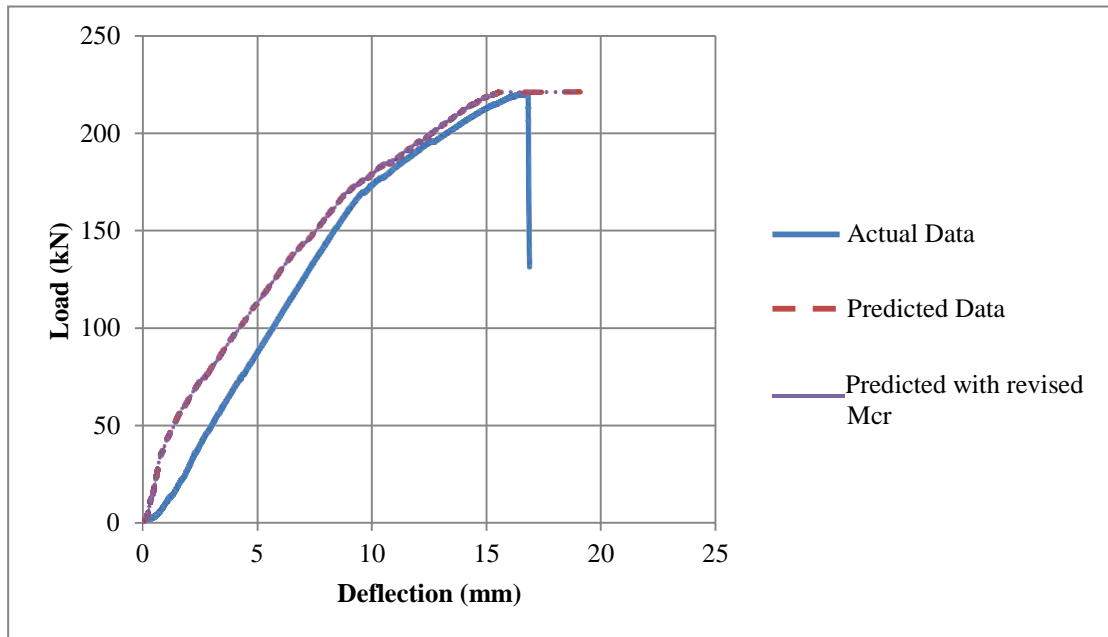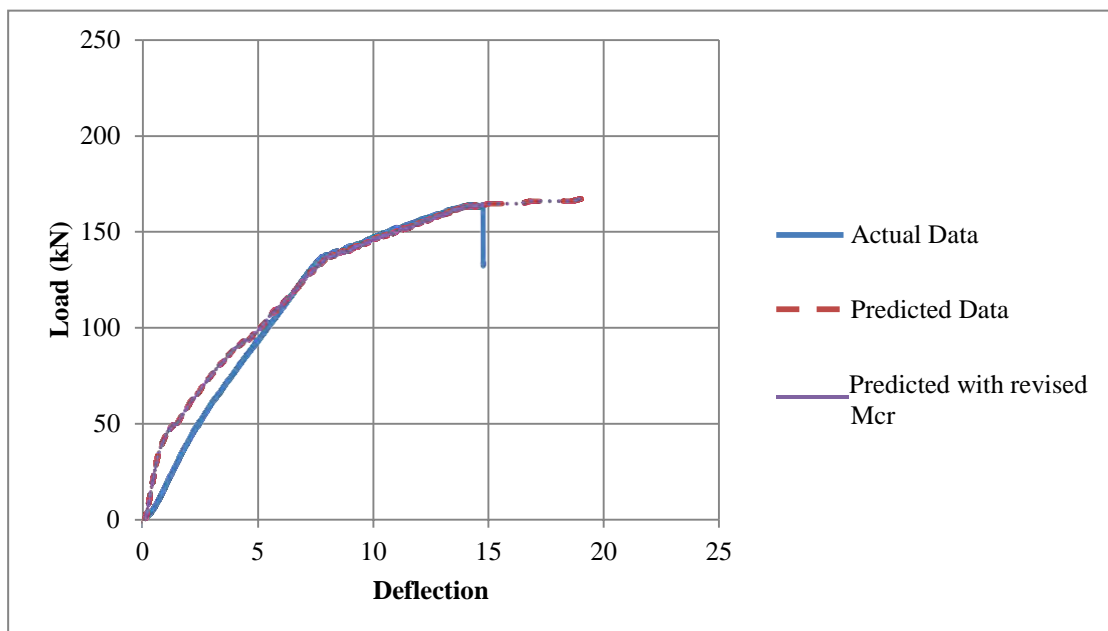
Figure 95: Beam (GB-SD-1) actual and predicted load-deflection curves

Figure 96: Beam (GB-SD-2) actual and predicted load-deflection curves

Figure 97: Beam (GB-SD-3) actual and predicted load-deflection curves
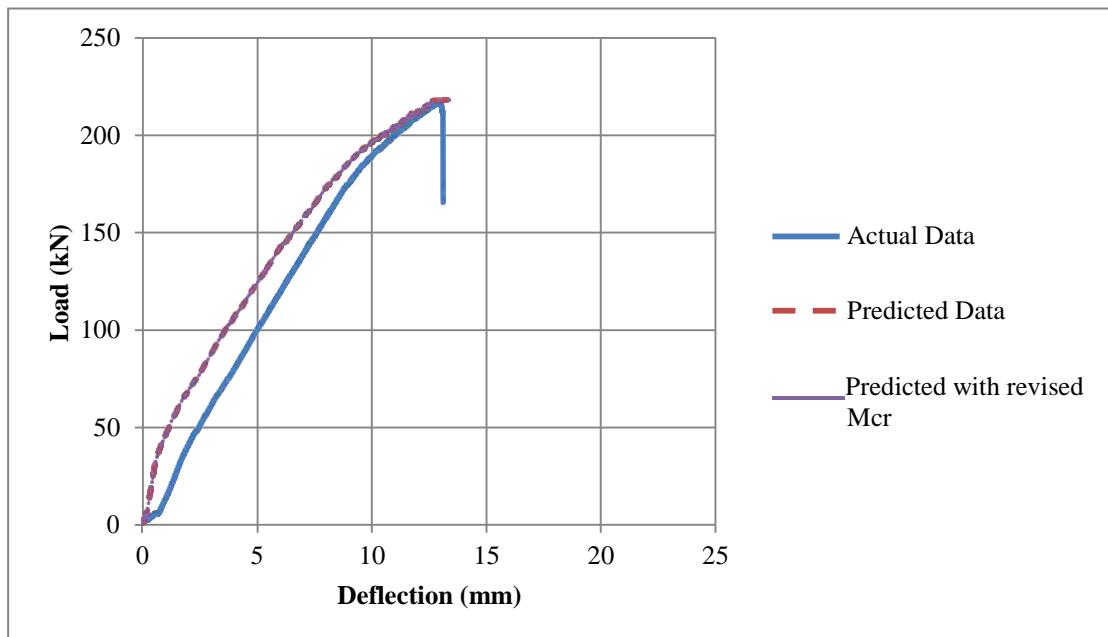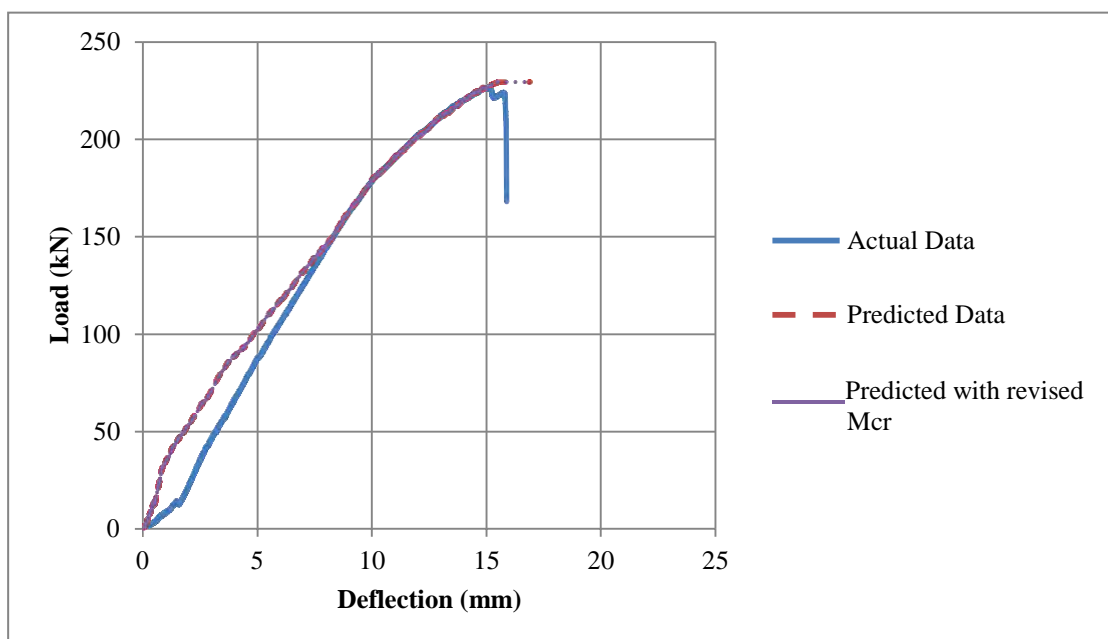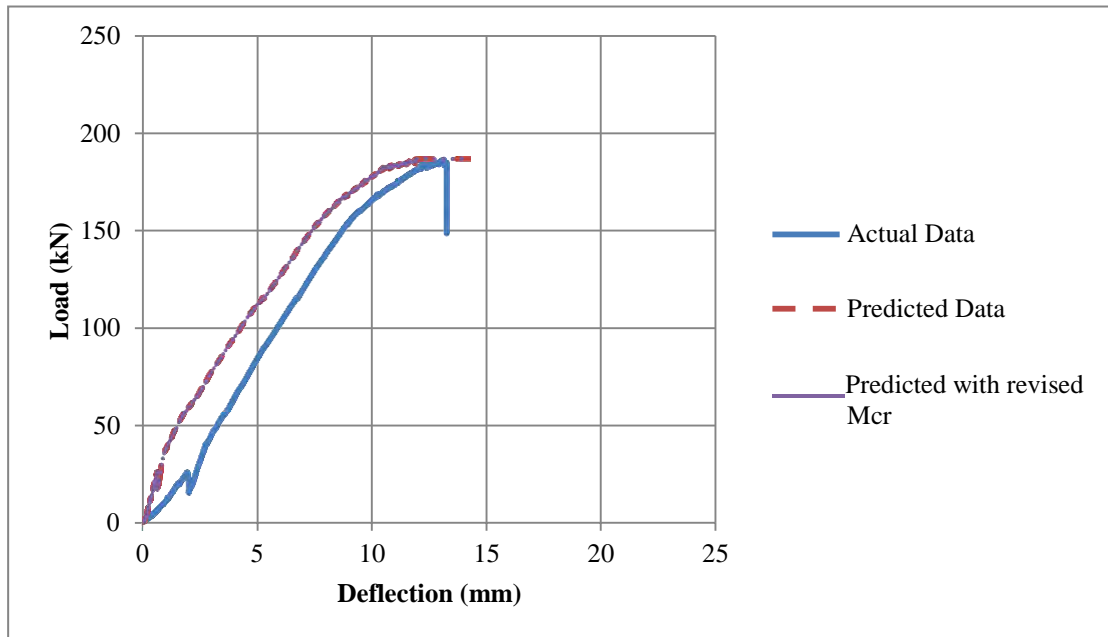
6.2.3 Group C
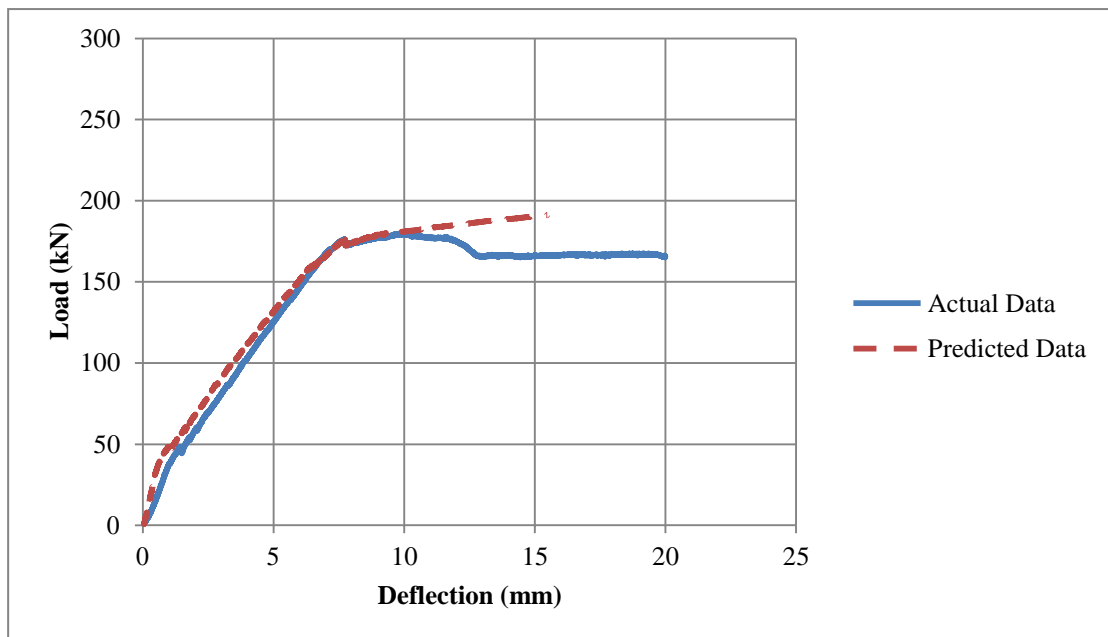
Figure 98: Beam (GC-C) actual and predicted load-deflection curves
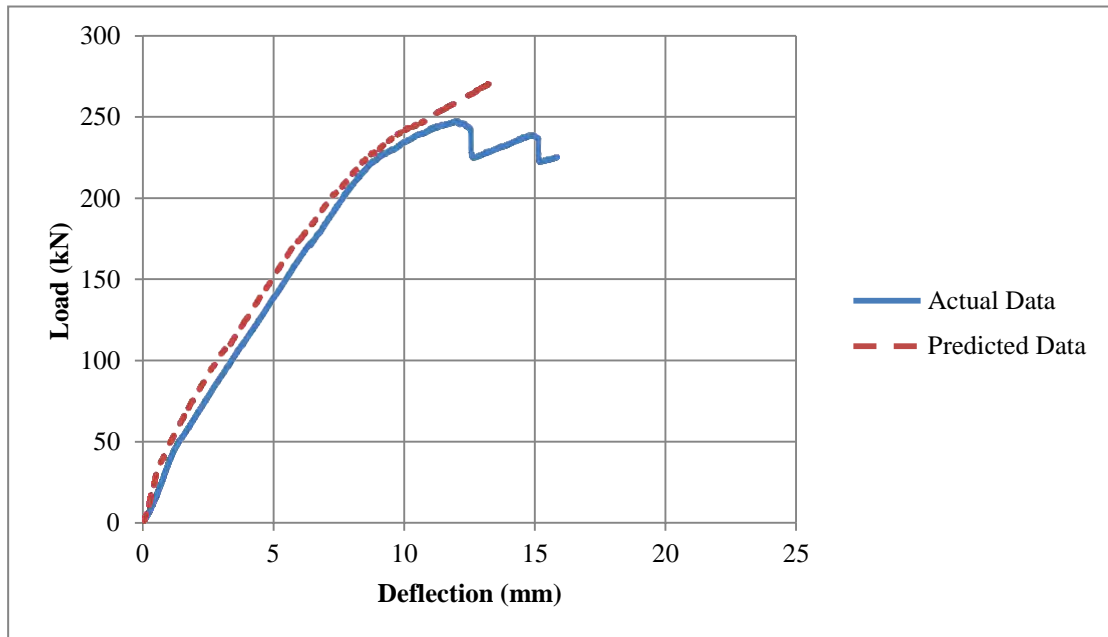
Figure 99: Beam (GC-BS) actual and predicted load-deflection curves
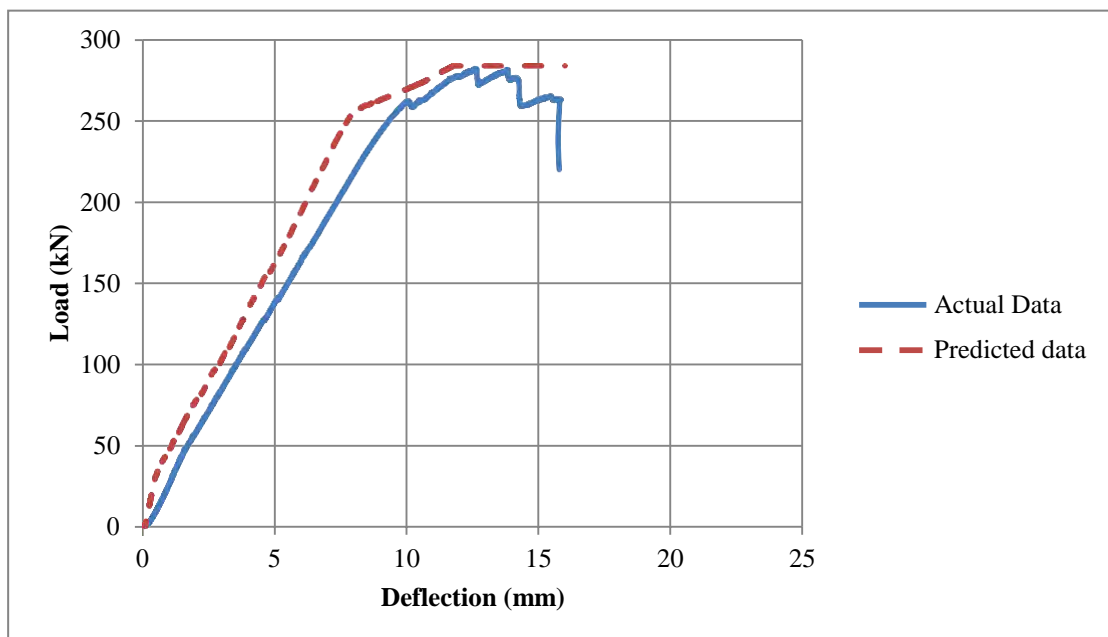
Figure 100: Beam (GC-BD) actual and predicted load-deflection curves
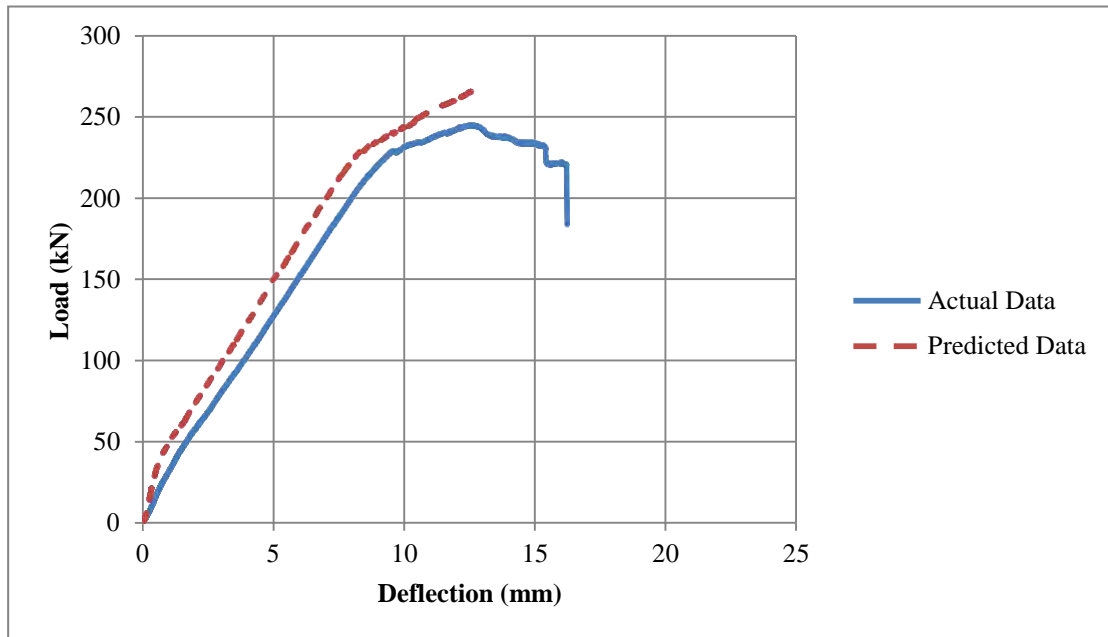
Figure 101: Beam (GC-SS) actual and predicted load-deflection curves
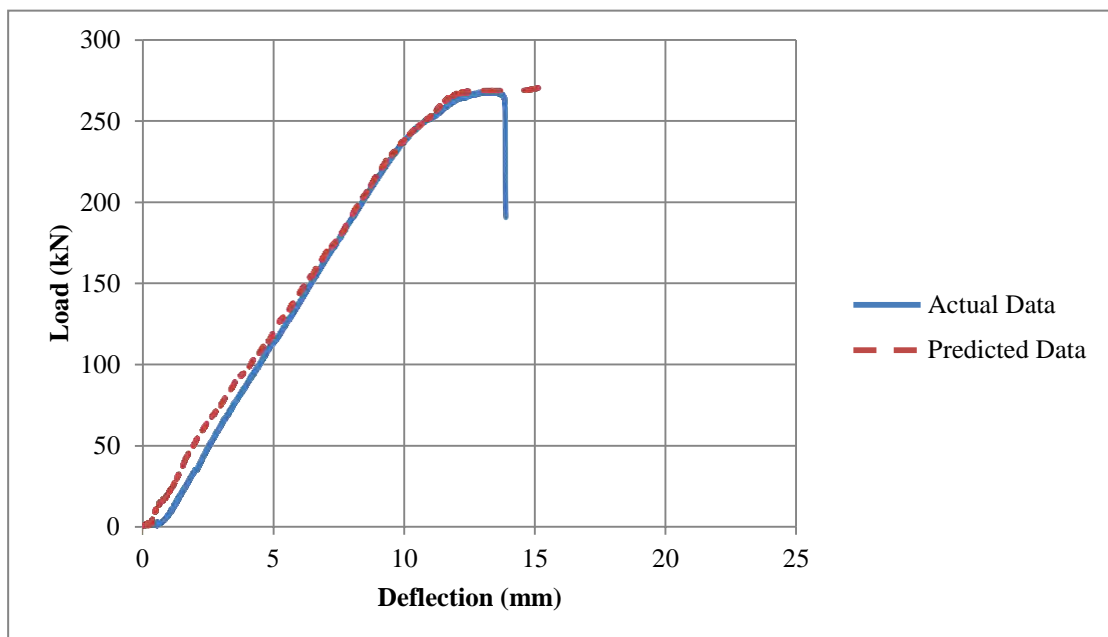
Figure 102: Beam (GC-SD) actual and predicted load-deflection curves

Generally, the graphs show that the cracking moment, the stiffness of an element is overestimated as the slope is higher than the actual values. Afterwards, when the load reaches the theoretical cracking moment, the model presents more precise deflection values within the elastic range of section. After reaching the ultimate limit state, the model deviates from the actual behavior, and it does not predict the failure mode. The ACI-440.2R-08 flexibility model validates the actual

results of the tested specimens; and the predictions shown previously are taking similar behavior trends to the actual load-deflection curves before reaching the inelastic range. In addition, the predicted response curves with the conventional cracking moment opposed to the modified one are matching; which mean the effect of the CFRP in the analytical model is minor and can be ignored.

6.3. Ultimate Moment Capacity Predictions

This section presents details of calculating the ultimate strength of an FRP strengthened beam; and then compares the predicted ultimate load to the actual one. ACI-440.2R-08 design guidelines provides equations to calculate the ultimate moment depending on strain compatibility and force equilibrium within the section.

The general assumptions to find the ultimate capacity of reinforced concrete in flexure are: 'Plane sections remain plane before and after bending' which means that the strain relationship varies linearly within the cross section. The tensile capacity of concrete is completely ignored. Moreover, perfect bond is assumed between the concrete and steel, which means they have the same strain on the steel level. The maximum compressive strain of the concrete is 0.003mm/mm and the stress beyond the yield point of the steel is assumed to be constant until failure.

The typical failure mode of the FRP-strengthened beams is yielding of the steel then crushing of the concrete without FRP brittle debonding failure. Figures 103 and 104 below show the forces introduced in the reinforced concrete cross section [5].
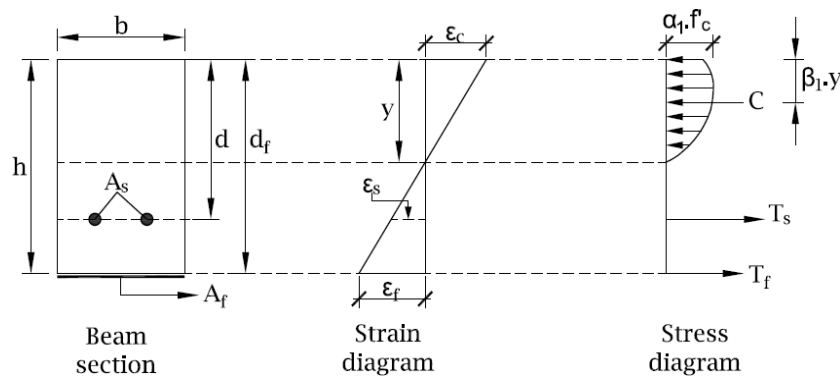

Figure 103: Stress and strain for bottom strengthening
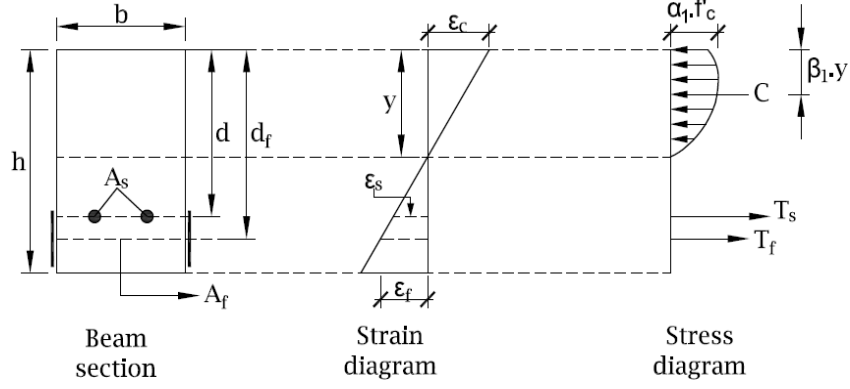
Figure 104: Stress and strain for side strengthening

The compressive force in the concrete (C) is found by the equation:

$$C = \alpha_1 \, \beta_1 \, f'_c \, b \, y \qquad (5)$$

While the tension force from the steel (T_S) is calculated by:

$$T_s = A_s \, \varepsilon_s \, E_s \qquad (6)$$

The strain of the FRP in the section (ε_f) is found by:

$$\varepsilon_s = \varepsilon_c \frac{d - y}{y} \qquad (7)$$

And the tension force from the FRP (T_S):

$$T_f = A_f \, E_f \, \varepsilon_f \qquad (8)$$

The strain of the FRP in the section (ε_f) is found by:

$$\varepsilon_f = \varepsilon_c \frac{d_f - y}{y} \qquad (9)$$

The balance of the forces produces the following equations:

$$(\alpha_1 \, \beta_1 \, b \, f'_c \, y) - (A_s \, \varepsilon_s \, E_s) - A_f \, E_f \, \varepsilon_f = 0 \qquad (10)$$

$$(0.5\alpha_1 \, \beta_1 \, b \, f'_c)y^2 + (A_s \, \varepsilon_s \, E_s)(d - y) + A_f \, E_f \, \varepsilon_f(d_f - y) = 0 \qquad (11)$$

After satisfying the equilibrium equations, the ultimate moment is calculated using this equation:

$$M_n = T_s \left(d - \frac{\beta_1 y}{2}\right) + T_f \left(d_f - \frac{\beta_1 y}{2}\right) \qquad (12)$$

Where: α_1 and β_1 are concrete compression block parameters.

Instead of solving the quadratic equation, an iterative process can be used. The procedure is to assume a mode of failure of the beam, and assume the depth of the neutral axis. Then, we need to recalculate the depth of the neutral axis and reiterate until force equilibrium and strain compatibility are satisfied. Note that all reduction factors are dropped from the calculation process, as the nominal capacity is required to be calculated not the factored one.

Table 16 shows the ultimate loads predicted and actual experimental loads; the results indicate that in most of the cases, the code gives conservative estimates for (P_n).

The results of the predicted values and the actual values were plotted in Figure 105, where P_u is represented in the y-axis and P_n is in the x-axis. A pseudo line was graphed which illustrates 100% utilization ($P_u / P_n = 1.0$). In fact, the purpose of this line is to easily compare and understand if the code is over or under estimating the ultimate capacity of the sections. In other words, the points which are above the inclined line are over-estimated by the code, and all the points below it are considered as conservative estimates. In addition, linear regression for all the points was carried out to determine the Coefficient of Determination (R^2), which equals to 0.9669. The R^2 value measures the precision of the data, which means ACI-440.2R-08 predictions are around the regression line 96.69% of the times.

Moreover, the ultimate loads of the side-bonded strengthened specimens are usually over-estimated. The reason behind that is that the calculations assume a uniform form distribution along the sheet, which is not the case in fact. Actually, the form is trapezoidal along the side-bonded fibers, which pushes the extreme lower fibers to reach the debonding strain. This failure mechanism was not captured properly in the ultimate load calculations. However, the error is still within an acceptable range considering the fact that the calculations did not include any materials reduction factors.

6.4.   Predicted Ultimate Loads using ACI-440.2R-08

Table 16: Summary of load predictions

Group	Specimen	$P_{u,,exp}$ (kN)	% $P_{u, exp}$ increase	$P_{u,,pred}$ (kN)	% Error	$P_{u,,exp}/P_{u,,pred}$
GA	C	97.3	-	75.1	22.8%	1.30
	BS	178.4	83.3%	174.2	2.4%	1.02
	BD	189.8	95.0%	186.3	1.8%	1.02
	SS	157.9	62.2%	150.9	4.4%	1.05
	SD	188.2	93.3%	190.2	-1.1%	0.99
GB	C	117.4	-	104.0	11.4%	1.13
	BS	190.2	62.0%	185.7	2.4%	1.02
	BD	225.4	92.0%	220.2	2.3%	1.02
	SS-1	194.9	66.0%	200.5	-2.9%	0.97
	SS-2	219.8	87.2%	204.9	6.8%	1.07
	SS-3	164.0	39.7%	161.2	1.7%	1.02
	SD-1	216.6	84.4%	230.5	-6.4%	0.94
	SD-2	227.1	93.4%	239.7	-5.6%	0.95
	SD-3	186.4	58.8%	183.9	1.3%	1.01
GC	C	179.9	-	175.8	2.3%	1.02
	BS	247.4	37.5%	239.6	3.1%	1.03
	BD	282.2	56.8%	276.0	2.2%	1.02
	SS	244.3	35.8%	248.6	-1.7%	0.98
	SD	268.6	49.3%	279.5	-4.0%	0.96

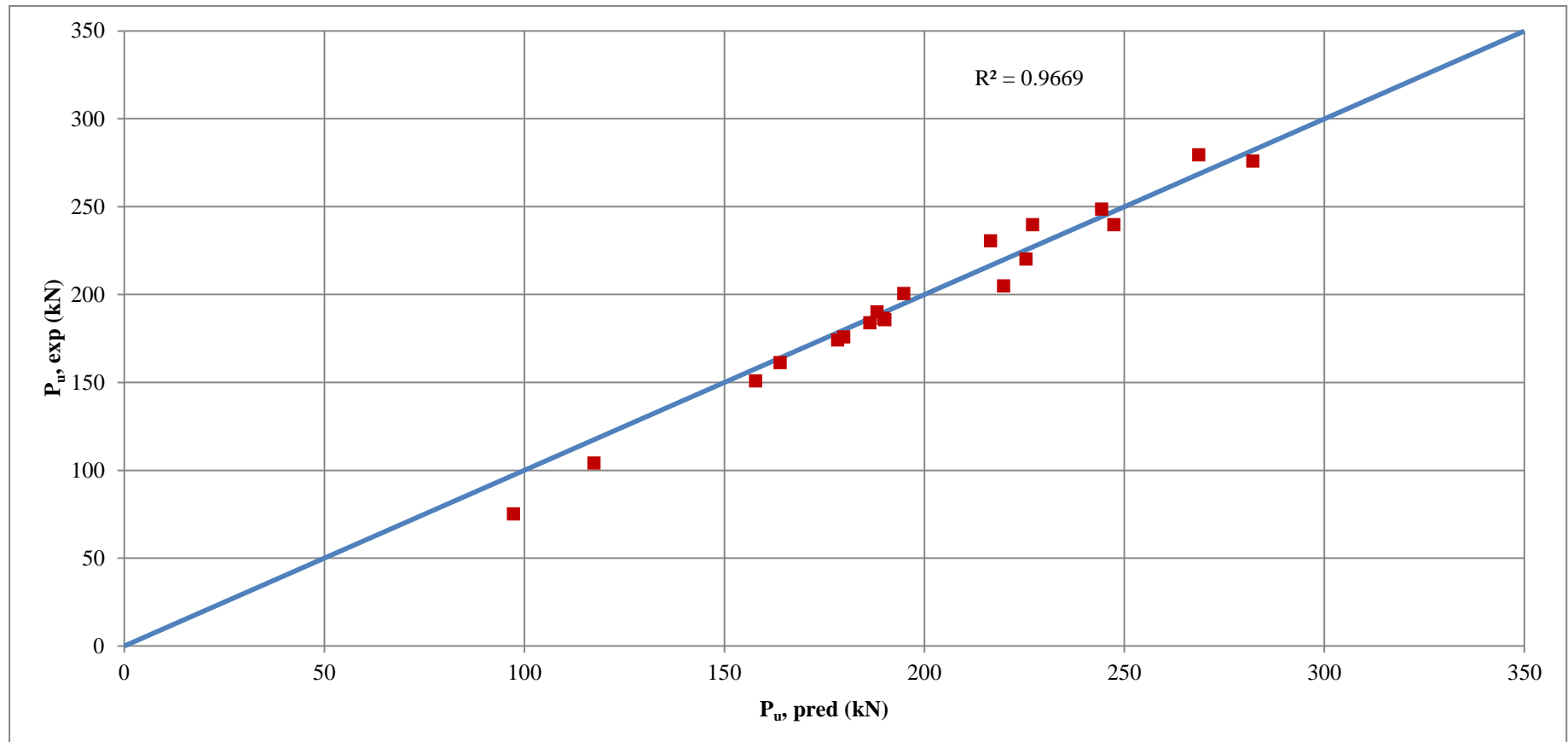## 6.5. Ultimate Loads - Actual versus Predicted

Figure 105: Experimental versus predicted ultimate loads

Chapter 7: Summary and Conclusion

Many techniques were developed to strengthen an existing structure or even repair it. Some of these methods were section enlargements, external post-tensioning, bonding steel plates to concrete structures, steel jacketing and the use of fiber reinforced polymers (FRP).

The use of FRP in civil engineering applications for strengthening of existing structures was developed as an alternative to the use of steel plates due to the many added advantages, such as: larger contact area, lack of corrosion, flexibility in construction, and design and greater ease of installation. Therefore, FRP is widely used to strengthen RC structural elements for axial, shear and moment. However, this study aimed to focus on the FRP flexural strengthening for conventional bending elements e.g. beams. The common method of flexural strengthening of RC beams is made by externally bonding FRP plates or sheets to the bottom tensile surface (soffit) of the beams. This project has addressed the beam flexural benefits of using side-bonded CFRP sheets as opposed to the soffit-bonded CFRP sheets on RC beams.

This study has focused on testing the flexural capacity of RC beams using externally side-bonded CFRP sheets. This topic was specifically chosen to further understand the increase in the RC beams strengthened with side-bonded CFRP sheets capacity as opposed to the increased capacity of soffit-bonded CFRP sheets.

Therefore, the experimental program included casting and strengthening 25 flexural specimens with three different reinforcement ratios. The beams were strengthened from the bottom as well as from the sides using different configurations. Afterwards, the specimens were tested using a third-point loading mechanism; and the results were closely examined and validated using ACI440.2R-08 code provisions.

The following observations and conclusions were drawn from this study:

- The experimental results showed that side-bonded strengthening is effective in flexural members. However, the bottom-bonded technique is more efficient and more economical by 33%.
- Side-bonded FRP is more effective with higher reinforcement ratios, as the performance and behavior get closer to the bottom-bonded technique.

- The percent increase in the flexural strength of the side-bonded strengthened RC beams reaches 95% over the control specimens.

- The high strength increase is accompanied with a high ductility reduction that reaches 60% lower than the un-strengthened beams.

- All the strengthened specimens have incurred steel yielding prior to the debonding of the FRP, and some of the beams have reached concrete crushing before the ultimate failure. Typically, when the effective reinforcement ratio increases, the concrete reaches crushing strain and dominates the failure in a brittle mode.

- The efficiency difference between the side-bonded and the bottom-bonded FRP is justified due to the fiber depth, which affects directly the moment arm within the section. Moreover, the stress distribution in the side-bonded laminates varies along the width of the sheets; which allows the extreme lower fibers to debond firstly and trigger the global failure.

- The increase in FRP width on the sides has indicated low improvement in strength as well as ductility, since the fibers get closer to neutral axis of the section. In group B, the strength improvement took a logarithmic trend, and the single ply side-bonded specimens have recorded 34% capacity enhancement by increasing the width of the FRP by 200%. For the double-ply side-bonded FRP specimens, the 200% fibers increase has led to only 22% strength growth.

- In all the groups (excluding specimens SS-2, SS-3, SD-2 and SD-3), the bottom-bonded scheme has recorded a ductility reduction of 54% for one ply of CFRP and 60% reduction for the double plies. On the other hand, the side-bonded FRP reduced the ductility at failure by 48% and 62% for single and double plies respectively.

- Generally, the analytical load-deflection curves indicate similar behavior for all the tested specimens. In fact, the model over-estimates the stiffness of the section in the uncracked region, and then follows the actual trend in the cracked elastic part. However, at ultimate the model deviates and it does not capture the plastic behavior of the materials.

- Considering the CFRP in the calculation of the cracking moment has an extremely small effect, and it does not change the global behavior of the load-deflection responses of the strengthened specimens using the analytical model.

- The strength predictions calculated using the design guidelines of ACI440.2R-08 code were very close to the actual ultimate attained loads of the tested specimens. The soffit bonded FRP members have recorded a maximum percentage difference of 7% compared to the predicted values.

- Nevertheless, the predictions of the side-bonded specimens have exceeded the actual ultimate attained load by 11%; which occurred due to the special mode of failure caused by uneven stress distribution along the FRP laminates. It should be noted that the ACI440 code provisions recommends using several strength material reduction factors, which were all dropped during this study.

Further studies can be developed on the basis of anchoring the side-bonded laminates, as this technique will enhance the bonding mechanism of the fibers and increase the efficiency of the strengthened beam specimens. Moreover, it is recommended to study the behavior of side-bonded strips. The smaller strips will avoid the global failure of the laminates when the extreme lower fibers reach the debonding strain.

In addition, a microscopic study can be developed on the debonding mechanism for the side-bonded FRP in flexure. This study should investigate the stress transfer plane between the concrete and the laminates, which will give a better understanding of the strain limits for side-bonded FRP. Nonetheless, the researcher should utilize different concrete types and strengths, to analyze the concrete influence on the global performance of side-bonded FRP.

Furthermore, cracking behavior for side-bonded FRP is different than the conventional bottom-bonded FRP, which affects the global behavior of the strengthened elements; therefore, further studies can be developed on the new strengthening technique by monitoring the crack behavior using different laminates and different configurations. Additionally, the researcher should investigate the effect of FRP on the concrete modulus of rupture experimentally; as this property is extremely important in understanding the global performance of elements strengthened with side-bonded FRP.

References

[1]   R. Z. Al-Zaid, A. I. Al-Negheimish, M. A. Al-Saawani, and A. K. El-Sayed, "Analytical study on RC beams strengthened for flexure with externally bonded FRP reinforcement," *Composites Part B,* vol. 43, pp. 129-141, 2012.

[2]   A. Nanni and M. S. Norris, "FRP jacketed concrete under flexure and combined flexure-compression," *Construction and Building Materials,* vol. 9, pp. 273-281, 1995.

[3]   A. Nanni, G. Loreto, and S. Babaeidarabad, "Flexural Strengthening of RC Beams with an Externally Bonded Fabric-Reinforced Cementitious Matrix," *Journal of Composites for Construction,* vol. 18, pp. 273-281, 2014.

[4]   J. L. Borgerson and W. L. Vogt, "Evaluation of Externally Bonded Fiber-Reinforced Polymer Systems to Concrete Structures," *Concrete Repair Bulletin,* pp. 18-21, 2011.

[5]   ACI, "ACI 440.2-08: Guide for the Design and Construction of Externally Bonded FRP Systems for Strengthening Concrete Structures," Farmington Hills, MI, 2008.

[6]   H. Toutanji, L. Zhao, and Y. Zhang, "Flexural behavior of reinforced concrete beams externally strengthened with CFRP sheets bonded with an inorganic matrix," *Engineering Structures,* vol. 28, pp. 557-566, 2006.

[7]   O. Buyukozturk, O. Gunes, and E. Karaca, "Progress on understanding debonding problems in reinforced concrete and steel members strengthened using FRP composites," *Construction and Building Materials,* vol. 18, pp. 9-19, 2004.

[8]   J. F. Bonacci and M. Maalej, "Behavioral Trends of RC Beams Strengthened with Externally Bonded FRP," *Journal of Composites for Construction,* vol. 5, pp. 102-113, 2001.

[9]   ISIS Canada Design Manual No.4, "Strengthening reinforced concrete structures with externally-bonded fiber reinforced polymers," ISIS Canada research network , Winnipeg, MB, Canada, Sep 2009.

[10]   Sika, " SikaWrap-430G: Glass Fiber for Structural Strengthening," in *Products Data Sheets*, ed. Zurich: Sika Schweiz AG, 2003, p. 2.

[11]   M. Ehsani, "Strengthening of Concrete and Masonry Structures with Fiber Reinforced Polymers (FRP)," the 30th Our World in Concrete and Structures (OWICs), Singapore, 2005.

[12]   M. M. Önal, "Strengthening Reinforced Concrete Beams with CFRP and GFRP," *Advances in Materials Science and Engineering,* vol. 2014, pp. 1-8, 2014.

[13]   S. P. Chiew, Q. Sun, and Y. Yu, "Flexural Strength of RC Beams with GFRP Laminates," *Journal of Composites for Construction,* vol. 11, pp. 497-506, 2007.

[14]   S. S. Mohite, D. M. M. Awati, and R. A. Patil, "Flexural Behaviour of R.C. Beams with Side Bonded G.F.R.P. Laminates," *International Journal of Emerging Technology and Advanced Engineering,* vol. 4, pp. 277-281, August 2014.

[15]   G. Murali and N. Pannirselvam, "Flexural Strengthening of Reinforced Concrete Beams Using Fibre Reinforced Polymer Laminate: A Review," *Journal of Engineering and Applied Sciences,* vol. 6, pp. 41-47, 2011.

[16]   D. S. Setunge and Others, "Review of Strengthening Techniques using Externally_Bonded Fiber Reinforced Polymer Composites," CRC Construction Innovation, Brisbane, Australia, 2002.

[17]   M. A. Rashid, M. A. Mansur, and P. Paramasivam, "Behavior of Aramid Fiber-Reinforced Polymer Reinforced High Strength Concrete Beams under Bending," *Journal of Composites for Construction,* vol. 9, pp. 117-127, 2005.

[18]   R. U. More and D. B. Kulkarni, "Flexural Behavioural Study on RC Beam with Externally Bonded Aramid Fiber Reinforced Polymer," *IJRET: International Journal of Research in Engineering and Technology,* vol. 3, pp. 316-312, 2014.

[19]   L. Structural Group, "V-Wrap™ C200-H: High Strength Carbon Fiber Fabric," in *Strengthening Solutions*, ed. U.S.A: Structural Technologies, LLC, 2016, p. 2.

[20]   A. Hutchinson and H. Rahimi, "Concrete Beams Strengthened with Externally Bonded FRP Plates," *Journal of Composites for Construction,* vol. 5, pp. 44-56, 2001.

[21]   F. Lu and A. Ayoub, "Evaluation of debonding failure of reinforced concrete girders strengthened in flexure with FRP laminates using finite element modeling," *Construction and Building Materials,* vol. 25, pp. 1963-1979, 2011.

[22]   R. Kotynia, H. Abdel Baky, K. W. Neale, and U. A. Ebead, "Flexural Strengthening of RC Beams with Externally Bonded CFRP Systems: Test Results and 3D Nonlinear FE Analysis," *Journal of Composites for Construction,* vol. 12, pp. 190-201, 2008.

[23]   A. F. Ashour, S. A. El-Refaie, and S. W. Garrity, "Flexural strengthening of RC continuous beams using CFRP laminates," *Cement and Concrete Composites,* vol. 26, pp. 765-775, 2004.

[24]   G. Li, Y. Guo, and X. Sun, "Investigation on Flexural Performance of RC Beams Flexurally Strengthened by Side-bonded CFRP Laminates," *The Open Civil Engineering Journal*, vol 6, no 1, p.26 – 32, 2012.

[25]   M. A. Hosen, M. Z. Jumaat, and A. Islam, "Side Near Surface Mounted

(SNSM) technique for flexural enhancement of RC beams," *Materials & Design,* vol. 83, pp. 587-597, 2015.

[26]   ACI Committee 318, "Building Code Requirements for Reinforced Concrete (ACI 318-14)', American Concrete Institute, Farmington Hills, MI, 2014

[27]   L. Structural Group, "V-Wrap™ 700: Epoxy Adhesive," in *Strengthening Solutions*, ed. U.S.A: Structural Technologies, LLC, 2011, p. 2.

[28]   ASTM. "D 3039/D 3039M - Standard Test Method for Tensile Properties of Polymer Matrix Composite Materials," 2000, pp. 105-116

[29]   L. Structural Group, "V-Wrap FRP System: Manual Number IM-16," in *Tensile Testing Manual*, ed. U.S.A: Structural Technologies, LLC, 2015, p. 11.

[30]   C. Dundar, A. K. Tanrikulu, and R. J. Frosch, "Prediction of load-deflection behavior of multi-span FRP and steel reinforced concrete beams," *Composite Structures,* vol. 132, pp. 680-693, 2015.

Appendix A

A. Testing Setups and Load versus Deflection Responses

A.1   Group A:

A.1.1 Control Beam (GA-C)
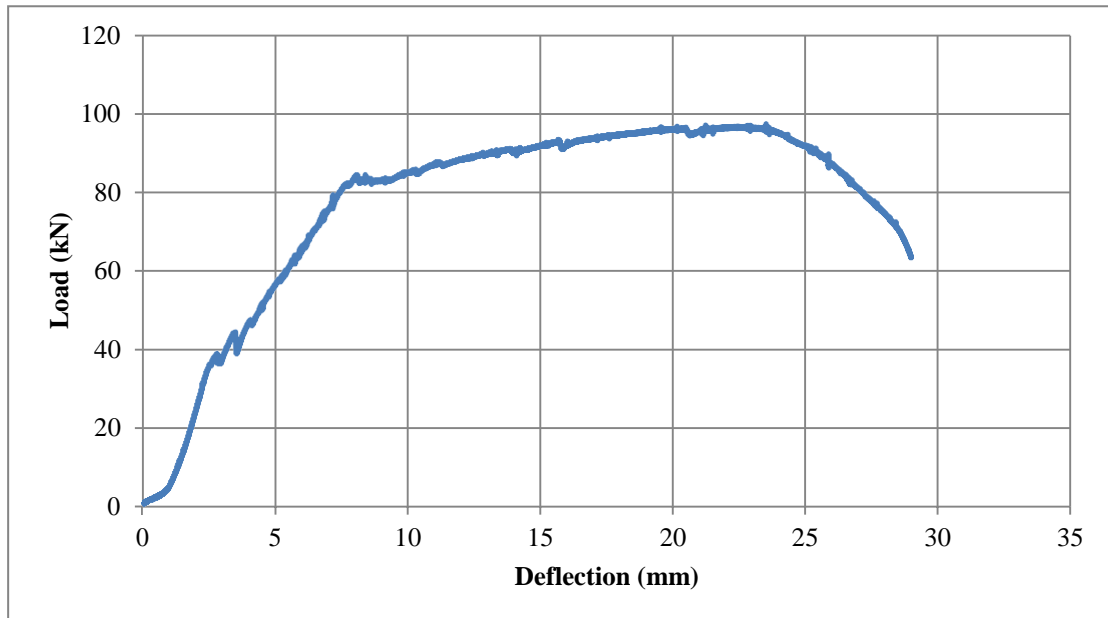
Figure 106: Control beam load (kN) versus deflection (mm)

Figure 107: Control beam set-up

Figure 108: Control beam steel yielding

A.1.2 Beam (GA-BS)
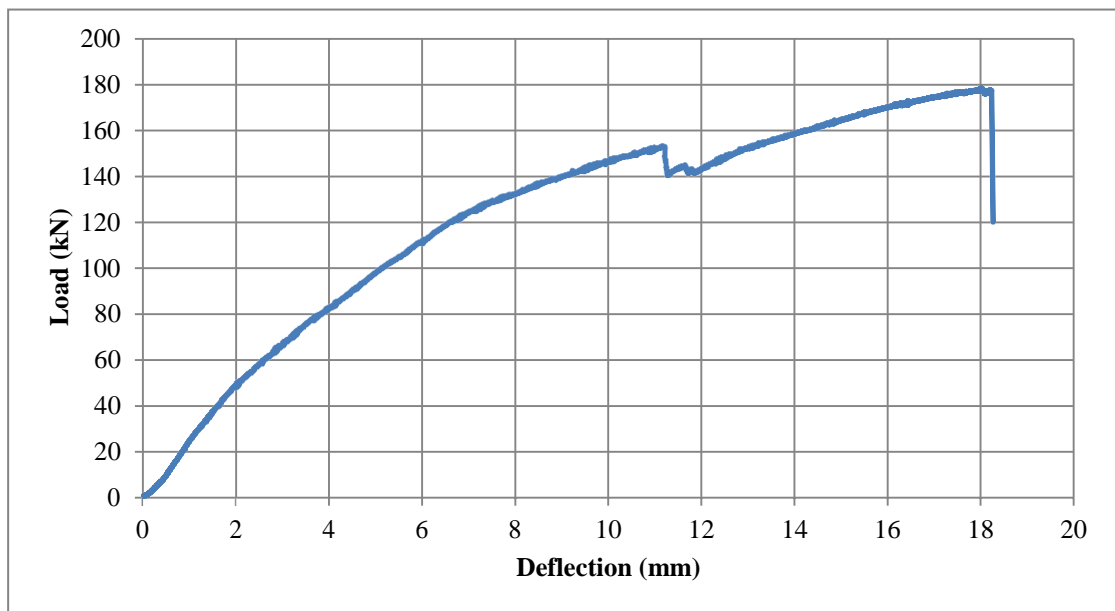
Figure 109: Beam BS load (kN) versus deflection (mm)

Figure 110: Beam (BS) set-up

Figure 111 Beam (BS) failure and FRP debonding

A.1.3 Beam (GA-BD)
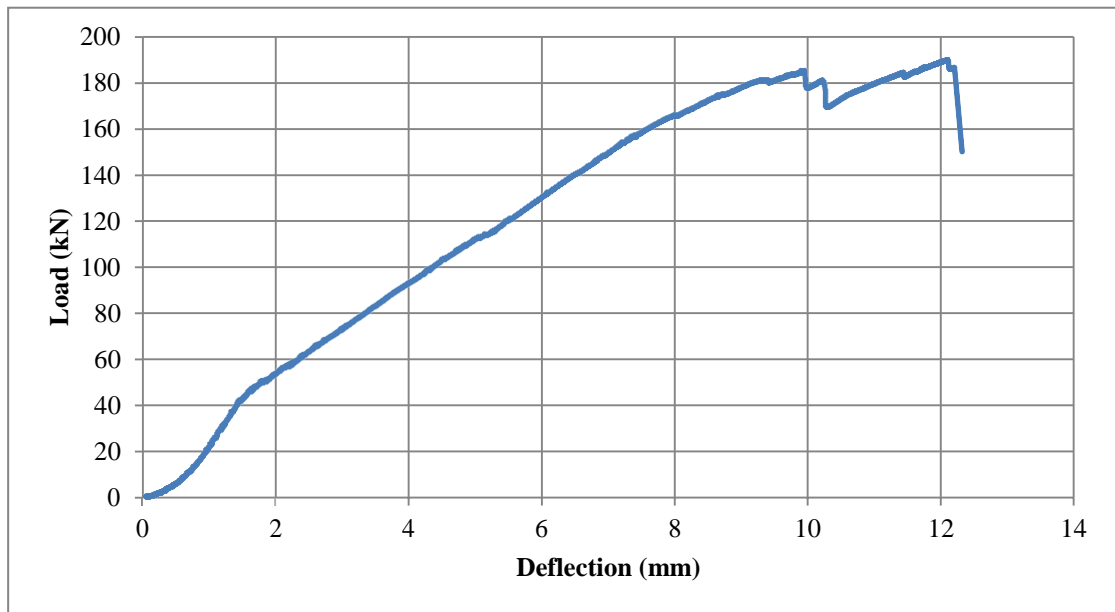
Figure 112: Beam (BD) load (kN) versus deflection (mm)

Figure 113: Beam (BD) set-up

Figure 114: Beam (BD) FRP debonding

A.1.4 Beam (GA-SS)
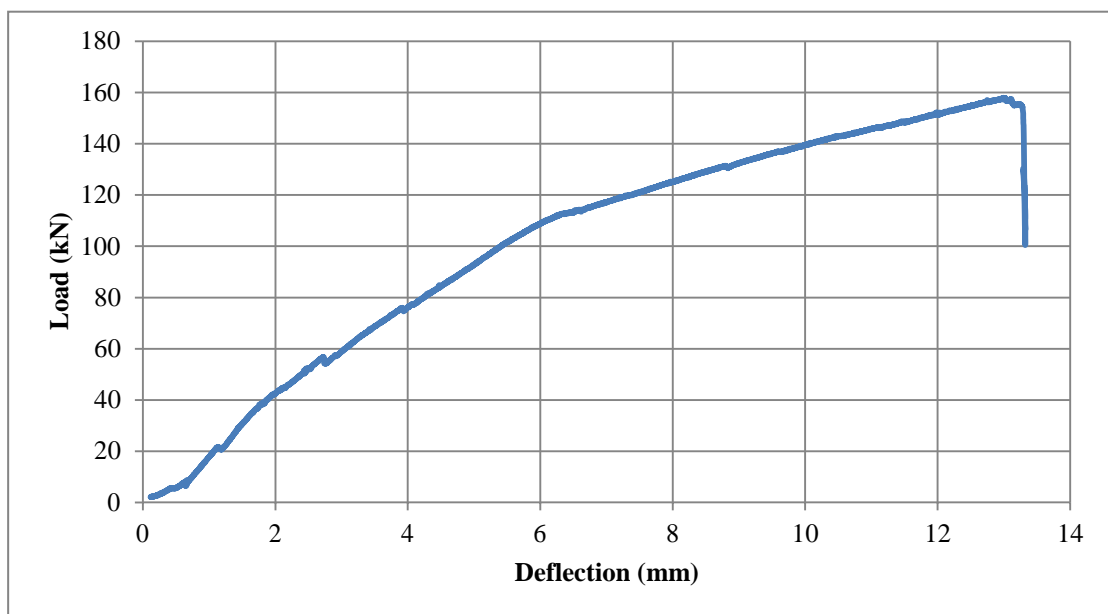
Figure 115: Beam (SS) load (kN) versus deflection (mm)

Figure 116: Beam (SS) set up

Figure 117: Beam (SS) debonding of FRP

A.1.5 Beam (GA-SD)
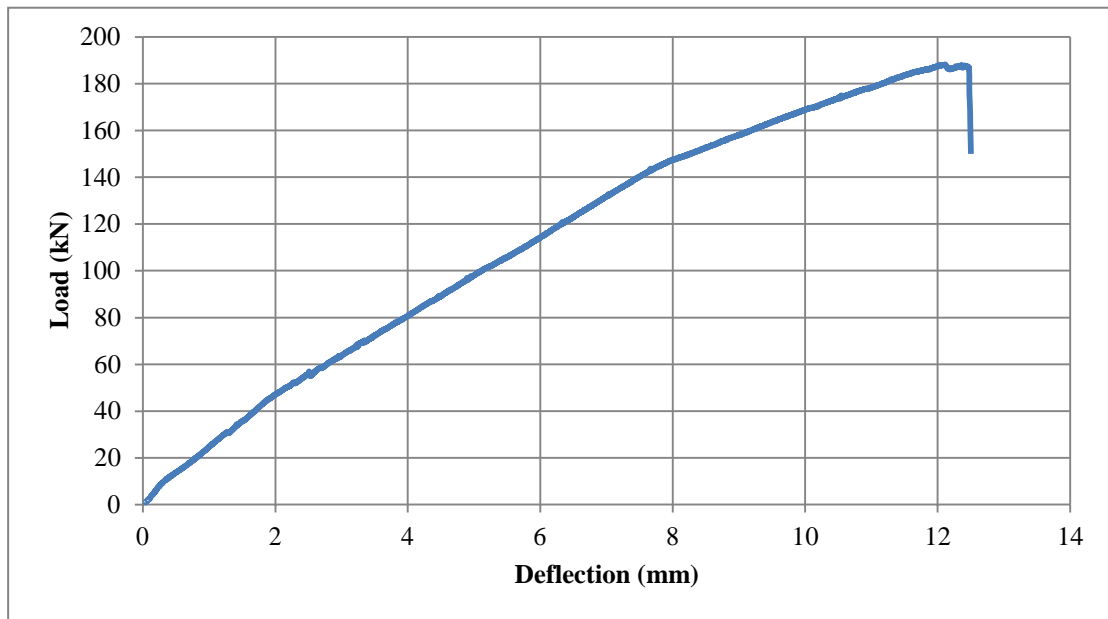
Figure 118: Beam (SD) load (kN) versus deflection (mm)

Figure 119: Beam (SD) set-up

Figure 120: Beam (SD) FRP debonding

A.2   Group B

A.2.1 Control Beam (GB-C)
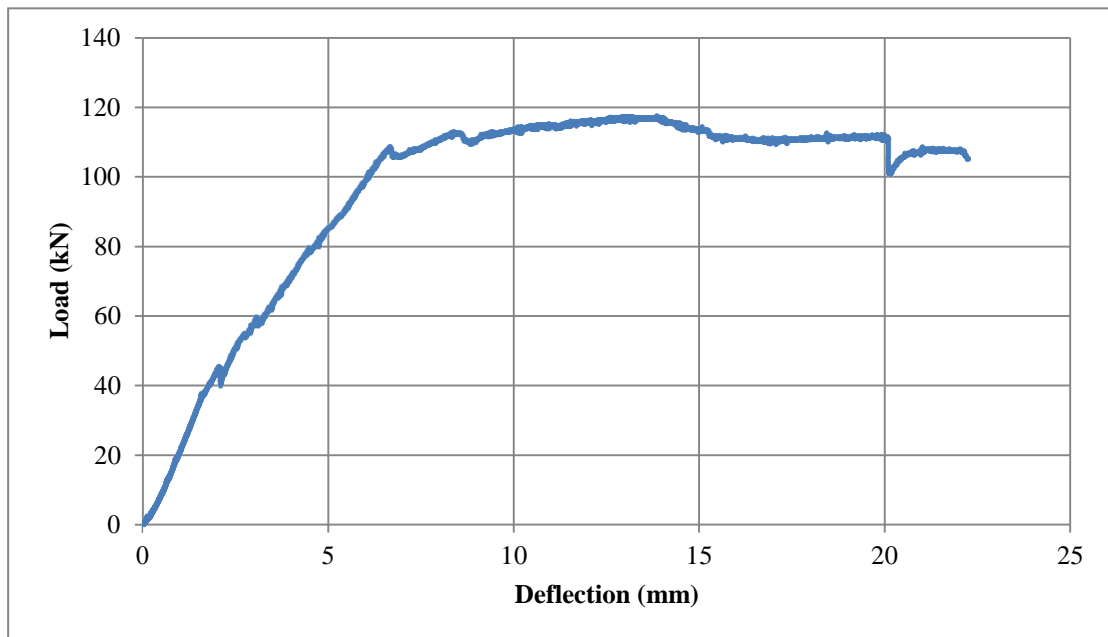
Figure 121: Control beam load (kN) versus deflection (mm)

Figure 122: Control beam set-up

Figure 123: Control beam at steel yielding

A.2.2 Beam (GB-BS)
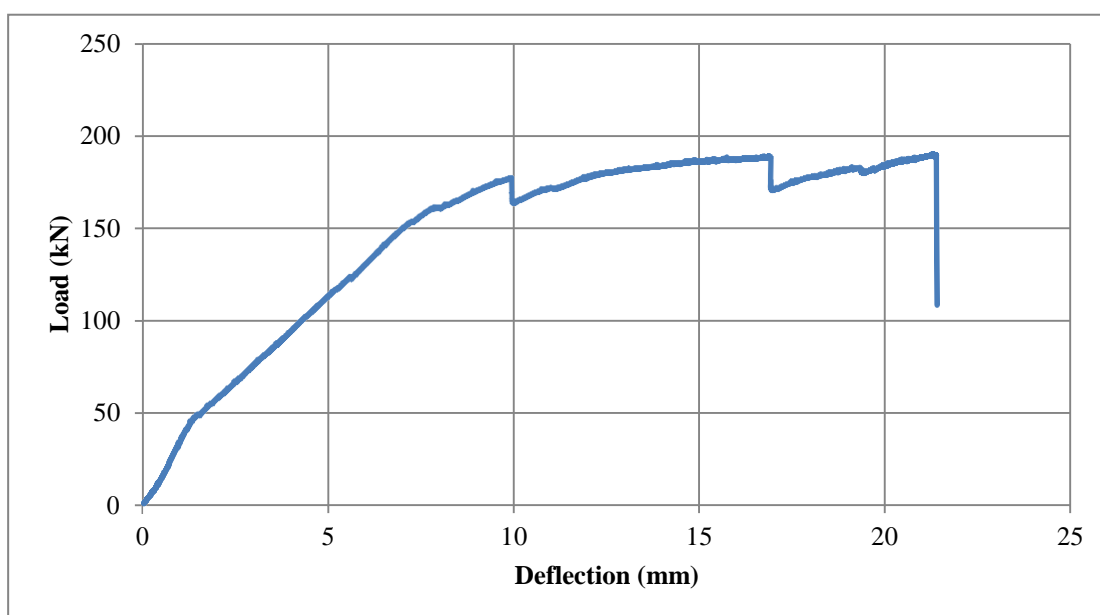
Figure 124: Beam (BS) load (kN) versus deflection (mm)

Figure 125: Beam (BS) set-up

Figure 126: Beam (BS) FRP debonding

A.2.3 Beam (GB-BD)
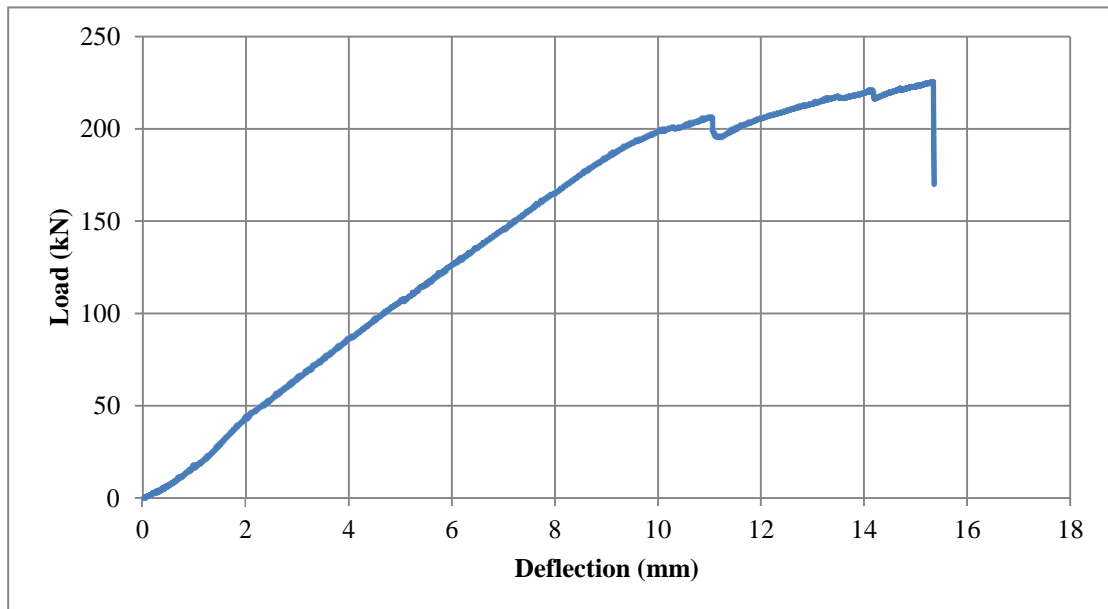
Figure 127: Beam (BD) load (kN) versus deflection (mm)

Figure 128: Beam (BD) set-Up

Figure 129: Beam (BD) FRP debonding

A.2.4 Beam (GB-SS-1)
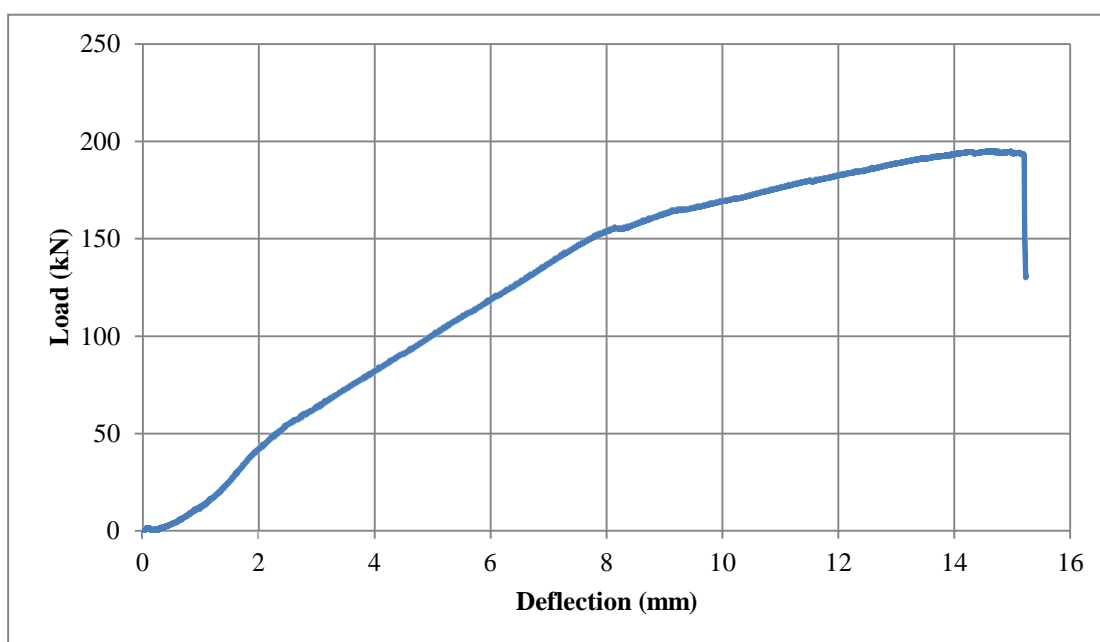
Figure 130: Beam (SS-1) load (kN) versus deflection (mm)

Figure 131: (SS-1) beam set-up

Figure 132: (SS-1) beam concrete crushing

## *A.2.5 Beam (GB-SS-2)*
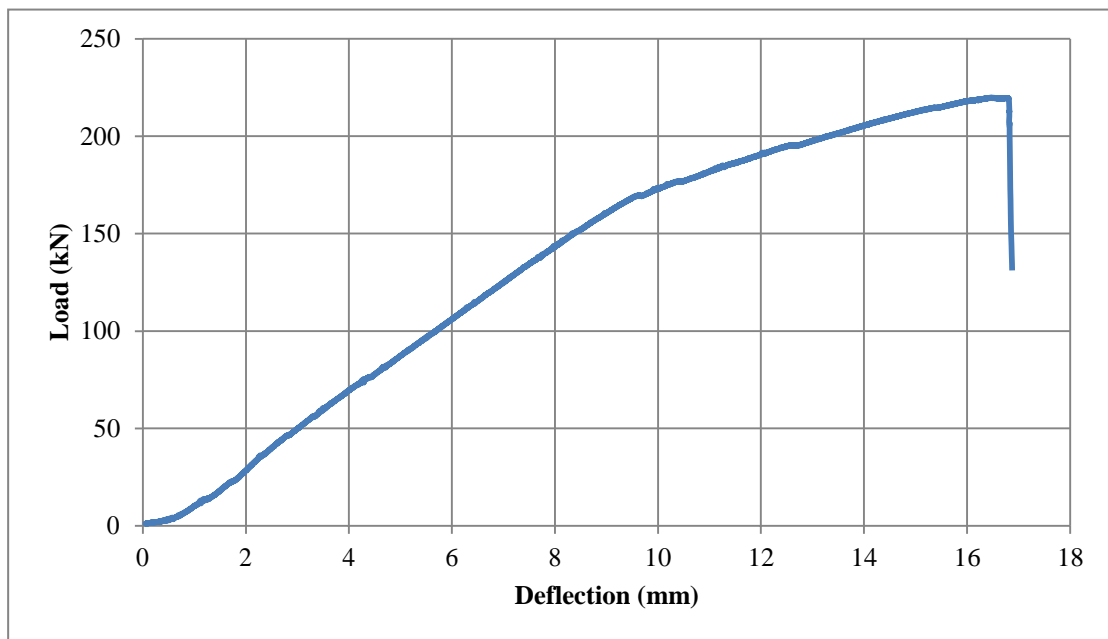
Figure 133: (SS-2) beam load (kN) versus deflection (mm)

124

Figure 134: (SS-2) beam set-up with 150mm side-bonded FRP

Figure 135: Beam (SS-2) FRP debonding

A.2.6 Beam (GB-SS-3)
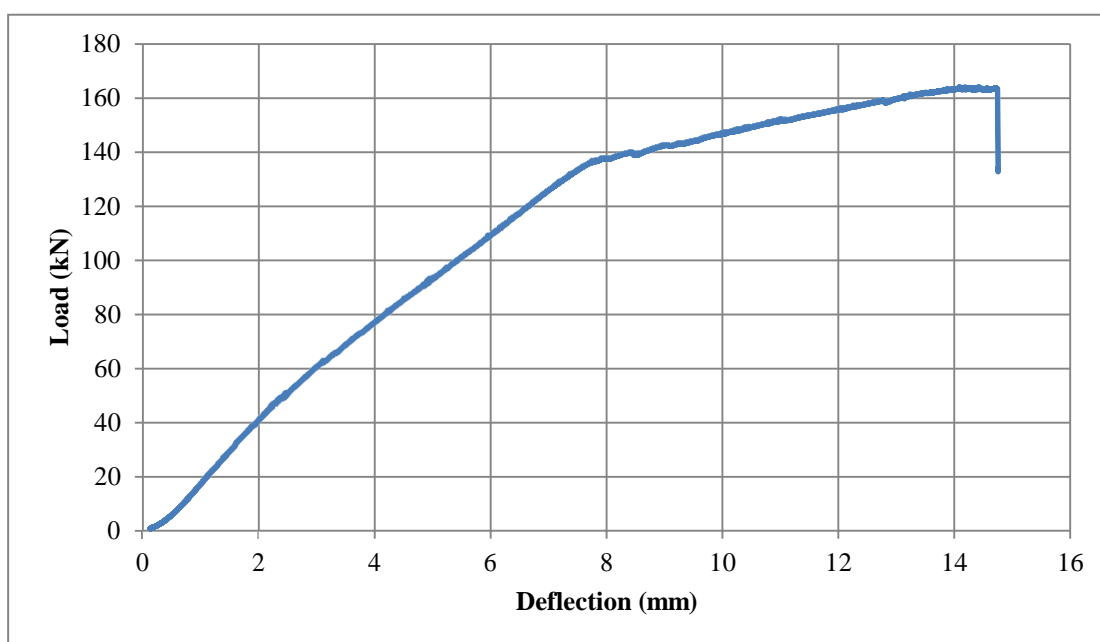
Figure 136: (SS-3) beam load (kN) versus deflection (mm)

Figure 137: beam (SS-3) set-up with 50mm side-bonded FRP

Figure 138: Beam (SS-3) FRP debonding

A.2.7 Beam (GB-SD-1)
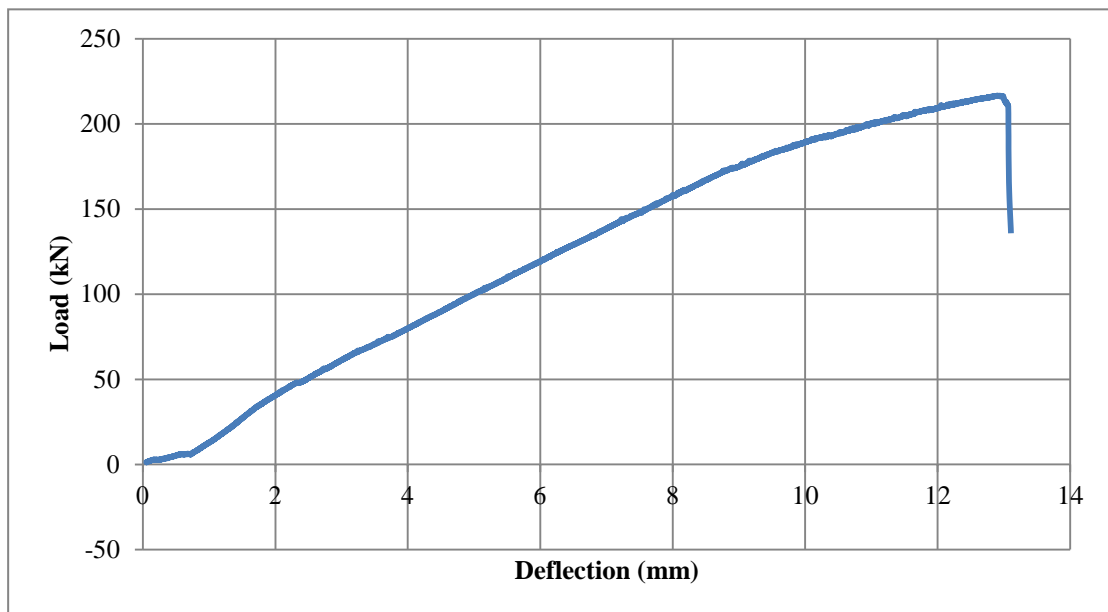
Figure 139: (SD-1) beam load (kN) versus deflection (mm)

Figure 140: (SD-1) beam set-up

Figure 141: Beam (SD-1) FRP debonding

A.2.8 Beam (GB-SD-2)
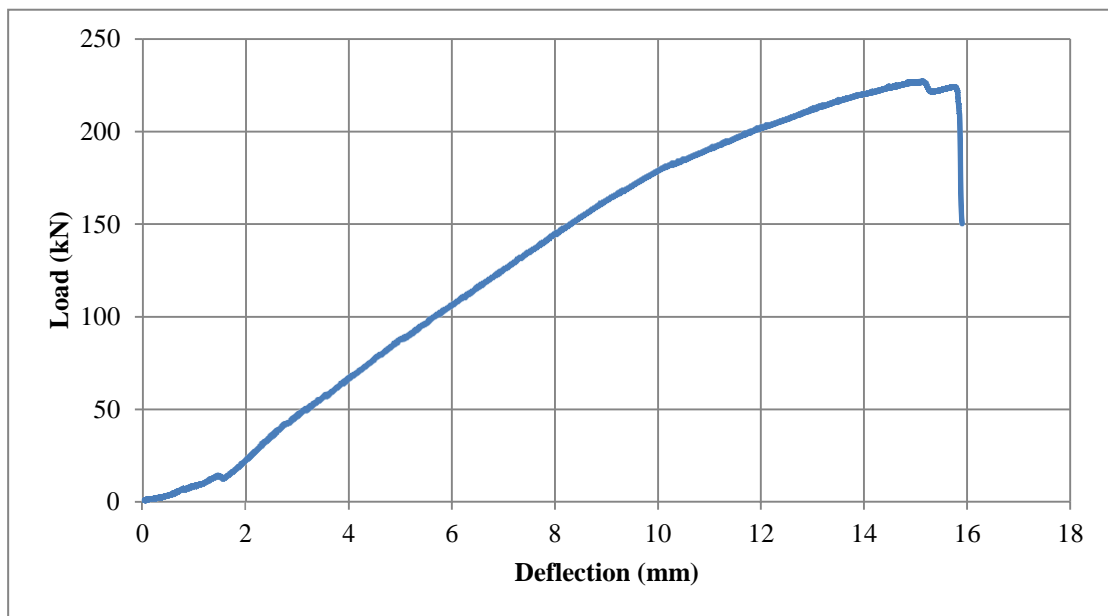
Figure 142: (SD-2) beam load (kN) versus deflection (mm)

Figure 143: Beam (SD-2) set-up with 150mm side-bonded FRP

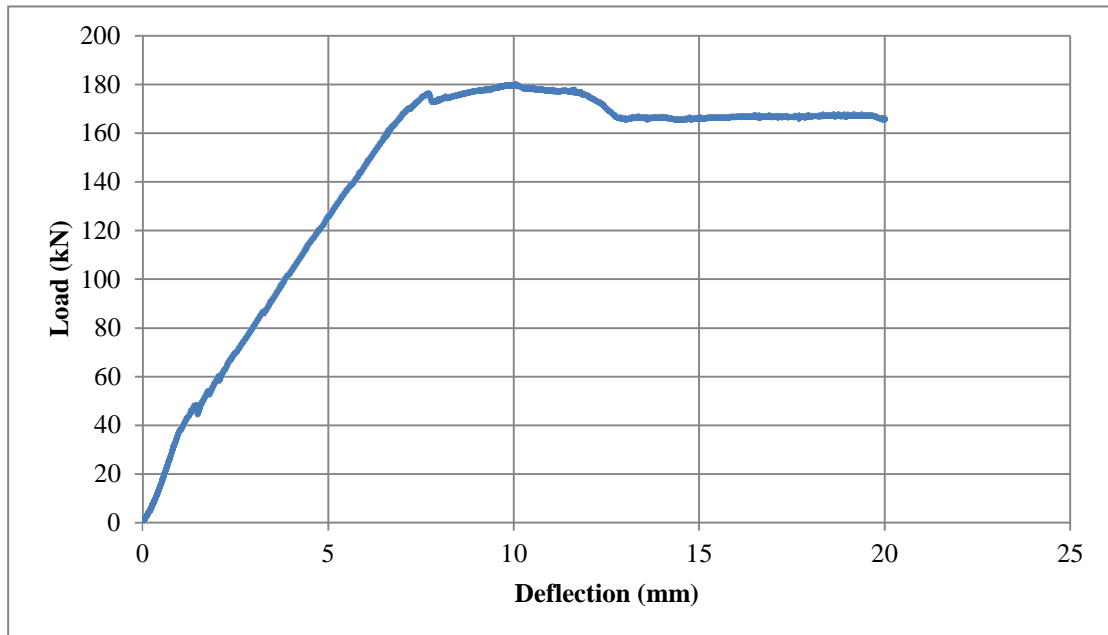Figure 144: Beam (SD-2) FRP debonding

A.2.9 Beam (GB-SD-3)
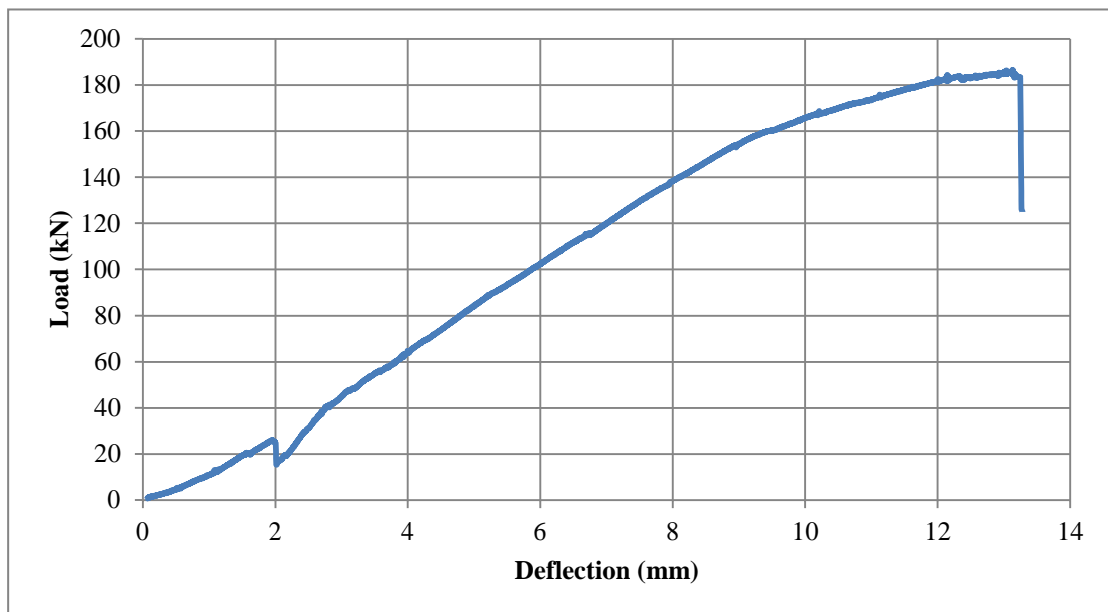
Figure 145: (SD-3) beam load (kN) versus deflection (mm)

Figure 146: Beam (SD-3) set-up with 50mm side-bonded FRP

Figure 147: Beam (SD-3) FRP debonding

A.3   Group C

A.3.1 Control Beam (GC-C)

Figure 148: Control beam load (kN) versus deflection (mm)

Figure 149: Control beam set-up

Figure 150: Control beam steel yielding and concrete crushing
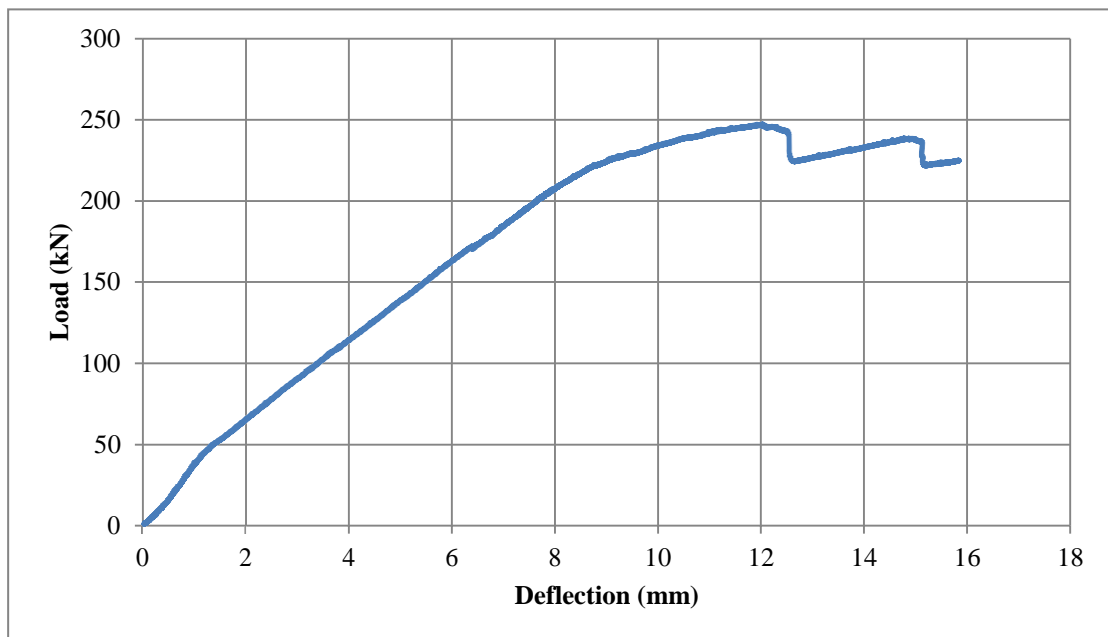
A.3.2 Beam (GC-BS)

Figure 151: (BS) beam load (kN) versus deflection (mm)
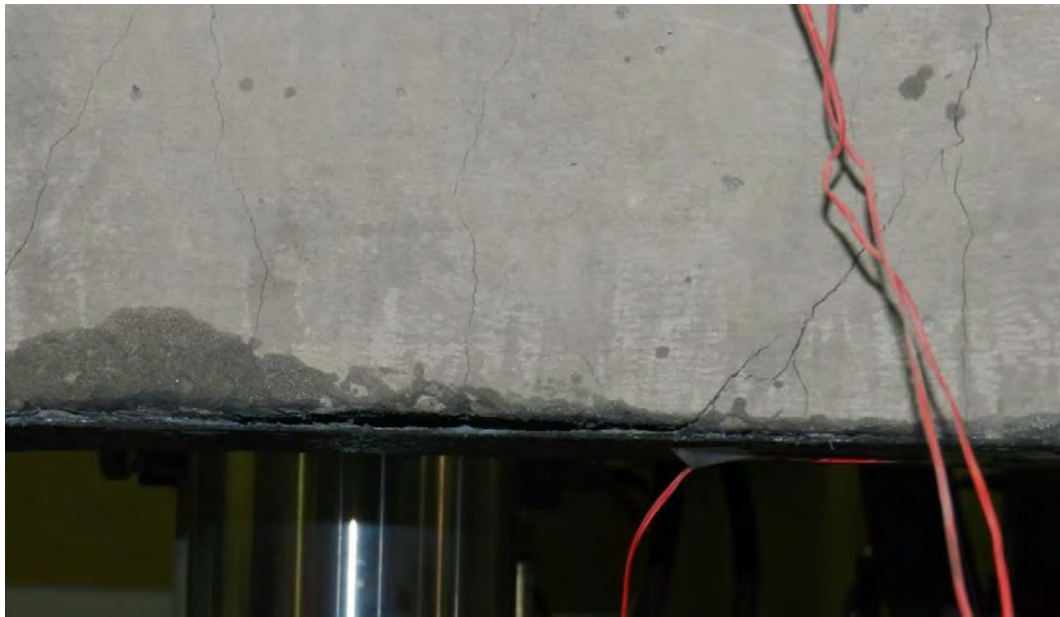
Figure 152: Beam (BS) set-up

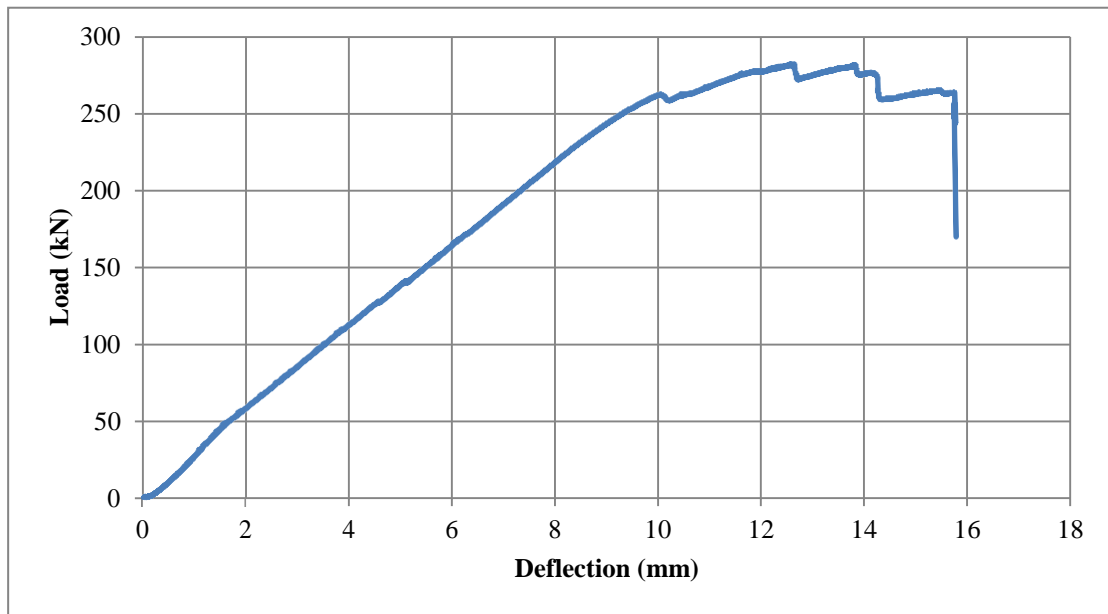Figure 153: Beam (BS) steel started to yield

A.3.3 Beam (GC-BD)

Figure 154: (BD) beam load (kN) versus deflection (mm)

Figure 155: (BD) beam set-up

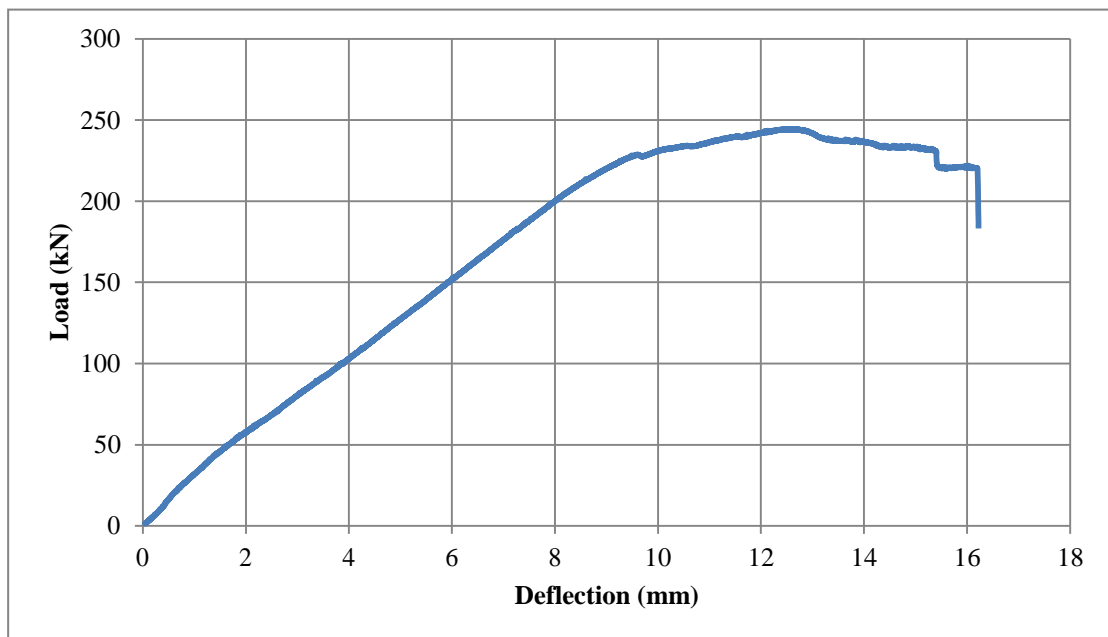Figure 156: Beam steel yielding and concrete started to crush

A.3.4 Beam (GC-SS)

Figure 157: (SS) beam load (kN) versus deflection (mm)

Figure 158: (SS) beam set-up

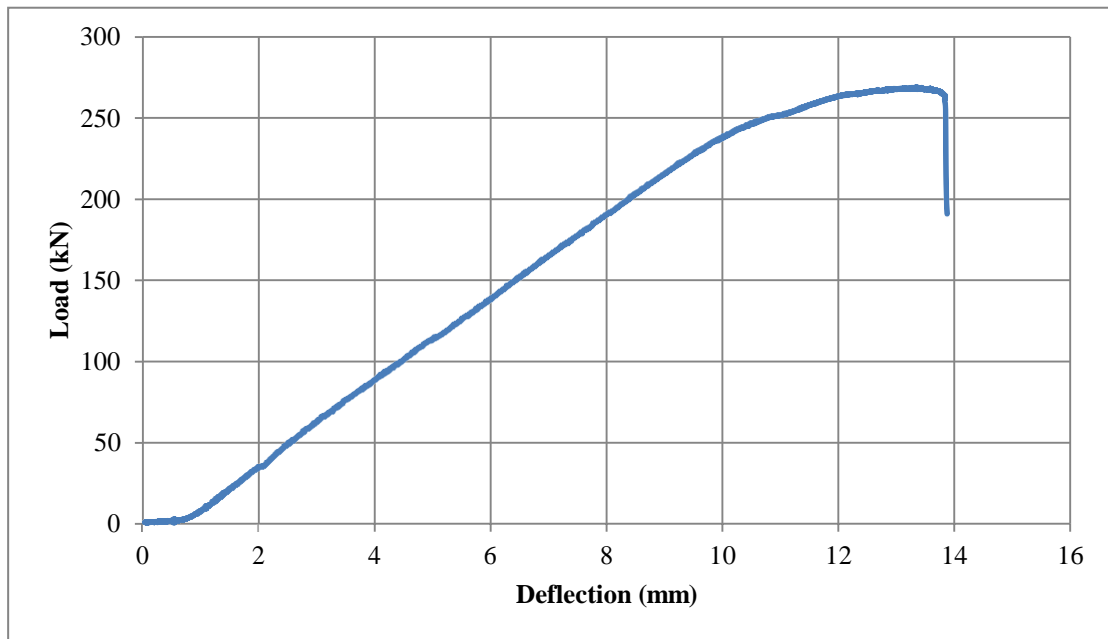Figure 159: Beam (SS) failure and FRP debonding

Figure 160: (SD) beam load (kN) versus deflection (mm)

Figure 161: (SD) beam set-up

Figure 162: FRP debonding of (SD) beam

Vita

Ahmad S.D. Salama was born in 1991, in Dubai, UAE. Ahmad graduated from Al-Shola Private School with honors in 2009. Afterwards, he joined the American University of Sharjah to pursue a Bachelor of Science degree in Civil Engineering. Mr. Salama completed his undergraduate studies with cum laude honors, in Spring 2013.

Mr. Salama started his career in Eng. Adnan Saffarini office as a structural engineer; meanwhile, he received an assistantship from AUS to pursue a Master of Science degree in Civil Engineering in Fall 2013, as he worked as a part-time Graduate Teaching Assistant.

During his master's studies, Mr. Salama found strengthening of reinforced structures using composites very interesting field. Therefore, in June 2014, he joined an American company called STRUCTURAL, RC strengthening specialist, as a Structural Engineer until the present time.